Study on Distortion Control in Nozzle Welding of Stainless Steel Pressure Vessels

by

Jinning Peng

A thesis
presented to the University of Waterloo
in fulfillment of the
thesis requirement for the degree of
Master of Applied Science
in
Mechanical Engineering

Waterloo, Ontario, Canada, 2011

I hereby declare that I am the sole author of this thesis. This is a true copy of the thesis, including any required final revisions, as accepted by my examiners.

I understand that my thesis may be made electronically available to the public.

Jinning Peng

Abstract

The welding of austenite stainless steel often results in large amount of welding distortion due to its high thermal expansion coefficient and low thermal conductivity. This has created great difficulty in the dimensional control of the welded stainless steel structure, ending up with high manufacturing cost. Researches on the welding distortion of stainless steels were very limited, especially for large weld structures with complex component shapes. The studies of this thesis were initiated with focus on the stainless steel nozzle-to-shell-can weld structures, a very typical structural configuration for pressure vessels used in petrochemical and nuclear power generation industries.

Both the experimental and the FEA (finite element analysis), i.e. computational simulation, approaches were taken in the studies which addressed the influences of the welding fixture, the welding sequence, and the welding process on the distortion caused by stainless steel nozzle-to-shell welding. The investigations employed single and multi-nozzle weld test models (called mockups in the thesis) or FEA models. Manual GTAW (gas tungsten arc welding) and SMAW (shielded metal arc welding) processes were selected to represent the most common practice for stainless steel nozzle welding. The FEA simulations were conducted with ABAQUS program using sequentially coupled transient analysis method with lumped weld passes to achieve high computing efficiency.

The investigations on the effect of the welding fixture concluded that the contour fixtures introduced in the thesis be effective for reducing the welding distortion for both

the single and the multi-nozzle welding. The contour fixtures tend to localize the welding distortion, hence yield less impact on the global distortion of the whole weld structure. The rib-bar fixture, a more common fixture type for multi-nozzle welding, was found resulting in a big jump in the shell plate distortion when the fixture was removed.

The studies on the influence of the welding sequence revealed that a progressive approach was more favorable for distortion control under the given nozzle-to-shell weld structure configurations. The best sequence suggested is to start welding at one nozzle, firstly on shell OD (outside diameter) side then on ID (inside diameter) side, then proceed to next neighboring nozzle. The effect of the welding direction of each weld pass was found affecting only the nozzle angular distortion.

The experimental data showed that the manual GTAW process developed much higher shell plate distortion than the SMAW process. The reason would be that a higher percentage of the welding heat had been consumed on the base metal. The influence of the weld bead size didn't appear to be significant. In the FEA study on the effect of the size of the lumped weld pass, the increase in weld bead size even resulted in a decrease in weld distortion. From the FEA simulation point of view, using large lumped pass would be a highly efficient choice without compromising too much in the precision of the distortion prediction. The FEA study confirmed that a decrease in cooling time after welding would result in more welding distortion.

The large scale multi-nozzle mockup with rib-bar fixture demonstrated a maximum out-of-plane shell distortion of 16.4mm after the welding of 10 nozzles with GTAW+SMAW process, which suggests that additional measures should be developed to further control the welding distortion.

Acknowledgments

I would like to thank my supervisor Prof. Norman Y. Zhou for his guidance and time during the period of the work of this thesis.

I would also like to thank Dr. Li Pan (Babcock & Wilcox Canada) and Dr. Wei Zhang (Oak Ridge National Lab) for their contributions in welding distortion simulation, and to Mr. Stephen Hamilton (Babcock & Wilcox Canada) for his help with mechanical drawings and machining. Thanks also go to Mr. Diab Keirouz (Babcock & Wilcox Canada) and Mr. Dorel Muth (Babcock & Wilcox Canada) for their support for the study of this thesis.

This work was financially supported by Babcock & Wilcox Canada.

To My Family

Table of Contents

List of Tables

List of Figures

Chapter 1 Introduction

Stainless steel's high resistance to corrosion, excellent formability, as well as its pleasant appearance make it an ideal material for many applications, such as kitchen cookware, appliances, surgical instruments, food processing equipments, hygienic equipments, storage tanks, petrochemical and nuclear power generation equipments [1~3]. The austenitic stainless steels, known as 300 series, are the most common ones, making up over 70% of the total stainless steel production [2].

During metal welding, the weld and the base metal materials around the weld are locally heated by the welding heat source. The temperature distribution around the weld joint is not uniform and changes as the welding progresses. Non-uniform stresses and strains are therefore developed during this process, resulting in plastic deformation and residual stresses after the welding is completed. The weldment shrinkage and various types of distortions are hence produced [4,5]. For austenitic stainless steels, due to their high thermal expansion coefficient and low thermal conductivity (Table 1-1), the welding distortion will be notably larger than that with carbon and low alloy steels [1].

Table 1-1 Physical Properties of Carbon and Austenitic Stainless Steels [1]

	Austenitic Stainless Steel	Carbon Steel
Thermal Conductivity (W/m-K),100°C	18.7~22.8	60
Mean Coeff. of Thermal Expansion (μm/(m-°C),0~538°C	17~19.2	11.7
Electrical Resistivity (nΩ-m)	690~1020	120
Melting Temperature Range (°C)	1400~1450	1538

For pressure vessels, the nozzle-to-shell-can or nozzle-to-head weld joints are normally, in the sense of welding distortion, the most complex weld structures among the vessel major welds. Even higher complexity would be found when a nozzle intersects with the shell surface at an angle, in which case we would see a saddled weld seam path with a typically varying weld groove cross-section.

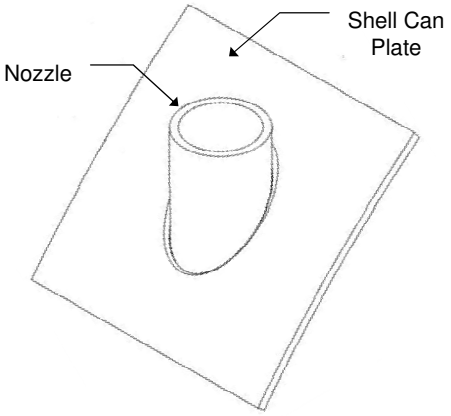

The control of the nozzle welding distortion would be very challenging when the shell can is of large diameter and thin wall and a high density of nozzles are to be welded onto the shell. Unfortunately there have been very limited studies that can be refereed to. Almost all the welding distortion studies were based on either flat metal plates with butt or fillet joints, or tubes / nozzles with girth groove welds (refer to Chapter 2), not to mention that a large portion of those studies were lab-based, not related to actual weld products. No published literature has been found addressing the nozzle-to-shell welding distortion. Although some general concepts may be extracted from available research results, such as that the fixture could help to reduce the distortion, the effective solution for specific application has to be developed on a case by case basis, through experiments or computational analyses under specific material and structural configurations [6]. It is therefore important to investigate and understand the distortion behaviors during the stainless steel nozzle-to-shell welding process.

Generally speaking the control of the welding distortion can be realized through pre- and post-weld application of mechanical loads or thermal heat, and careful design of

the weld joint, the welding constraints (fixtures, clamping), the welding sequences, and the welding procedure [4,6,7]. In other words, there are three types of distortion control approaches: pre-weld control such as pre-straining, in-process control such as the application of welding fixture, and post-weld control such as thermal straightening. In the case of stainless steel multi-nozzle welding where the weld joint structures are more complicated than plat plate or tube girth joints, the pre-weld control would be hard to apply except for the optimization of the weld joint design. The post-weld control approach would also be hard to do due to the stainless steel's unique thermal properties (Table 1-1). The studies of this thesis were therefore focused on aspects of in-process distortion control, involving welding fixture, sequence and process.

The objectives of the studies on stainless steel nozzle welding distortion are as follows,

- Comparative evaluation of existing and new welding approaches/techniques in terms of welding distortion, so that an optimal welding procedure could be developed to minimize the shell and nozzle distortions
- Assessment of the actual distortion level so that proper actions could be determined to maintain the welding distortion within tolerable limits
- Application of finite element analysis (FEA) method for prediction of nozzle welding distortion. This would be an important technological advance for efficient study of the nozzle welding distortion.

Both nozzle weld model (called mockup in the thesis) tests and FEA simulations were carried out for the distortion studies. The FEA method provides an excellent opportunity that the evaluation of multiple process variations could be completed within

restricted time frame and limited budget. Sometimes conducting an experiment may not be possible due to such as the material availability, in which case the computational approach would be the most effective solution [8]. Because of the structural complexity of the nozzle-to-shell welds, the lumped pass transient analysis technique [6,7,9] has been employed to simplify the FEA computation. The lumped pass technique was further simplified in the thesis for the analyses of multi-nozzle large weld structures.

To represent the possible manufacturing conditions, the manual gas tungsten arc welding (GTAW) and shielded metal arc welding (SMAW) processes had been chosen for the mockup tests, which bring in an uncertainty in terms of process consistency. In other words, even under nominally the same welding condition, the welding distortion of the mockup sample would often to some extent be different from the distortion of the actual product. The main focus of the thesis was therefore placed on the relative comparison of the distortions under different welding conditions. For the same reason plus the use of lumped pass technique, it is hard to develop a FEA heat source model to precisely reflect the multi-pass manual welding process. The distortion values from FEA simulations were hence used primarily for relative comparisons among FEA results. Nevertheless, the direct comparisons between the FEA and the experimental results were made where such a comparison is appropriate.

The thesis starts with a literature review on welding distortion theory, researches and findings. Chapter 3 describes the experiment mockup designs, the test procedures, the distortion analysis method, and the techniques employed in the FEA simulation studies. The studies on the influences of the welding fixtures were summarized in Chapter 4. Chapter 5 presents the findings of the studies on the influences of different

welding sequences. The impacts of different welding processes, weld bead sizes and cooling conditions are presented in Chapter 6. The experimental results of multi-nozzle weld mockup are listed in Chapter 7. The conclusions from the experimental and the FEA simulation studies are given in Chapter 8.

Chapter 2 Literature Review

The welding distortion as the most visible quality issue of a welded structure has drawn continuous attention. Large amount of research works were carried out to study the distortion behaviors under various welding application conditions in order to find out effective measures to minimize the welding distortion. Early welding distortion studies were conducted through welding experiments. Over the past thirty years or so, along with the emerging and maturing of the finite element analysis technology and the rapid growth of the computer computing power, more and more efforts have been devoted to the computational simulation of the welding process to predict the welding distortions [5~43]. Very often the FEA studies were accompanied by supporting experiments. A few publications were also found using artificial neural networks for welding distortion studies [44~46]. This chapter summarized the welding distortion basics, the application areas of the welding distortion studies, the influences of the welding procedure variables, and the available FEA techniques for welding distortion prediction.

2.1 Welding Distortion Concepts, Mechanisms and Control

2.1.1 Welding Distortion Concepts and Mechanisms

The non-uniform temperature distribution created by the welding process results in non-uniform residual stresses and deformations in the weldment. In the case of flat plate weld joints, the weldment deformation is composed of three basic elements (Figure 2-1) [4,8,10],

- Transverse shrinkage
- Longitudinal shrinkage
- Angular change

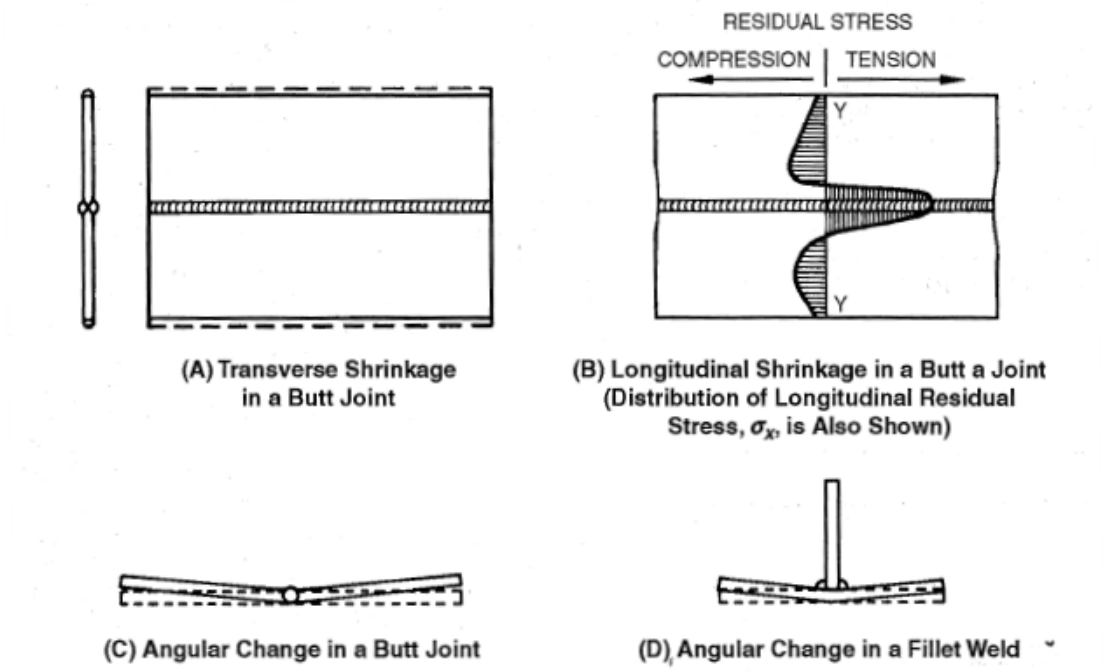

Figure 2-1 Fundamental Dimensional Changes in Weldments [4]

Depending on the specific structure characteristics, these basic deformations would develop into different types of distortions. The longitudinal shrinkage could cause bending distortion along the weld seam direction, or buckling distortion when with thin plate. The buckling distortion is due to the compression stress in the region just beside the weld seam (Figure 2-1 (B)). Typical examples were given by Reference [47], showing the buckling of an overlap joint welded with 1mm thick DP600 steel plates, and the bending of a T-joint welded with 6mm thick S355 plates. Some literatures mentioned about out-of-plane deformation [28,48]. It is a term applicable for all types of welding distortions except the plate shrinkages.

Apart from the thermal expansion / contraction, the phase transformations of the weld and the heat affected zone (HAZ) during the heating and cooling processes also play

an important role in determining the welding residual stresses and distortions. As shown in Figure 2-2, when a carbon steel base metal is heated above A1 (cementite disappearance temperature) temperature, the pearlite–ferrite microstructure which is of body centered cubic (BCC) structure gradually transforms into austenite microstructure which is of face centered cubic (FCC) structure , resulting in reduction of the material volume. During rapid cooling, the austenite with FCC structure changes to martensite with a body centered tetragonal structure, and the volume increases. For carbon and low alloy steels, the higher the carbon or carbon equivalent content, the more impact the phase transformation will have on the welding residual stress and the distortion. An example was given in Reference [12] showing that a compressive stress had been produced in the weld fusion zone in the welding direction, where tensile stress would normally be expected. It confirms clearly the influence of the material phase transformation. However, for austenite stainless steels, no such phase transformation will take place.

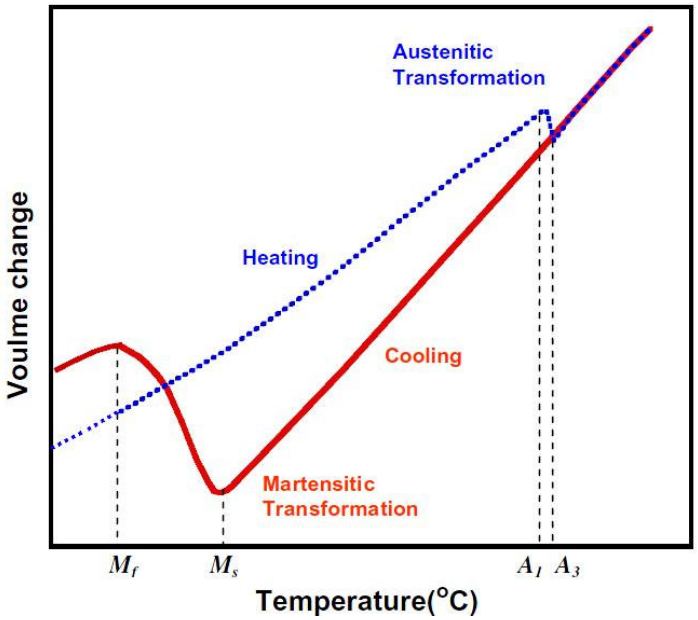

Figure 2-2 Schematic Diagram of Volume Change Due to Phase Transformation [12]

2.1.2 Control of Welding Distortion

Pre-weld Distortion Control

The pre-weld distortion control techniques are applied before the start of the welding process. Two basic approaches as follows were recommended [4,6],

- Optimization of weld joint design to reduce the weld size and balance the weld groove geometry to avoid over-deposition of the weld metal on one side of the workpiece or structure
- Bend the workpieces or set the workpiece orientations in a direction opposite to the predicted or known welding distortion, to counterbalance the consequence of the welding process.

The typical examples of the second approach include pre-straining [4,7], pre-bending [6,13], and workpiece presetting [4]. These methods are applicable to relatively simple weld structures where the welding distortions are of simple shape (for example bending, rather than buckling) so that the pre-weld forming or setting of the workpieces could be realized [4].

Regarding the weld joint design, the first rule is that the weld seam size shall be minimized to scale down the driving force of the welding distortion. Examples are the reduction of the number of weld passes [49], the use of narrow groove design [50]. It was also highlighted by some studies that the initial weld groove gap, usually called root gap, has a significant effect on the final welding distortion, therefore shall be reduced if feasible [4,32].

It is commonly understood that for butt welding of thick plates the double V or double U groove design, as compared to single V or single U, would help to reduce the

welding distortion. Reference [4] presented a few research results revealing that, to achieve minimum distortion on a butt weld joint, the ideal ratio between the groove depths of the first and the second welded sides depended on the actual joint configuration and plate thickness. For example, with 19mm thick plate, the ideal ratio of the groove depths between the first and the second welded sides was 7:3, while with 32mm thick plate, the ideal ratio was found to be 1:1. However, for butt weld of a washer shape flat plate, the ideal ratio was 11:6 when the plate thickness was 19mm.

In Process Distortion Control

Various techniques have been investigated for distortion control during the welding process, such as the application of fixture or clamping, the optimization of welding sequence, mechanical tensioning, thermal tensioning, pre-cambering, preheat, and vibratory weld conditioning [4,6,7,51,52]. They can in fact be separated into two categories:

- External methods: use external mechanical device/load or thermal power to create resistance to the shrinkages of the weld metal
- Internal method: sequence the deposition of the weld beads so that the resistance to weld metal shrinkages could be generated through the interactions between the weld beads

Among the above the most common distortion control methods are fixture design and weld sequence optimization. The mechanical tensioning and thermal tensioning techniques were proposed for longitudinal weld seams [52]. The pre-cambering technique requires that the workpieces be elastically bent then welded [6]. After the welding the pre-camber is released and the fabricated structure springs back to its final shape. This is

similar to the mechanical tensioning, except that the pre-cambering method is more dedicated to bending or angular distortion.

The influences of the welding process type and parameters were also investigated, addressing heat source density, heat input, welding travel speed, and weld bead size [3,4,6,21,37,38,50,53]. All these factors are related to the heat source characteristics. For stainless steel welding, reference [1] recommended to use heat sink to take away part of the weld heat in order to reduce the welding distortion.

Post-weld Distortion Correction

Two approaches are available for correcting the welding distortions produced by welding [4,6,7,48],

- Mechanical straightening
- Thermal or flame straightening

The purpose of straightening operation is to remove the distortion by producing adequate plastic deformation in the distorted member or section [4]. It is apparent that this type of correction is not always possible or allowed. The best practice would be to optimize the weld joint design, apply sufficient constraint through fixture or clamping, and optimize the welding sequence.

2.2 Application Areas of Welding Distortion Studies

Most of the welding distortion studies were based on butt or fillet welds of flat metal plates [3~5,9,13~18,21,24,27,28,31,35,38,41,47,48,50,53~55]. The typical applications include shipbuilding [5,32,35,41,48,53], automobile [31,32,41], trains and bridges [37]. The plate thicknesses in these studies were mostly 1~12mm. The rests of the distortion studies were conducted with tubular/pipe butt joints, or plate/flange to pipe girth welds [5,9,19,22,23,29,51].

The welding processes involved in the welding distortion studies include gas tungsten arc welding (GTAW), pulsed GTAW, gas metal arc welding (GMAW), pulsed GMAW, laser beam welding (LBW), submerged arc welding (SAW), and electron beam welding (EBW). No literature was found addressing the effect of manual welding processes on welding distortion, such as shielded metal arc welding (SMAW) or manual GTAW. Besides, although there were a few references heading into multi-pass welding distortion [19,41,50,56], the knowhow obtained has been very limited regarding the welding distortion behaviors specific for multi-pass welding.

Regarding the base metals, the mostly investigated materials were low carbon and high strength low alloy (HSLA) steels [4,12,21,22,31,35,41,42,47,48]. The next mostly studied material type was stainless steel [3,26,41,42,49,56~59].

2.3 Welding Distortion Studies on Influences of Welding Procedure Variables

2.3.1 Studies on Influences of Welding Constraints

Many researches were conducted to investigate the influences of the weld fixtures or clamping on the welding distortion [1,4,6,7,13,14,30,41,47,49,53,55,57,59,60]. Tack weld was also categorized into this group [4,57]. The studies demonstrated that the application of welding constraints had effectively reduced the welding distortion, especially for angular distortion [13,59]. Reference [47] even investigated into the effects of specific clamping technique details like the clamping time, the clamp release time, and the clamp preheating.

While restricting the welding distortion, the fixture or clamping also resulted in higher internal plastic deformation and higher residual stress [4,47]. This might become a concern for some applications. Reference [1] also pointed out that, for metal plates thicker than 6.35mm, other distortion control measures such as the optimization of weld bead deposition sequence may be required in addition to the application of the weld fixture/clamping.

2.3.2 Studies on Influences of Welding Sequences

The influences of the welding sequence on welding distortion have attracted the attentions of many researchers [1,6,7,11,13,18,20,41,44,53,57,61~63]. The studies involved the sequencing of different weld seams, different weld passes/segments of the same weld seam, and different welding directions. Reference [6] proposed to classify these sequencing types as local (e.g. back stepping) and global sequencing. A common characteristic of these studies is that, the sequencing solutions were very much application-oriented. For example, the best welding sequences (sequence "d" in Figure 2-3) concluded from reference [62] would be valid only for the flat plate T-joint structure under the analysis conditions. In other words, there is no universal solution in terms of welding sequence. Dedicated studies are necessary for specific welding applications.

2.3.3 Studies on Influences of Welding Process

Comparative studies on the effects of different welding processes on welding distortion were presented in reference [38], involving GMAW, pulsed GMAW, SAW, Fronius cold metal transfer process, and LBW. The laser (LBW) and pulsed GMAW processes were found the best for welding distortion control. Reference [50] also

concluded that, at given welding heat input, the pulsed GMAW process created less welding distortion than the GMAW process. The effects of the pulse frequency, amplitude and duration of the pulsed GTAW process were studied in reference [3] for the welding of austenite stainless steels. An explanation of the advantage of the pulsed welding process was that the higher frequency enhances the energy density of the welding heat source, thereby reduces the welding distortion [3].

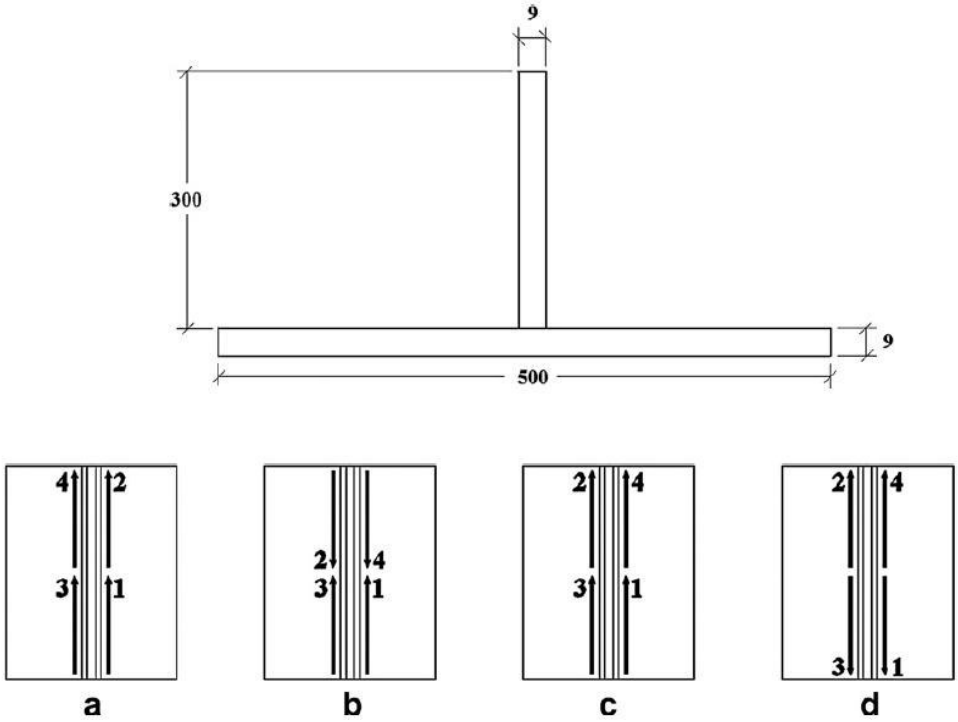

Figure 2-3 T-Joint Weld Structure and Weld Sequences [62]

For given welding process, the heat input (welding power per unit length of weld) is usually considered the deterministic factor for the weld quality including welding distortion. The studies on the effect of the heat input suggested that the heat input be reduced in order to achieve low welding distortion [38,53,55]. However, it should be aware that this conclusion was only based on single-pass welding. The situation would become complicated when dealing with multi-pass welding.

Studies were also carried out by some researchers on the influences of the welding speed on welding distortion [6,21]. An in-depth study on the influence of welding speed was conducted in reference [64], through applying the same heat input but different welding speeds. It was revealed that the welding speed had clear impact on transient temperature field, microstructure grain size and workpiece material hardness. Although the welding distortion was not addressed in reference [64], it would be expected that the welding distortion would change along with the changes of the temperature field.

Reference [37] described a study with double-sided double arc welding process. The effects of the arc distance and welding parameters were investigated.

For multi-pass welding, it was found that using larger-sized weld electrodes (accordingly, larger weld bead size) would result in a decrease in the overall weldment transverse shrinkage [4]. Figure 2-4 shows the gradual increase of the transverse shrinkage along with the deposition of each additional weld pass, indicating that the first a few passes play the major role in determining the welding distortion [4]. The larger the size of the initial passes, the less the final overall welding distortion.

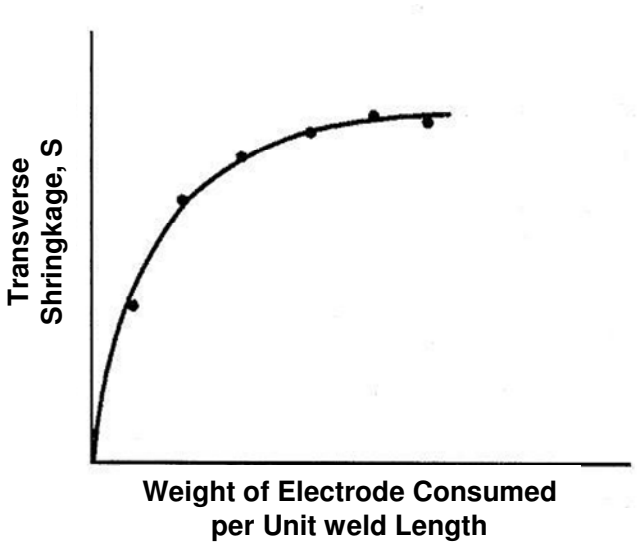

Figure 2-4 Increase of Transverse Shrinkage along with Addition of Weld Passes [4]

2.4 Finite Element Method for Welding Distortion Simulation

2.4.1 Basic Concepts and Techniques

The application of the finite element method for predicting the welding distortion relies on the following information,

- Temperature-dependant material properties
- Weldment structure and weld joint design
- Boundary conditions: fixtures / clamping / forces, workpiece and ambient temperatures, cooling condition
- Welding heat: heat input, weld speed, thermal cycle
- Weld sequences

The numerical simulation involves the interaction of thermal, mechanical and metallurgical phenomena. The welding process has transient characteristics where a local heated zone travels through an elastic structure, causing heating up, melting, solidifying, and cooling down, often accompanied by complex microstructure changes [5]. The welding power was thus called transient moving heat source. A finite element analysis of the welding process can be based on a 3D FEA model of the weld structure, using nonlinear transient analysis techniques incorporating the interactions of all phenomena at every analysis time step. For a complex weld structure, this is going to be very time consuming. Some early researches found out that the heat transfer analysis could be separated, or normally called uncoupled, from the stress-strain analysis without hurting the analysis quality [8]. In other words, the thermal analysis is performed first, followed by the structural analysis using the temperature predicted in thermal analysis as the thermal load in conjunction with any additional mechanical loads or constraints [6]. This

technique is called sequentially coupled thermal and structural analysis, or sequentially coupled thermal, metallurgical and structural analysis when phase transformations are involved [6,8,12]. It has become the standard approach for welding process simulations and been implemented into major FEA software packages for welding.

Before starting the FEA prediction of the welding distortion, the critical step is to establish an appropriate heat source model. The heat source model reflects the combining effect of the welding heat input, the welding speed, and the power source heat density and distribution. The double ellipsoid model, proposed by Prof Goldak, is the mostly employed one (Figure 2-5) [8]. Its heat flux features Gaussian distribution. In the welding FEA software SYSWELD, standard heat source models for GTAW and GMAW processes are provided [42,43]. Calibration of the standard models is required in order to match the actual application, using either the heat input and the welding travel speed, or the information of the thermal cycle or weldpiece microstructures / hardness [43].

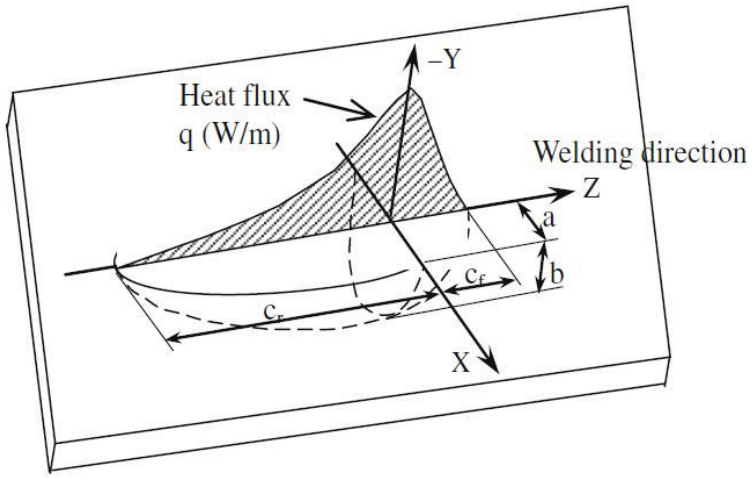

Figure 2-5 Double-ellipsoid Heat Source Model [8]

2.4.2 FEA Software

There are currently three major FEA software platforms employed for welding distortion simulations,

- ABAQUS, working together with dedicated ABAQUS subroutines or extensions [6,7,9,12,21,32,39,47,55]
- SYSWELD, an independent software for welding process simulation [41-43]
- ANSYS [18,20,23,57]

SYSWELD was developed by ESI Group and AREVA for numerical simulation of welding and heat treatment processes [41]. An outstanding feature of SYSWELD is its capability in handling CCT (continuous cooling transformation) diagrams of carbon and low alloy steels [42], based on which the simulation of phase transformation is performed. The outputs of a SYSWELD analysis include temperature field, distortions, residual stresses, microstructures, hardness, and plastic strains.

The most successful welding simulation tool on the ABAQUS platform is the Virtual Fabrication Technology (VFT) modeling procedure, developed by Battelle Memorial Institute in conjunction with Caterpillar Incorporated [7]. With the VFT tool, ABAQUS is able to accurately model complex welding procedures. Graphical User Interface is provided for the assignment of welding paths, parameters and material properties [9]. These data are imported from Comprehensive Thermal Solution Procedure (CTSP) and user material subroutine UMAT35. For large fabricated structures, very coarse meshes are suggested for global distortion predictions [6]. But this is inadequate for thermal gradients and cooling rates during the welding process. CTSP was thus developed for global distortion prediction of production components. Apart from the

applications at Caterpillar, VFT has been used in the US shipbuilding and power generation industries. The addition of VFT to ABAQUS has resulted in 58~85% of saving in computing time [9].

2.4.3 Simplifications for Welding Distortion Simulation

Because of the complexity of welding processes and welded structures, the computing time for numerical prediction of the welding distortion is still a challenge. Various efforts have been made to simplify the FEA analysis. Typical simplification techniques are summarized in this section.

FEA Model Design and Meshing

It has become a common practice for large weld structure that the weld seam and nearby regions are treated as 3D solid model and the area of a large plate away from the weld as shell model, as shown in Figure 2-6 [39,41]. Full analysis was performed on the local 3D model for weld joints, and simplified analysis on the shell model. High density meshes were created at the weld seam. The further away from the weld, the coarser meshing [5,18].

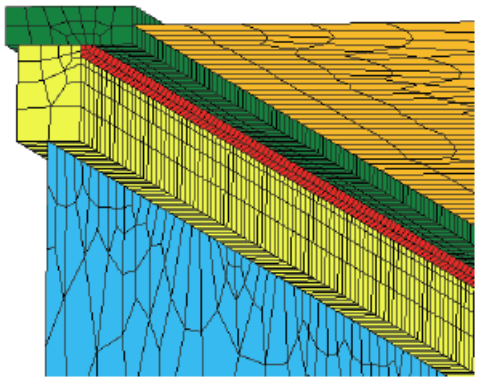

Figure 2-6 Typical FEA Model and Meshing [39]

Block Dumping Technique

Block dumping technique was introduced to speed up the FEA computation and has now become a widely accepted approach [7]. It is also called lumped pass analysis when the dumped block is a complete weld pass. During block dumping analysis, the whole weld metal of the selected weld pass or segment is added and heated up simultaneously. Then the analysis will move on to the next weld pass or segment. In other words, it reduces the number of solution steps by grouping a few element-wise steps into one step [6]. For example, with a moving heat source the analysis of one weld pass may take dozens of steps. While with block dumping approach the analysis could be completed in one step. The saving in computing time is apparently high. However, the challenge is how to develop an equivalent heat input and heating duration for the lumped step. One approach recommended in reference [6] is to match the size of the heat affected zone (HAZ) by comparing the lumped heating with the ordinary moving arc solution. It was claimed by reference [7] that, with the block dumping technique, the ABAQUS-based VFT tool can model extremely large and complicated structural fabrications used in pressure vessels, nuclear piping and ship components.

One reported concern with the block dumping approach was that the block addition of large amounts of hot metal to a cold model tends to cause convergence issues with the VFT program, which would result in analysis failing to complete [9].

The studies in reference [19] introduced a variation of the block dumping method. In stead of using fixed size block, a series of variable length heating blocks were added to a multi-pass joint per schedule shown in Figure 2-7. In comparison to the analysis with a moving heat source, the computing time was cut down from 200 hrs to 91 hrs. With

heating blocks of fixed length of the whole circle, the computing time dropped down dramatically to only 3.2 hrs. It should be aware that a large saving in computing time would usually be accompanied by less precise prediction. This may not be a concern for studies based on relative comparison, but might become a problem if the focus is on the absolute value of the predicted distortions.

Number of weld pass	Length of heat source	Image of heat source
1–2	1/36 (L_0)	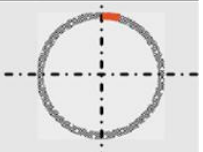
3–5	1/4 (L_0)	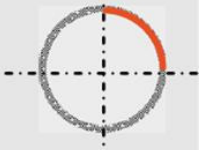
6–10	1/2 (L_0)	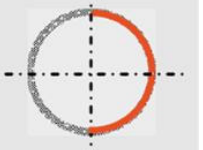
11–14	1/4(L_0)	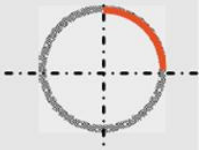
15–16	1/36(L_0)	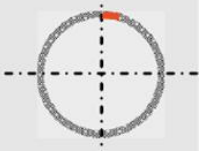

L_0 is the circumference of the corresponding weld pass.

Figure 2-7 Multi-pass Welding Simulation with Varied Length of Dumped Heating Blocks [19]

Simplified Two Stage Analysis Based on Inherent Strain Theory

The inherent strain theory was established based on an assumption that the complex nonlinear thermal, metallurgical and elastic-plastic processes occur only at the weld seam and on the immediate neighboring base metals. All remote areas experience

only elastic loads. The inherent strain was defined as the residual plastic strain of the weld joint [29]. Assuming the inherent strain is the initial strain, the welding distortion can easily be calculated with elastic FE analysis, omitting the complicated thermal elastic-plastic analysis. The following procedure was therefore proposed [29,31,32,35],

- Stage I: estimate the inherent strains for different typical weld joints, using thermal elastic–plastic finite element method
- Stage II: use the inherent strains obtained from Stage I to predict the welding distortions of large welded structures with elastic finite element method

Reference [13] introduced a technique called Iterative Substructure Method (ISM), with which the distortion prediction was composed of two steps, dealing with respectively a large structure linear problem and a small nonlinear region with moving heat. It falls in the same philosophy of the inherent strain theory.

Shrinkage Volume Method

A very simple FEA method - linear elastic shrinkage volume method was developed by Prof Tsai [16,34]. It is a steady-state finite-element approach that assumes that the main driving force for distortion is linear thermal contraction of the weld metal as it cools from elevated to room temperature. This contraction is resisted by the surrounding parent metal, resulting in the formation of internal forces. The parent metal distorts to accommodate these shrinkage forces until equilibrium is achieved. No thermal or metallurgical analysis is required by this method.

2D FEA Models for Simple Weld Structures

For welding of flat plate butt joint, a simplified 2D thermal and plane-strain elastic-plastic model was employed in reference [38]. The 2D model was orientated in a plane transverse to the welding direction. The stress field from the 2D analysis was then

applied to a 3D elastic model to predict the welding distortion. This approach is similar to the techniques using inherent strain theory, except that the 2D model is applicable only to simple weld structures. In reference [14], a 2D cross-section thermal model was used for thermal transient analysis of plate butt weld.

2.5 Summary

Welding distortions are caused by non-uniform temperature distribution during welding process and often with contribution from phase transformations. The transverse shrinkage, longitudinal shrinkage and angular change are the basic deformations which work together to produce various types of welding distortions.

The researches on welding distortion were mostly based on flat plate butt/fillet welds or tube/pipe/nozzle girth welds, involving various types of welding processes. No study was found on manual SMAW or manual GTAW. Most studies dealt with single pass weld only.

Various types of distortion control techniques were investigated. The pre- and post-weld distortion control methods (except joint design) were primarily applied for simple weld structures. Major in-process distortion controls were realized through fixture/clamping, welding sequence, and welding process selection and heat control.

The influences of the welding sequence on welding distortion were studied under specific application conditions. No universal solution was proposed.

Related researches suggest that the welding distortion could be reduced through the application of high power density welding process such as laser welding. For multi-pass weld joint, large weld bead size was found resulting in less final welding distortion.

The sequentially coupled thermal and structural transient analysis was the mostly employed technique for the finite element simulation of the welding distortions. The simplification of the FEA simulation was found necessary for complex weld structures. The most common simplification techniques include the use of shell model for remote area on the weld plate, block dumping or lumped pass method, and inherent strain theory. Simplified FEA analysis was usually accompanied by lower prediction precise.

Chapter 3 Design of Experiments and FEA Studies

3.1 Introduction

Based on the purposes of the studies on stainless steel nozzle welding distortion the following types of tasks were proposed,

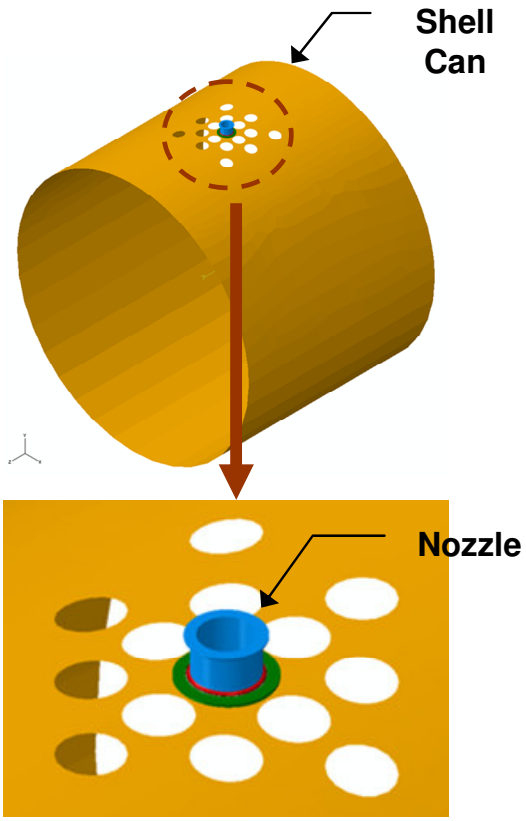

1) Relative comparison of welding technique options or possibilities through FEA analysis, involving fixture designs, welding sequences, weld bead sizes and cooling times
2) Experimental comparison of welding technique options or possibilities, especially those that are difficult to establish relevant FEA models. Areas of focus include welding processes, fixture, welding directions, and weld bead sizes
3) Determination of the level of the actual welding distortion through nozzle weld mockups

In reference to typical pressure vessel applications, it was determined that all experimental mockups and FEA models be designed to represent stainless steel nozzle-to-shell welding with the following dimensions,

- Shell can: 7500mm outside diameter, 31.75mm thickness
- Nozzle: 290mm outside diameter, 25.4mm wall thickness
- Nozzle spacing on shell can: 380mm

3.2 Mockup Designs

Two levels of mockups were designed,

- Single nozzle mockups for comparison between different welding techniques, so that optimal welding procedure could be developed to produce minimum welding distortion
- Multi-nozzle large mockups for determining the level of shell distortion that reflects the effect of constraint conditions and the interaction between the welding of different nozzles.

The shell plate material is SA-240 Type 304L and the nozzle SA-182 Grade F304L.

3.2.1 Single Nozzle Weld Mockups

Stainless steel plates of 900mm x 900mm in dimensions were used for single nozzle weld mockup. The plate was pressed to the shape of the shell can of 7500mm OD (outside diameter), representing a cut-off section of the shell, with one straight edge in parallel to the shell axis. The nozzle axis intersects with the plate at the plate surface center, with the nozzle end at shell ID (inside diameter) side being saddled to flush with the plate.

Three types of single nozzle weld mockups were designed,

1) Nozzle axis normal to the shell plate surface

2) Nozzle intersects with the plate at 45° angle, in which case unbalanced welding distortion would normally happen, causing nozzle angular distortion.

3) Nozzle intersects with the plate at 45° angle, with a carbon steel (A36 material) contour fixture being tightened with four bolts onto the ID side of the shell plate (Figure 3-1). The contour fixture is a 50.8mm thick strongback with surface profile matching the shell can ID surface. This is a very typical fixture for small weldment to restrict the welding distortion. Stainless steel washers were placed in between the shell plate and the contour fixture to prevent contamination from carbon steel. Stainless steel plate strongback could be another option but would be more expensive, and prone to distortion under welding heat.

Most of the single nozzle mockups belong to the last two types, as they represent the worst case scenarios regarding welding distortion.

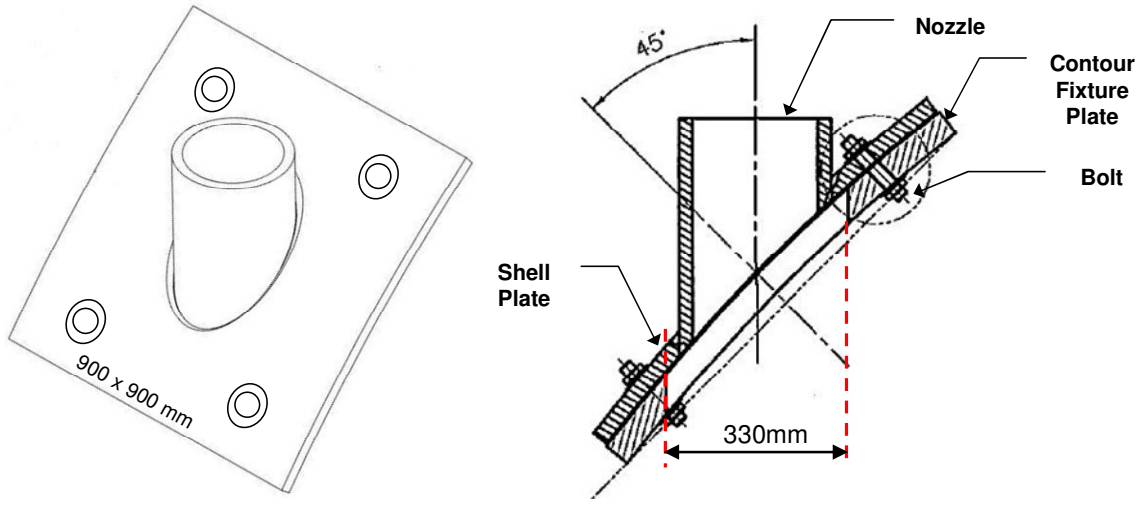

Figure 3-1 Single Nozzle Weld Mockup with Contour Fixture

3.2.2 Multi-nozzle Weld Mockup

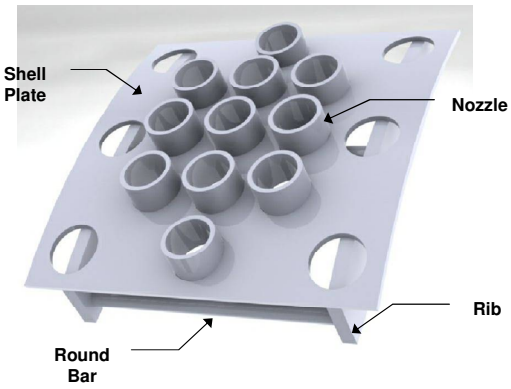

The multi-nozzle weld mockup was built on a 2000mm x 2000mm stainless steel plate that was pressed to the shape of the shell of 7500mm OD, with one edge in parallel to the shell axis. A series of nozzle openings was designed with 11 at the middle to be welded with nozzles. The gap between neighboring nozzles is 90mm, corresponding to a nozzle spacing of 380mm. The nozzle bottom was saddled to flush with the shell ID surface.

The nozzle at the center was with J groove and welded without fixture in order to examine the worst case scenario of welding distortion. The other nozzles were with double bevel groove and welded with a rib-bar fixture attached to the ID side of the shell plate (Figure 3-2). The rib-bar fixture is a typical design for the welding of large pressure vessel assemblies. They were made of A36 carbon steel. The 76.2mm thick rib strongbacks were braced with three pieces of 114.3mm diameter tubes.

3.3 Weld Preparation

The studies of this thesis used three types of weld groove designs,

1) Modified double J groove (Figure 3-3)

   This is a complicated groove design, used for single nozzle welding studies. The groove details were engineered as such that equal cross-section area be maintained all way around the nozzle weld seam, specifically for the cases

where the nozzle is on a shell surface location of such as 45^{o} slope. To achieve this, the bevel angle and the width of the root flat portion of the groove have to be adjusted along with the location of the weld cross-section. The purpose of the special design is to eliminate the chance of unbalanced weld distortion due to the variation in weld seam cross-section area. It can also better facilitate the potential automation of the welding process. Figure 3-3 shows the groove design data when the nozzle is normal to the shell plate.

Besides, the unique concept of locating the machined portions of the groove on both the shell plate and the nozzle has greatly simplified the machining process. Otherwise a complex 5 axes CNC machine would be required in order to machine the shell ID side of the prep.

2) Modified double bevel groove (Figure 3-4)

This groove design was primarily used for multi-nozzle welding studies, with intention of reducing the development cost. For the same reason for the modified double J groove, the shell ID side of the prep was machined on the nozzle bottom end, while shell ID side on the shell plate.

3) J groove (Figure 3-5)

J groove was used for the welding of the center nozzle in the multi-nozzle weld mockup.

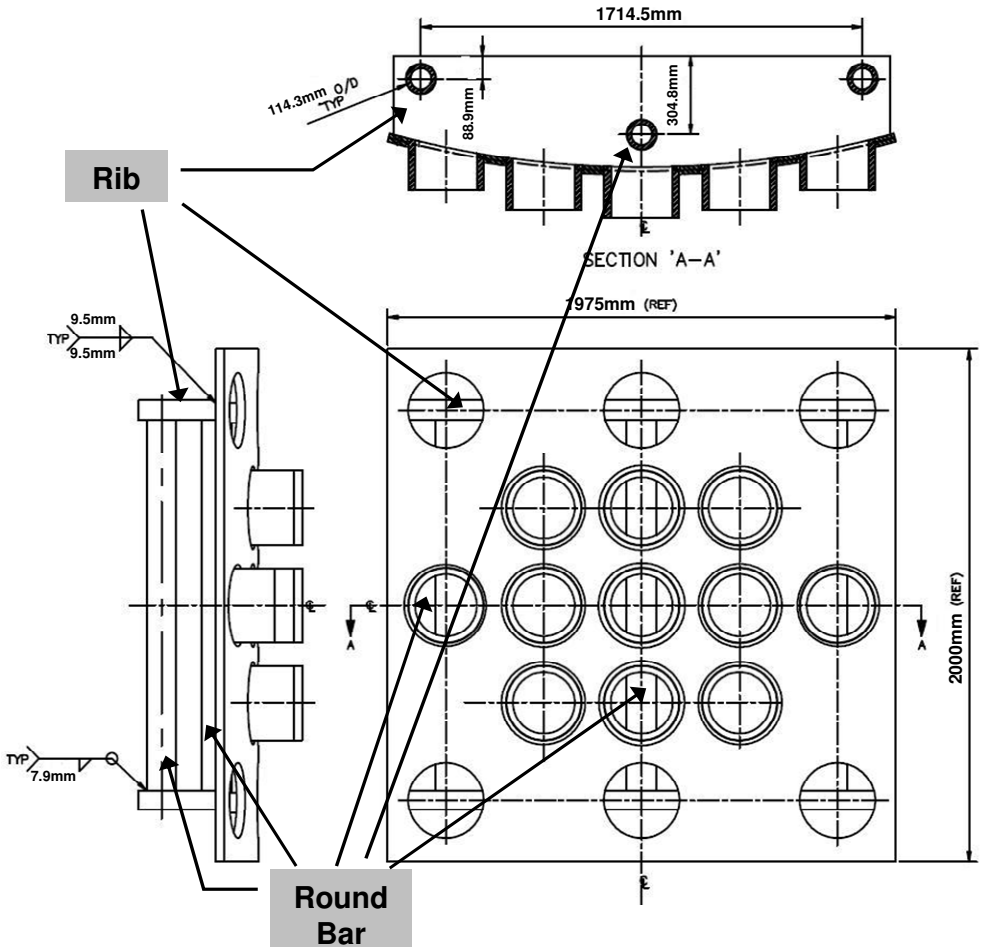

Figure 3-2 Multi-nozzle Weld Mockup with Rib-Bar Fixture

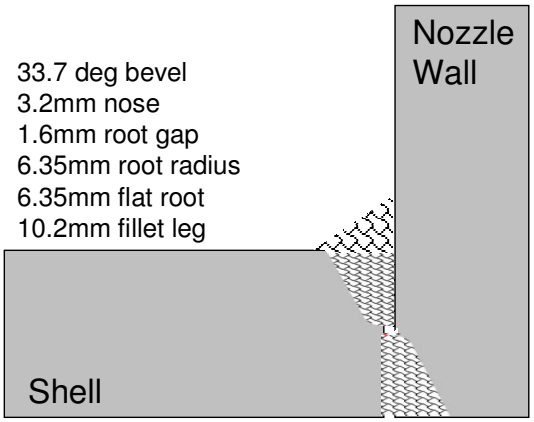

Figure 3-3 Modified Double J Groove When Nozzle Normal to Shell Plate

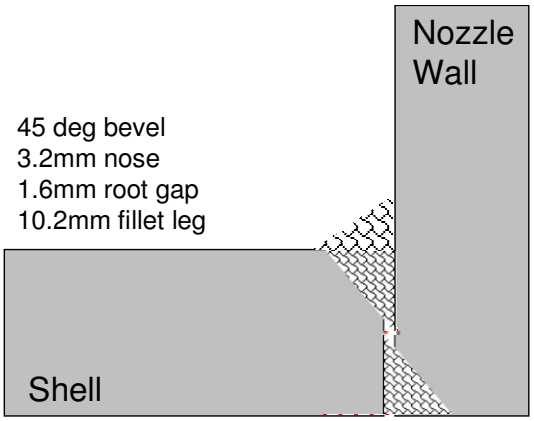

Figure 3-4 Modified Double Bevel Weld Groove Design

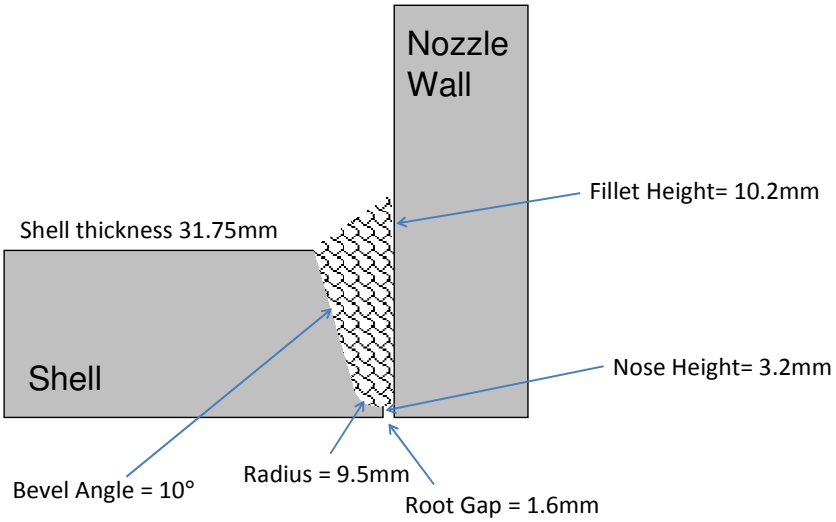

Figure 3-5 J Type Weld Groove Design

3.4 Experimental Procedure

Manual GTAW and SMAW are the most commonly used welding processes for nozzle-to-shell weld seams, therefore were selected for the studies of this thesis. However, as it is known, the heat input and the welding thermal cycle by these processes are hard to keep consistent. It was expected that, because of the size of the nozzle weld in the study which requires dozens of weld passes, the impact of the variation in heat input etc could be statistically balanced out. This would be of even less concern for multi-

nozzle weld mockup. For the selected comparative studies of this thesis the impact would also be minor.

The following was the general procedure of mockup tests,

a) Shell plate forming and cut
b) Cut of shell openings for nozzle welds
c) Weld prep machining
d) Attaching / welding fixture to workpiece and pre-weld measurement of shell plate surface profile. For single nozzle mockup with fixture, the measurement was performed before attaching the fixture. For multi-nozzle mockup with fixture, the measurement was conducted after the fixture had been welded onto the shell plate.
e) Welding
f) Post-weld measurement of shell plate surface profile and shell plate distortion analysis. For single nozzle mockup with fixture, the measurement was performed after the removal of the fixture. For multi-nozzle mockup with fixture, the measurement was conducted with the fixture staying on the shell plate.

3.4.1 Single Nozzle Welding Procedure

The welding procedure for specific mockup varies from case to case. The procedure details will be given under corresponding sections of the thesis. One common requirement applied across all cases is on the interpass temperature, 176.7^{o}C max.

3.4.2 Multi-Nozzle Welding Procedure

Welding Sequence

Figure 3-6 shows the nozzle welding sequence of the multi-nozzle weld mockup. Nozzle #1 (with J groove) was welded from the shell OD side. The welding of nozzles #2~#11 (with double bevel groove) was started from the shell OD side, and the shell ID side was welded after the OD side of all nozzles had been completed.

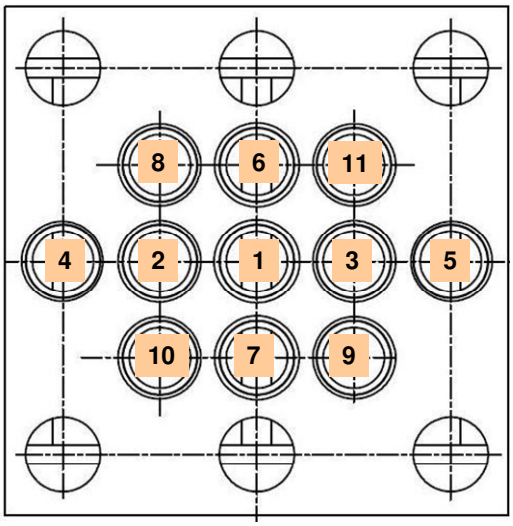

Figure 3-6 Multi-nozzle Mockup Nozzle Welding Sequence

Welding Procedure

- No preheat, interpass temperature 177°C max
- Welding parameters recorded from the mockup tests are listed in Table 3-1

Table 3-1 Multi-nozzle Mockup Welding Parameters

Weld Pass	Process	Electrode	Electrode Size (mm)	Current (A)	Voltage (V)	Speed (cm/min)
Nozzle #1 Welding						
All	GTAW	ER308L	2.4	170	19~22	7.5~10
Nozzle #2~#11 Welding						
Root	GTAW	ER308L	2.4	130~150	12~16	2.5~5
Others	SMAW	E308L	3.2	115~135	21~25	10~30
Others	SMAW	E308L	4	140~160	25~30	25~35

3.5 Measurement of Welding Distortion

3.5.1 Measurement of Single Nozzle Weld Mockup

The reference coordinate system for single nozzle mockup distortion measurement is shown in Figure 3-7. Measurements were taken before and after welding,

- On shell OD side of the mockup plate surface along EF and OA, to obtain the distortion data
- On nozzle top surface, combined with the measured plate surface data, for determining the nozzle angular distortion in YZ plane. See Figure 3-7 for the definition of nozzle angle in reference to the shell plate.

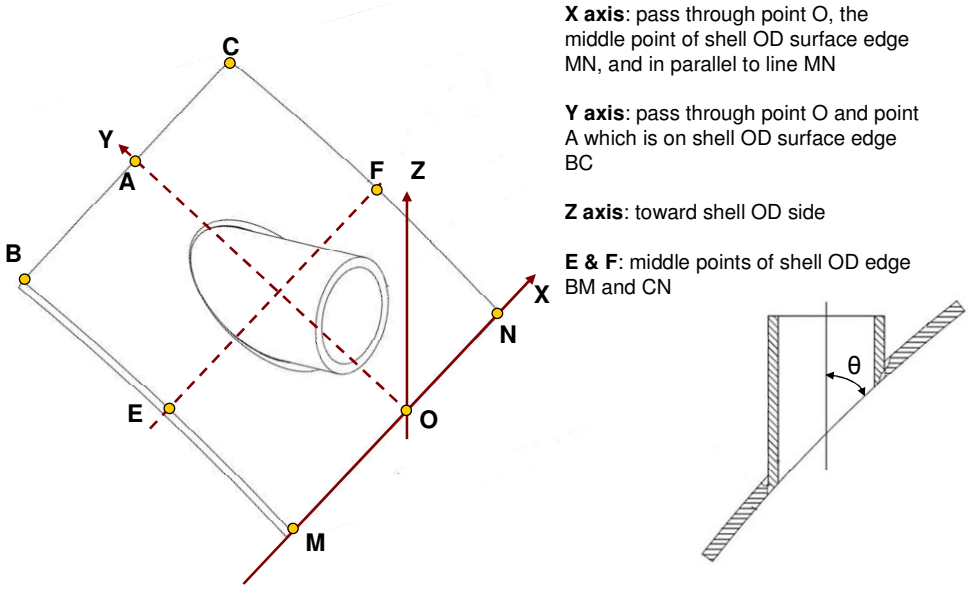

Figure 3-7 Coordinate System for Measurement of Single Nozzle Mockup Profile

The measurement was conducted with high precision portable CMM device FARO-ARM Platinum (Figure 3-8) manufactured by FARO Technologies, Inc. Punch marks were created on the shell plate surface at locations to be measured, so that the pre-

weld and post-weld measurements could be taken from the same points and the distortion values be calculated afterwards.

Figure 3-8 Single Nozzle Weld Distortion Measurement with FARO-ARM Platinum

3.5.2 Measurement of Multi-nozzle Weld Mockup

The reference coordinate system for multi-nozzle mockup distortion measurement is shown in Figure 3-9.

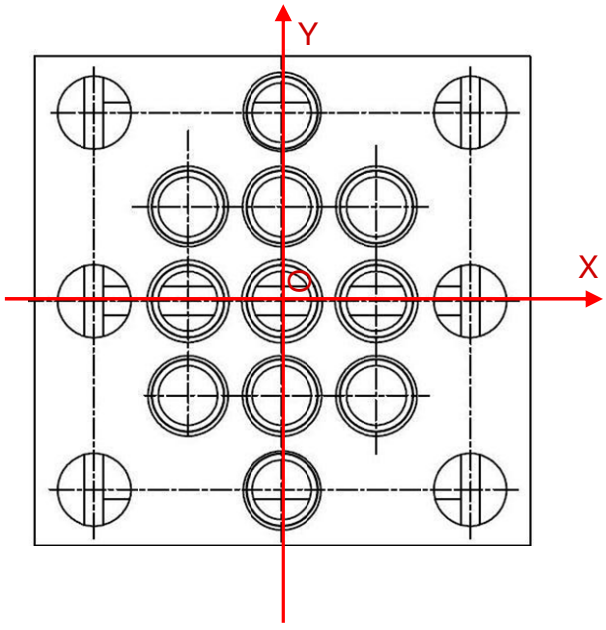

Figure 3-9 Coordinate System for Measurement of Multi-nozzle Mockup Profile

The shell plate distortion after the welding of the center nozzle (nozzle #1) was measured with high precision portable CMM device FARO-ARM Platinum. Punch marks were created on the shell plate surface at locations to be measured, so that the pre-weld and post-weld measurements could be taken from the same points and the distortion values be calculated afterwards.

The shell plate surface profiles before and after the welding of nozzle #2~#11 were obtained using laser scan device Handyscan 3D^{TM} EXAscan (Figure 3-10). A 3D model of the shell plate was established based on the laser scan data. The welding distortion information was then extracted by comparing the shell plate 3D models obtained before and after welding. This was performed automatically with the inspection software for the laser scan device. The four corners of the shell plate were used as reference points for aligning the pre- and post-weld measurement data.

Figure 3-10 3D Laser Scan of Multi-nozzle Mockup Plate

3.6 Analysis of Welding Distortion

The nozzle-to-shell welding distortion was evaluated using the following indicators,

1) **Max Z Distortion**: **c = b –a**

   Refer to Figure 3-11 for the definitions of a, b and c

2) **RMS** (Root Mean Square) **Z Distortion**: $\sqrt{\frac{(\Delta Z_0)^2 + (\Delta Z_1)^2 + ... + (\Delta Z_n)^2}{n}}$

   Refer to Figure 3-12 for the meanings of the symbols in the formula above

3) **X Direction Shrinkage** and **Y Direction Shrinkage** (Figure 3-13)

4) **Nozzle Angle Change**

   Refer to Figure 3-7 for the definition of nozzle angle

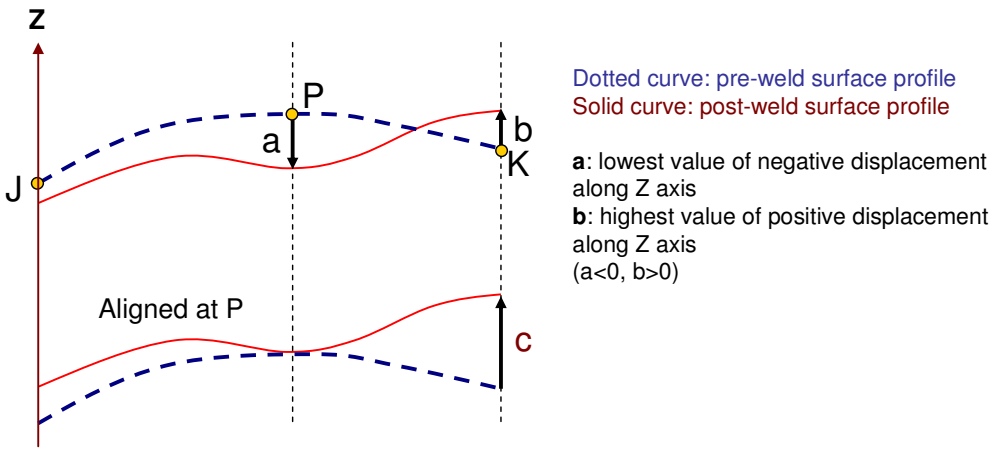

Figure 3-11 Sketch for Definition of Max Z Distortion

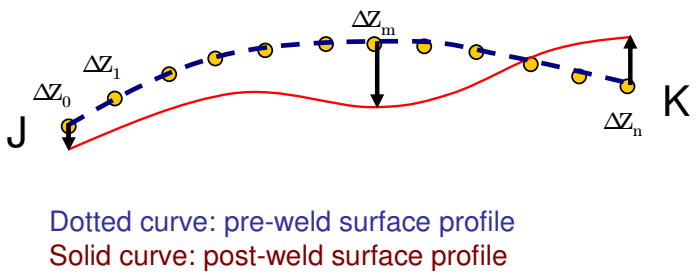

Figure 3-12 Sketch for Definition of RMS Z Distortion

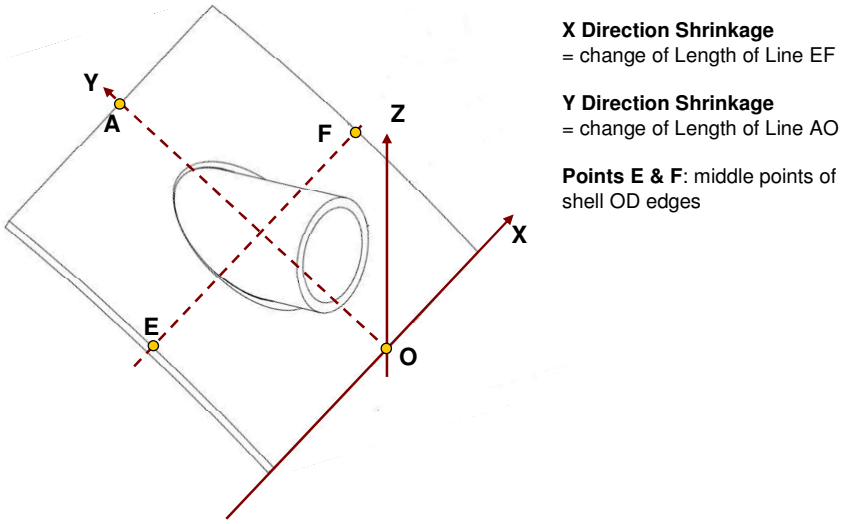

Figure 3-13 Definition of Plate Shrinkages in Single Nozzle Weld Mockup

3.7 Design of FEA Studies

3.7.1 Types of FEA Models

The shell plates and the nozzles in FEA studies were designed to the same dimensions as that in experimental mockups. Two groups of FEA models were developed.

FEA Model Group A – single nozzle on small shell plate

The nozzle with 45° nozzle angle is welded to a 900mm x 900mm plate. This type of FEA models was used for investigations on the effects of fixture, weld pass deposit sequence, weld bead size, and cooling time. Most of them were configured with a contour fixture, as shown in Figure 3-13. This is a modified version of the contour fixture used in mockups, consisting of a 50.8mm thick 900mm x 700mm carbon steel plate and a 3.175mm thick stainless steel washer in between the stainless steel shell and the carbon steel fixture plate. The three components are tied together at interfaces.

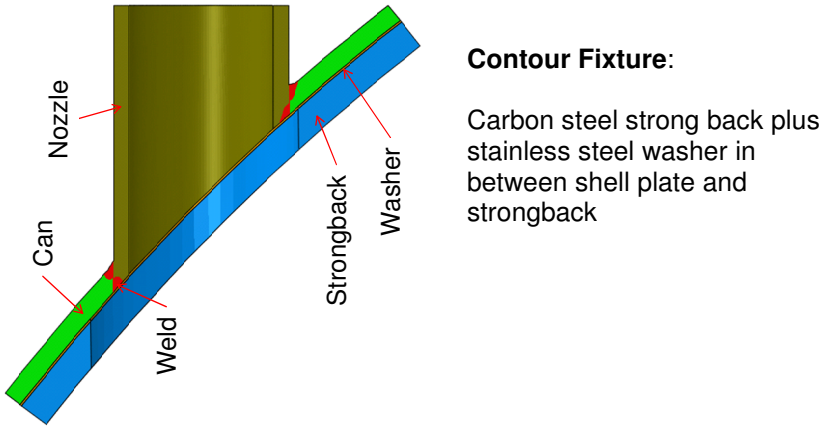

Figure 3-14 Single Nozzle FEA Model with Contour Fixture

<u>FEA Model Group B</u> – multi-nozzle on large shell plate

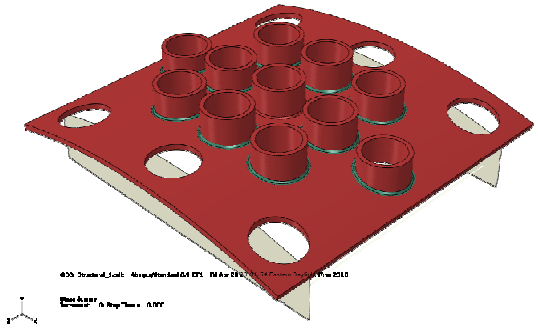

The nozzles are welded onto a 2000mm x 2000mm shell plate for studies on the effects of different fixture designs, nozzle sequences, and weld pass deposit sequences. The fixture designs involved under this FEA model category will be described in detail in Chapter 4.

3.7.2 FEA Simulation Techniques

Software package ABAQUS was employed for the FEA studies, using nonlinear sequentially coupled thermal-structural transient analysis method [6,8]. Lumped weld pass method, a type of block dumping techniques [7], was used to model the deposition of filler metal and the welding thermal cycle. The use of lump pass has made the FEA tool efficient enough for its application to the simulation of the nozzle-to-shell welding process, especially for multi-nozzle welding. In the thermal transient analysis, a time-varying heat flux was applied to each pass to melt the filler metal and some base metal. It was followed by cooling for certain time before the next pass starts. Then the nonlinear elastic-plastic structural analysis was performed using the temperature field calculated in the thermal transient analysis.

Techniques for FEA Model Group A

Based on the symmetric characteristics of the model structure, only half of the model was used for FEA calculation, as shown in Figure 3-14. It is a 3D model with fine elements at and around the weld seam and coarse elements at the far ends of the nozzle and the plate. During the simulation process, each weld pass was dumped into the weld groove as a whole pass, i.e. lump pass.

Techniques for FEA Model Group B

This group of FEA models involve 7~11 nozzles with a shell plate much larger than those in the model group A. They are 3D models with up to 266,000 elements after meshing. The shell, nozzles and filler metal are modeled with solid elements, and the ribs and bars with shell and beam elements. For simplification, all the weld passes on shell OD side are lumped into one pass and all the ID passes are lumped into another pass.

With the combined lump pass approach, a complete run of the group B models took between 32 to 67 hours with 8 CPUs.

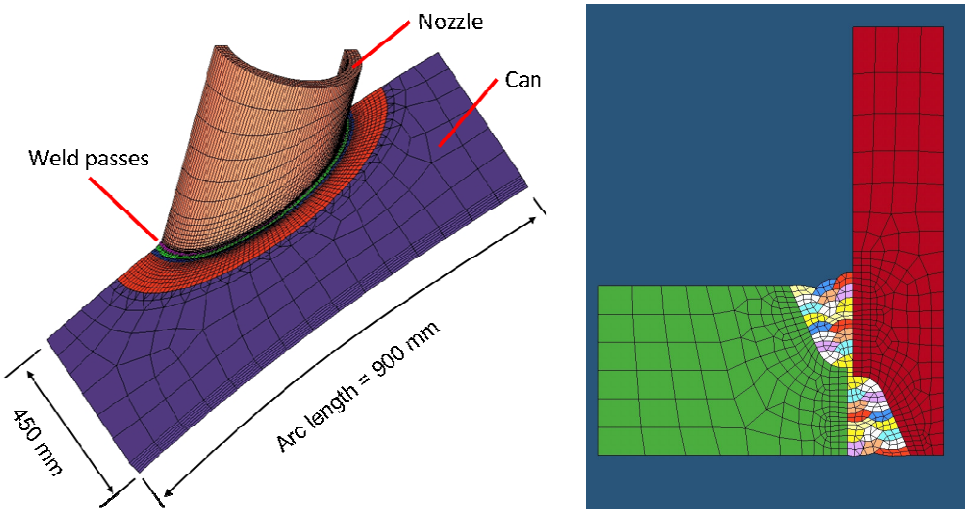

Figure 3-15 Single Nozzle FEA Model Simplification and Meshing

3.7.3 FEA Distortion Analysis

The nozzle welding distortion results from the FEA prediction were represented in reference to coordinate systems similar to those for nozzle welding mockups (Figures 3-7, 3-9), so that the comparison between mockup and FEA results be possible. Apart from the colored distortion plots for visual comparison, the Max Z Distortion defined earlier was also calculated based on the predicted distortion data, as an indicator of the overall distortion for each FEA model.

Chapter 4 Effect of Fixtures on Nozzle Welding Distortion

Fixtures are the most common solution for welding distortion control [4,6]. The FEA method has provided an excellent tool for comparing the effectiveness of different welding fixture designs. The studies in this chapter consist of FEA analyses of the distortions caused by single and multi-nozzle welding with different types of fixtures. A single nozzle weld mockup was made to check the actual distortion amount and to evaluate the results from FEA studies.

4.1 Single Nozzle Weld Mockup with Contour Fixture

The mockup with contour fixture was tested against a mockup without fixture.

- **Welding conditions**: nozzle angle 45^{o}, modified double J groove, SMAW process, shell ID side was welded first, uphill welding direction
- **Welding parameters**: see Table 4-1

Figure 4-1 Completed Single Nozzle Weld Mockup Welded with Contour Fixture

The mockup was measured

- After tacking the nozzle but before attaching the fixture and welding
- After welding, cooling down, then taking off the fixture

The measured mockup plate surface profiles are shown in Figures 4-2 and 4-3. Welding distortions were summarized in Table 4-2, which indicates that the distortion with contour fixture was only about 60% of the distortion when without fixture. The angular distortion was reduced to 35% of the level when without fixture. The ratio of Y Direction Shrinkage was not calculated because the difference between the two mockup cases is very minor.

Table 4-1 Welding Parameters for Mockup Study on Fixture

Condition	# of Weld Passes	Heat Input (kJ/cm)	Travel Speed (cm/min)	Estimated Total Heat Input (Mega J)
No fixture	26	19.7	8.4	57.2
With contour fixture	28	15.7	10.2	49.3

Table 4-2 Single Nozzle Weld Distortion from Mockup Study on Fixture

	MAX Z Distortion (mm)	RMS Z Distortion (mm)	X Direction Shrinkage (mm)	Y Direction Shrinkage (mm)	Nozzle Angle Change (deg)
No fixture	11.53	3.78	3.20	0.28	3.4
With contour fixture	6.99	2.01	2.16	0.36	1.2
Distortion Ratio (With / without fixture)	61%	53%	67%	-	35%

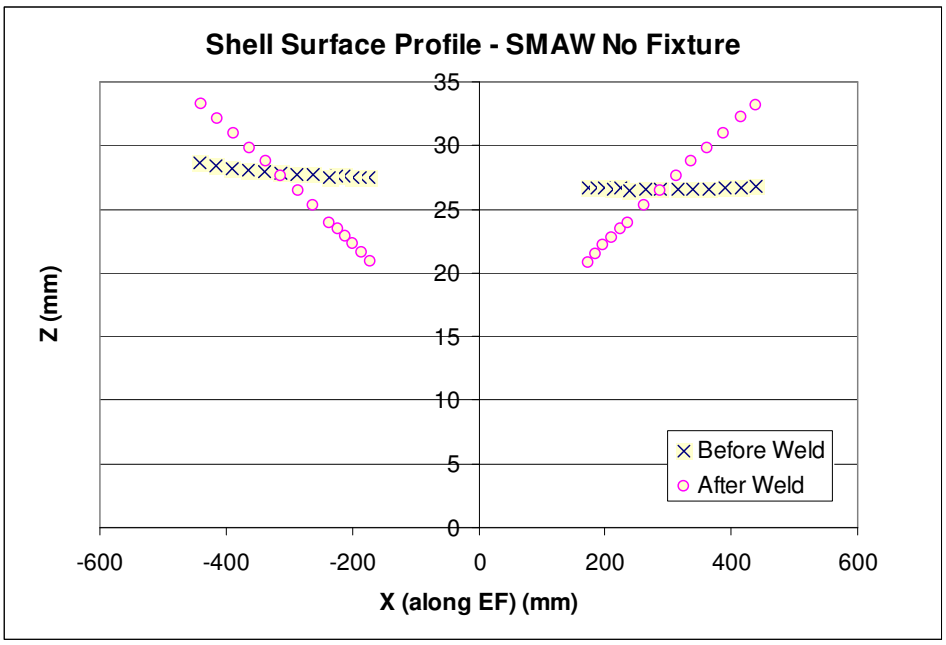

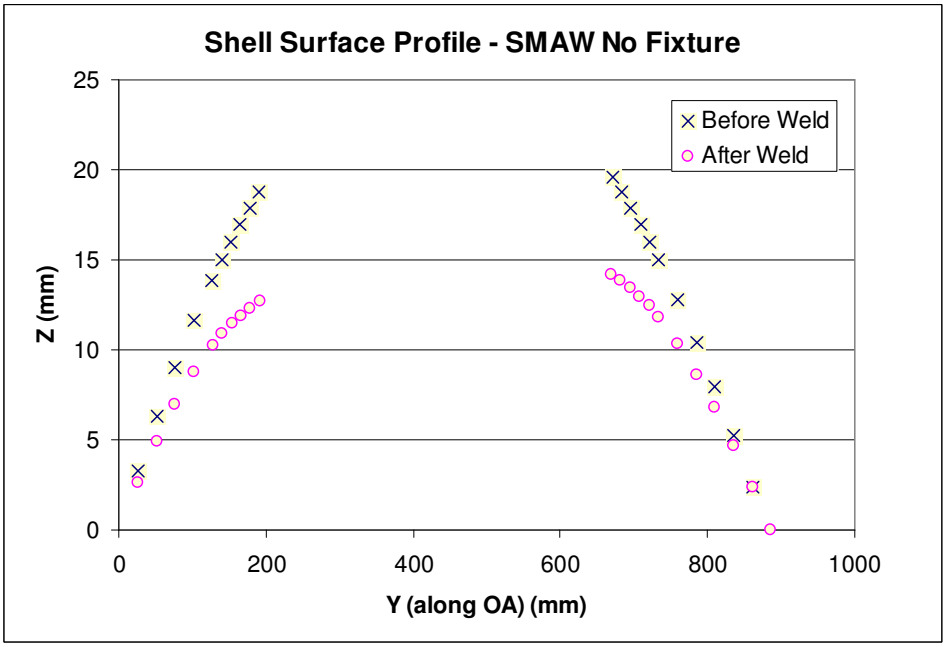

Figure 4-2 Single Nozzle Weld Mockup Distortion – No Fixture

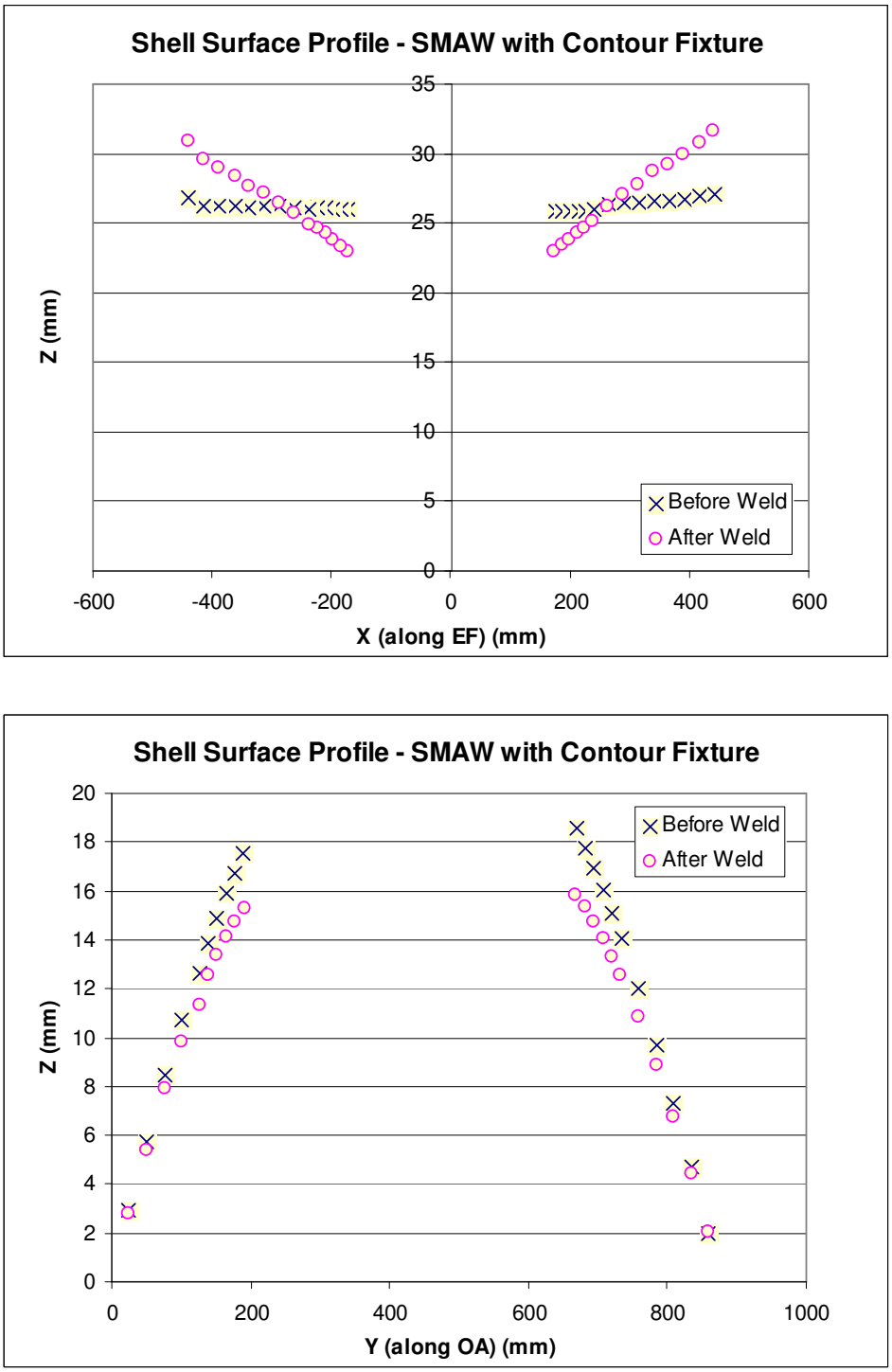

Figure 4-3 Single Nozzle Weld Mockup Distortion – Contour Fixture

4.2 Simulation of Single Nozzle Welding with Contour Fixture

The FEA model with modified contour fixture (Figure 3-13) was compared against a model without fixture.

- **Welding conditions**: nozzle angle 45^{o}, modified double J groove, shell ID side welded first
- **Welding parameters**: 36 weld passes. The FEA heat flux was worked out to match the heat input of 13.8 KJ/cm and weld travel speed of 7.6 cm/min. The total heat input is about 55 Mega J.

The predicted shell plate distortions (after removal of fixture for the case with contour fixture) are shown in Figures 4-4 and 4-5. A comparison of the distortions of the two FEA cases is presented in Table 4-3, which shows that the Max Z Distortion with contour fixture will be about 58% of the distortion when without fixture, very close to the ratio of 61% obtained from the mockup tests in Section 4.1. This would indicate that the modified contour fixture in the FEA model be effective for the simulation of the contour fixture used in the mockup. The absolute levels of the predicted Max Z Distortion appear to agree very well with the mockup results (Table 4-2), confirming the validity of the FEA approach.

Table 4-3 Single Nozzle Weld Distortion from FEA Study on Fixture

Condition	Displacement Min (mm)	Displacement Max (mm)	Max Z Distortion (mm)	Distortion Ratio
No fixture	-3.585	5.974	9.559	
With contour fixture	-2.265	3.242	5.507	58%

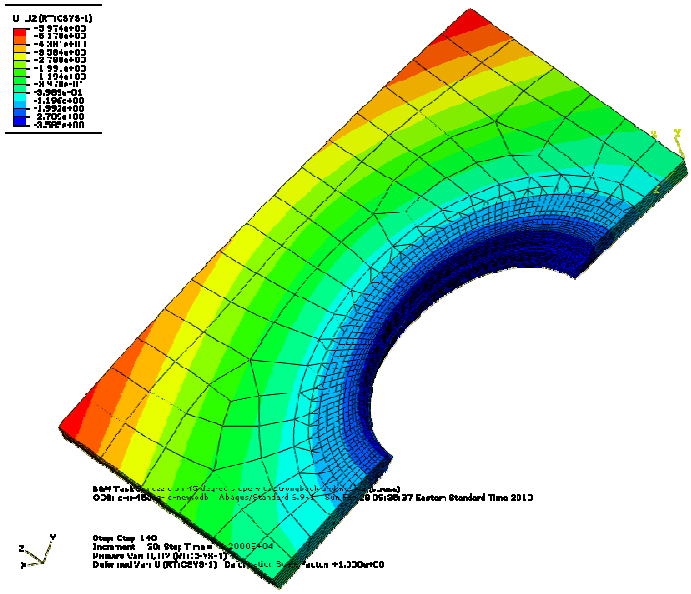

Figure 4-4 Predicted Single Nozzle Weld Distortion – No Fixture

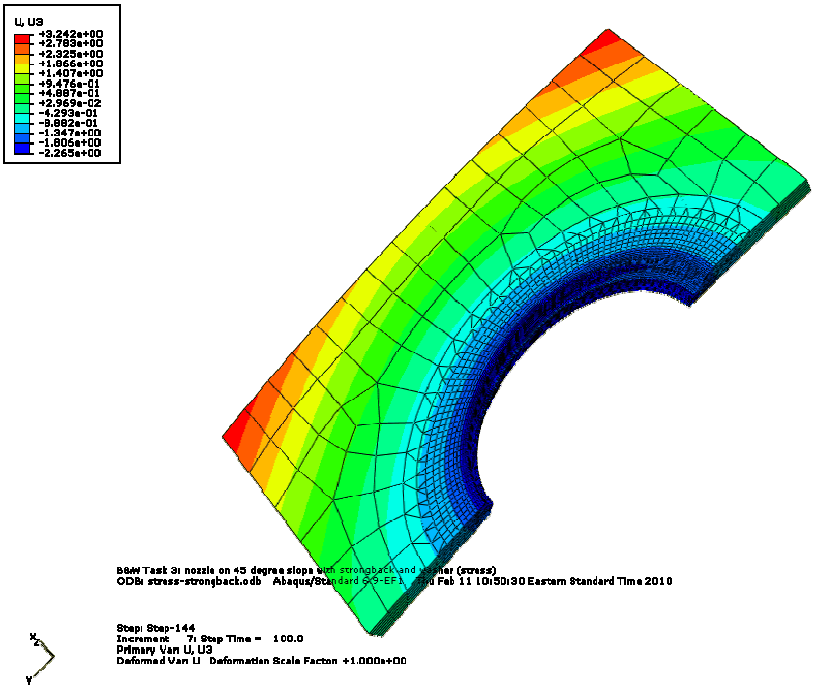

Figure 4-5 Predicted Single Nozzle Weld Distortion – Contour Fixture

4.3 Simulation of Multi-Nozzle Welding with Different Fixtures

A common practice for preventing welding distortion of a pressure vessel shell can is to install a supporting ring toward the inside surface of the shell can. An equivalent fixture design, rib-bar fixture (Figure 4-6), was developed for the multi-nozzle weld mockup and evaluated here with FEA method against other fixture designs proposed in this thesis.

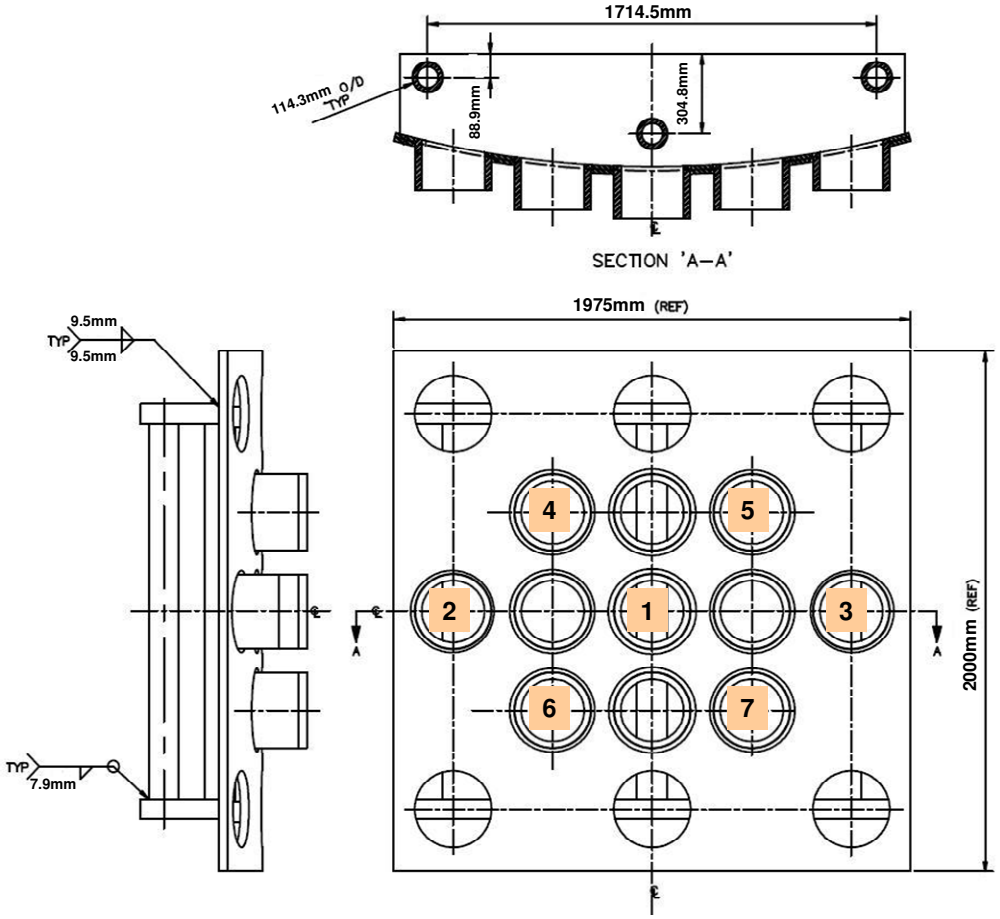

Figure 4-6 Multi-nozzle Weld Sequence with Rib-Bar Fixture – FEA Study

4.3.1 Fixture Design Types

Three fixture designs were studied,

1) **Rib-bar fixture** (Figure 4-6)
2) **Contour fixture with full surface contact** (Figure 4-7), representing a tight fit between the fixture and the shell plate. The 50.8mm thick carbon steel contour fixture is attached under the ID surface of the shell plate, with openings at the locations of nozzle #1~#7 in Figure 4-6. A 3.2mm thick stainless steel shim is placed between the contour plate and the shell plate. The purpose of the stainless steel shim is to prevent chemical contamination from the carbon steel.
3) **Contour fixture with ring shape partial surface contact** (Figure 4-8), representing a less tight fit between the fixture and the shell plate by using bolts. Stainless steel washers of 296.4mm ID, 347.2mm OD and 3.175mm thickness are placed around the nozzle openings in between the carbon steel contour plate and the shell plate. The complete FEA model is shown on the right in Figure 4-8. On the left, the shell is removed to reveal the circular washer rings.

All the FEA multi-nozzle weld models use double bevel weld groove design, with the shell OD side of the groove being welded first.

The apparent benefits of contour-type fixture design include:

- Possibility of reducing / eliminating welding between the fixture and the shell, avoiding thermal impact on the shell plate (distortion, residual stress, concern of chemical contamination)

- More space on shell ID side for welding operation access
- Higher possibility for using automatic welding equipments because of the improved clearance inside the shell can
- Flexibility in fixture setup (the same fixture curvature, applicable anywhere on shell ID) and possibly less setup time for welding operation

The influence of the contour-type fixture on the shell distortion in multi-nozzle welding was studied and the analysis results were summarized in the following section.

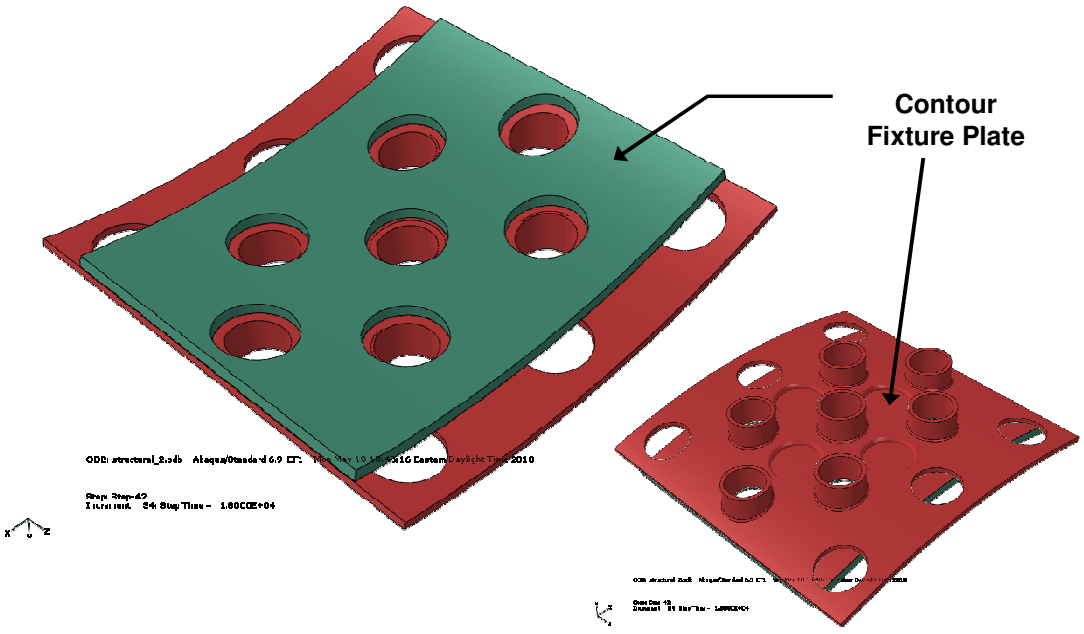

Figure 4-7 Multi-nozzle FEA Model with Full Contact Contour Fixture

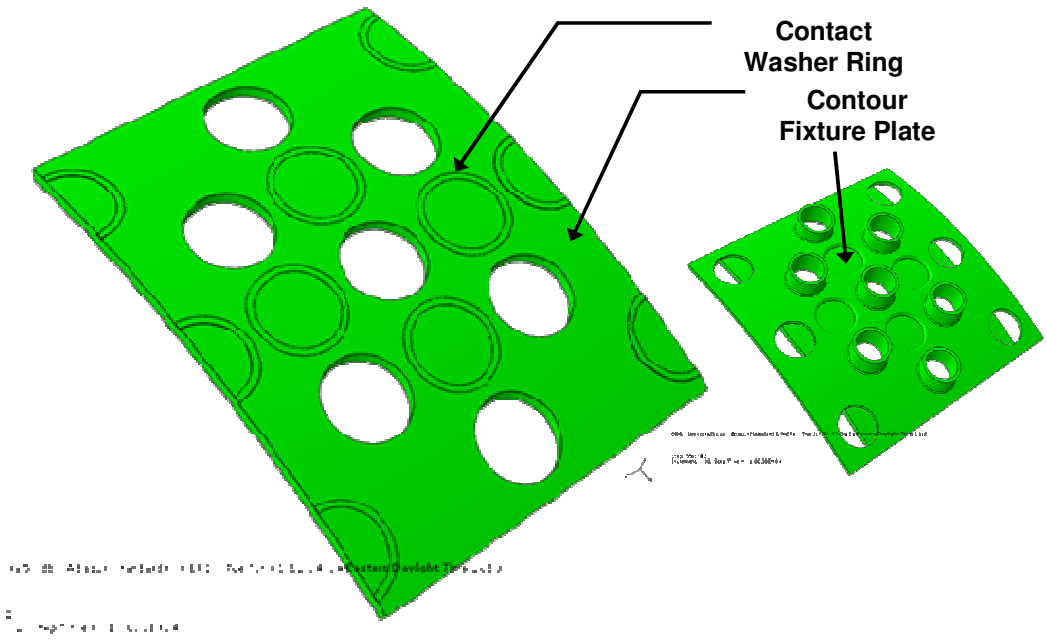

Figure 4-8 Multi-nozzle FEA Model with Ring Contact Contour Fixture

4.3.2 Effect of Fixture Design on Welding Distortion

The predicted welding distortions from different fixture designs are shown in Figures 4-9, 4-10 and 4-11. A comparison of the distortion data is listed in Table 4-4.

Table 4-4 Multi-nozzle Weld Distortion from FEA Study on Fixtures

	With Fixture				After Fixture Removal			
	Displacement Min (mm)	Displacement Max (mm)	Max Z Distortion (mm)	Distortion Ratio	Displacement Min (mm)	Displacement Max (mm)	Max Z Distortion (mm)	Distortion Ratio
Rib-bar fixture	-16.4	1.7	18.1		-16.1	12.5	28.6	
Contour fixture with complete surface contact	-13.6	0.2	13.8	**76%**	-15.4	0.3	15.7	**55%**
Contour fixture with ring-style surface contact	-22.1	0.1	22.2	**123%**	-12.7	3.2	15.9	**56%**

General distortion characteristics

In comparison to the rib-bar fixture design, an outstanding characteristic of the distortions with contour fixtures is that the distortion distribution is localized (Figures 4-10 & 4-11), especially before the removal of the fixtures. In other words, the contour

fixture design appears able to restrict the welding distortion to local area. This would be beneficial for the distortion control of large weld structures.

Distortions before taking off the fixtures

The least distortion was produced with full contact contour fixture, about 76% of the distortion in welding with the rib-bar fixture. However, the model with ring contact contour fixture did show a higher level of distortion than the model with rib-bar fixture. This is because the ring style connection was provided by a 3.175mm thick, 25.4mm wide stainless steel washer, which may not be strong enough. Nevertheless, unlike rib-bar fixture, the distortion with ring contact contour fixture has been well kept locally around the welded nozzles (Figure 4-11), suggesting less concern of the impact of the distortion on remote areas. By reinforcing the connection strength between the fixture and the shell, the magnitude of the distortion would be reduced and the distortion distribution would be compressed further toward the center, leaving less impact on remote areas.

Distortions after taking off the fixtures

The most apparent phenomenon as suggested by the FEA results in Table 4-4 is that both the models with contour fixture ended up with much less distortion than the model with rib-bar fixture. In other words, after the removal of the fixture, both cases are much better than the rib-bar fixture design for distortion control.

Regarding the distortion distribution, the stronger the connection between the contour fixture and the shell, the more localized the distortion (compare Figures 4-10 & 4-11). On contrary, the application of rib-bar fixture has developed a skewed distribution (Figure 4-9), with high levels (in positive and negative directions) away from the welded nozzles, suggesting distortion impact on remote areas.

Distortion change when taking off the fixture

Table 4-4 shows that there was a big distortion jump after taking off the rib-bar fixture, indicating the release of a high magnitude of welding residual stress. From the production distortion control point of view, it would mean that the rib-bar fixture should be kept in place until the assembly of the nozzle-to-shell weld subassemblies has been completed. However, for contour fixture with complete surface contact, the distortion increase was very small, suggesting that the fixture could be taken off before the final assembly of the nozzle-to-shell weld subassemblies. More interesting is that, after the removal of the contour fixture with ring-style surface contact, the distortion even showed a large decrease. In other words, the fixture should be removed before the final assembly of the nozzle-to-shell weld subassemblies. This type of findings is very valuable for proper scheduling of the manufacturing process in order to achieve low welding distortion, effective and efficient fixture tooling, and high productivity.

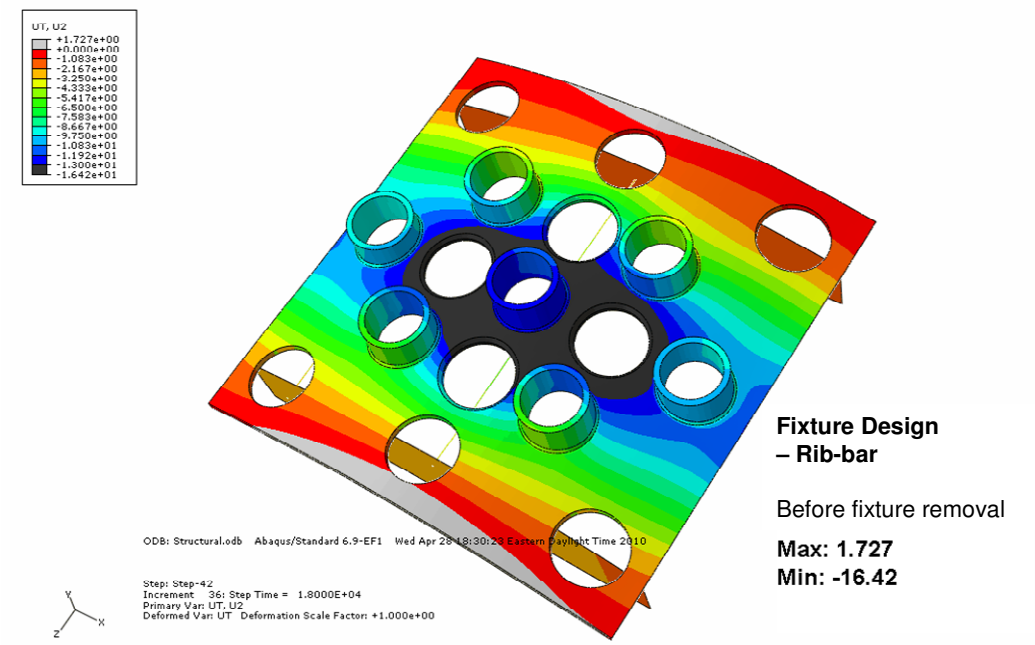

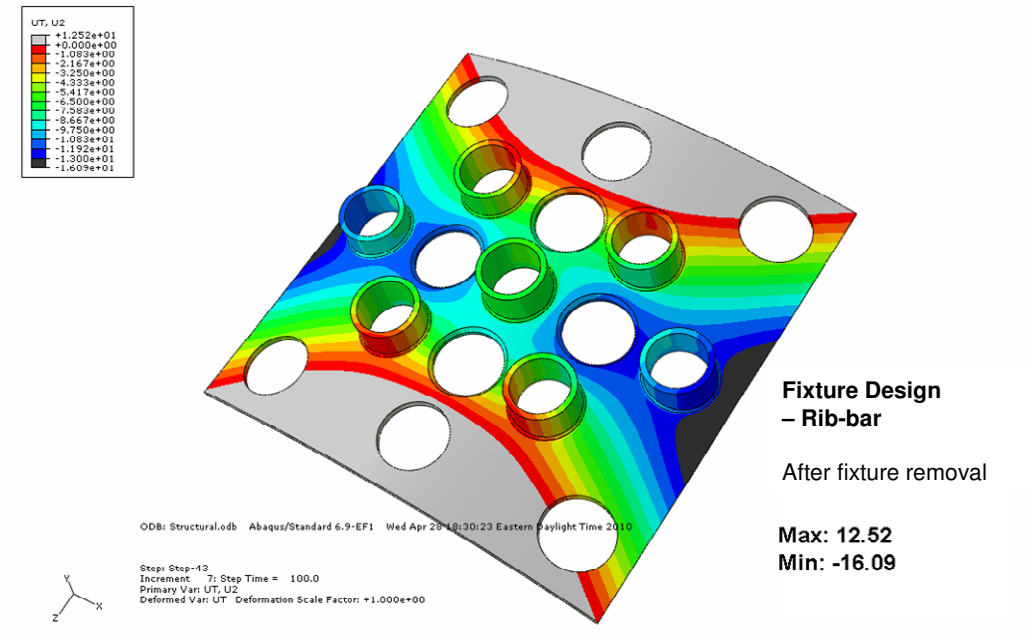

Figure 4-9 Predicted Multi-nozzle Weld Distortion – Rib-Bar Fixture

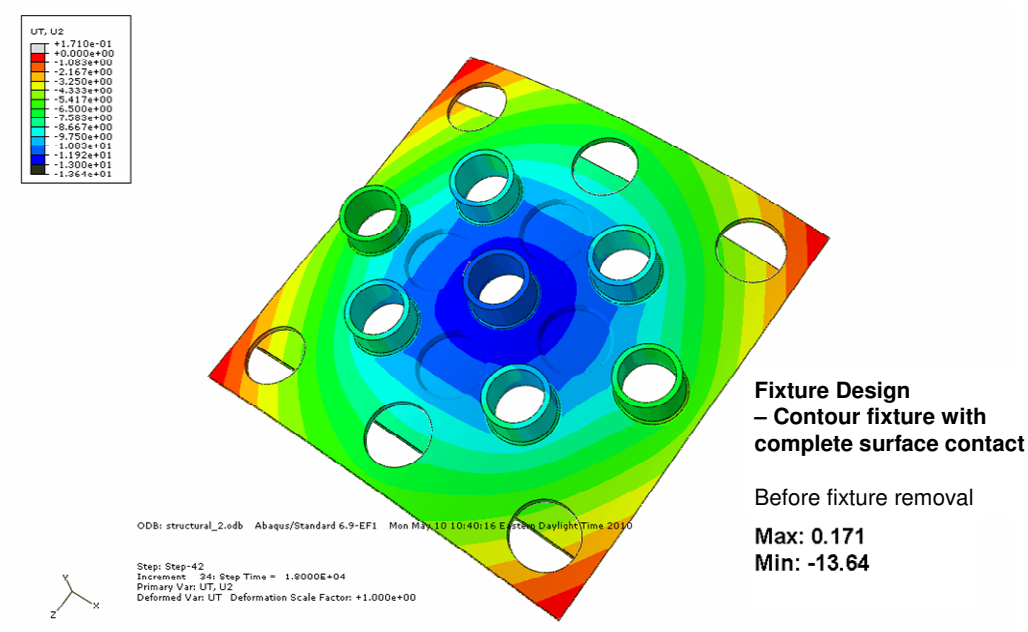

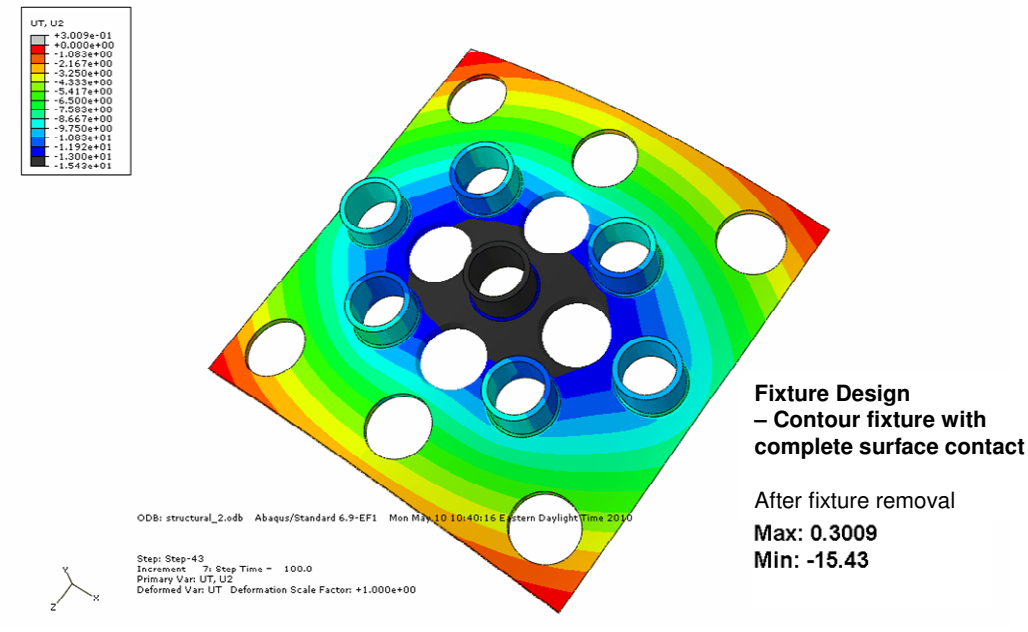

Figure 4-10 Predicted Multi-nozzle Weld Distortion – Full Contact Contour Fixture

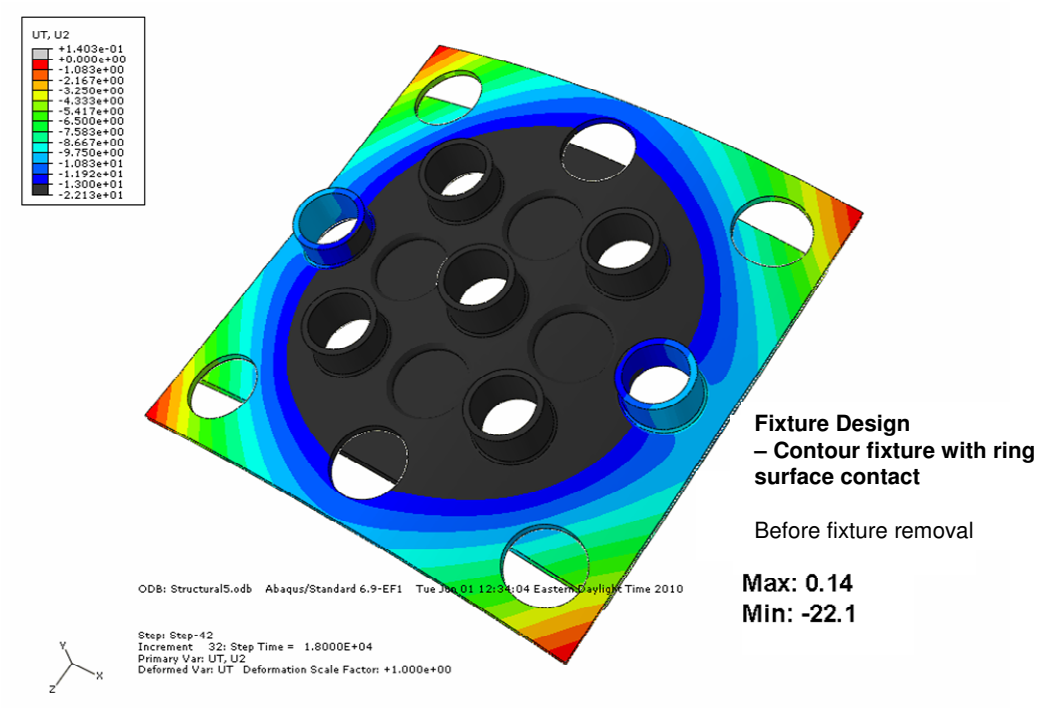

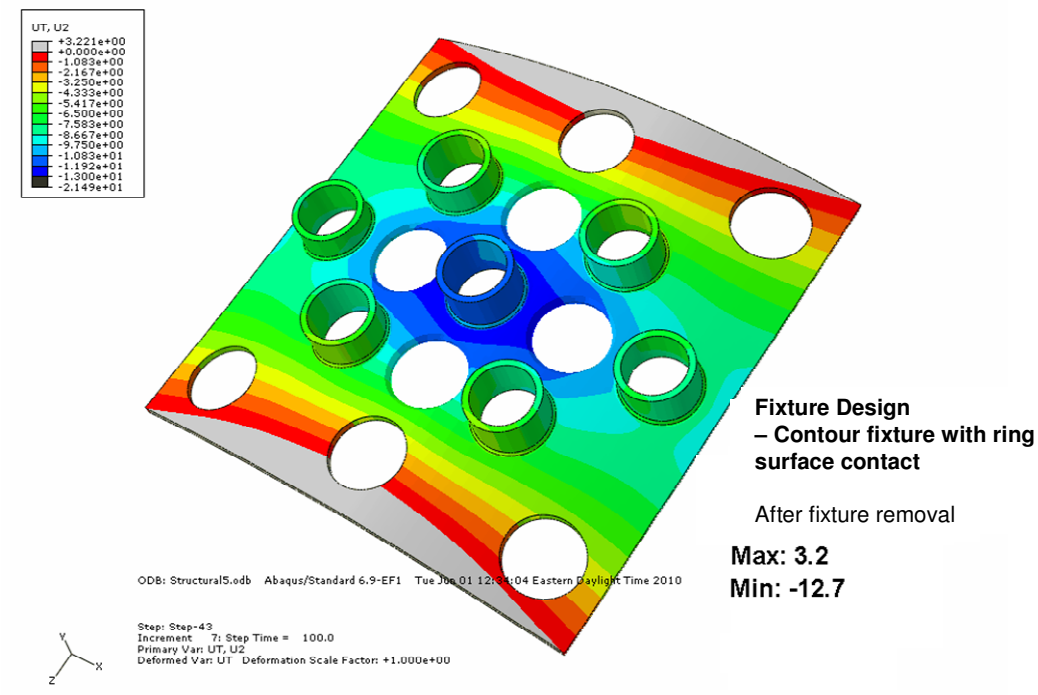

Figure 4-11 Predicted Multi-nozzle Weld Distortion – Ring Contact Contour Fixture

4.4 Summary

The influence of fixtures on the welding distortion of stainless steel nozzle-to-shell-can weld assemblies was investigated through finite element analyses and mockup tests, involving the welding of single and multiple nozzles.

Both the FEA simulations and .the mockup tests of single nozzle welding, with similar total heat input, revealed that the level of the welding distortions with contour fixtures was about 60% of the level of the distortions without fixture under the given structure and welding conditions. The agreement between the FEA and the mockup results appears to confirm that the modified contour fixture employed in the FEA simulation is an effective representation of the contour fixture used in the mockup test. The comparison of the absolute values of the welding distortion confirmed also that the FEA methods were able to give fairly precise prediction of the welding distortion.

The FEA simulations of multi-nozzle welding with different fixture designs indicated that the welding distortions with contour fixtures were more localized than the distortion with rib-bar fixture. After the removal of the fixtures, the distortions associated with contour fixtures were less than the distortion with rib-bar fixture. However, when the shell plate was not tied tightly with the contour fixture (ring-style surface contact), the distortion before the removal of the contour fixture was found higher than the distortion with rib-bar fixture. The stronger the link between the shell plate and the contour fixture, the less the distortion before the removal of the fixture.

The fixture removal schedule shall be evaluated on a case by case basis in order to achieve minimum final welding distortion. Under the given structure and welding conditions in this chapter, the rib-bar fixture has to be kept in place until the completion

of the final nozzle-to-shell weld assembly, while the contour fixtures appeared better to be removed right after the completion of a nozzle weld subassembly.

Chapter 5 Effect of Welding Sequence and Direction on Nozzle Welding Distortion

Welding distortion control through proper design of the welding sequence has been proved to be effective in the fabrication of sheet metal structures, primarily for carbon or mild steels [1,6,7,18,20,53,61~63]. However, it is still an under-developed area for stainless steel complex structures. The studies in this aspect were carried out mainly using FEA method, except the experimental mockup for study on the impact of the welding direction when the weldment is in out-of-flat welding position.

5.1 Simulation of Multi-nozzle Welding with Different Nozzle Welding Sequences

Two welding sequences as shown in Figure 5-1 were studied.

1) Progressive nozzle weld sequence
2) Jumped nozzle weld sequence

Both cases use rib-bar fixture and modified double bevel weld groove (Figure 3-4). Each nozzle is welded first from the shell OD side. As the boundary conditions for the FEA simulation, the displacements at the four corners of the shell plate were set to zero along the nozzle axial direction. In other words, the four corners were taken as the reference points for the evaluation of the shell distortion.

The FEA simulation results are shown in Figure 5-2 and 5-3. The comparison between the weld distortions of the two cases is listed in Table 5-1, which indicates that for the given components and joint configurations the progressive welding sequence is better for distortion control (22% less distortion when with fixture, 12% less after fixture removal). An explanation for this would be that, with the jumped weld sequence, the first a few nozzles are welded with less constraint from their surrounding structures, hence have developed a higher level of distortions. The data in Table 5-1 also confirmed the finding from the FEA simulation results listed on Table 4-4, i.e. a large distortion jump after taking off the rib-bar fixture.

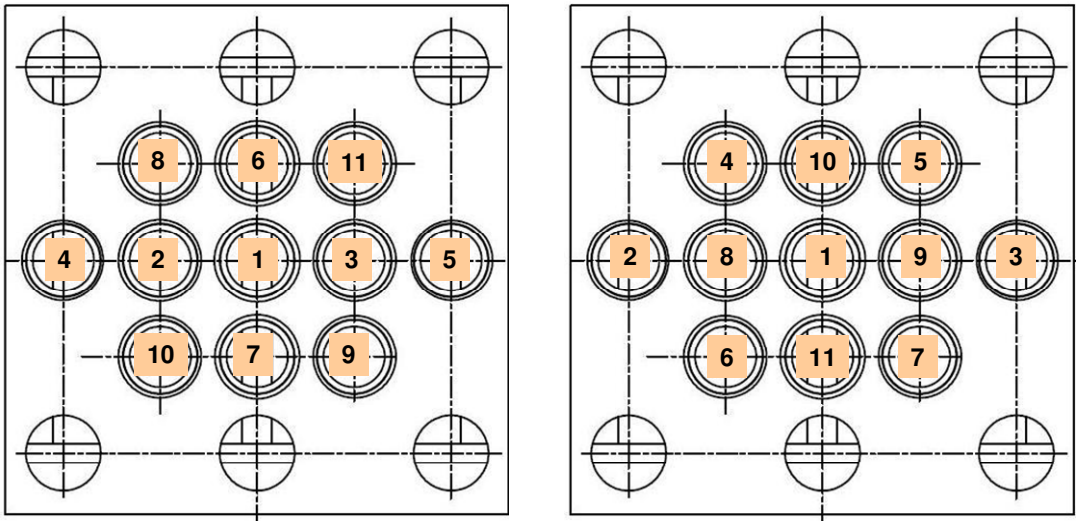

Progressive Sequence Jumped Sequence

Figure 5-1 Multi-nozzle Welding Sequences – FEA Study

Table 5-1 Multi-nozzle Weld Distortion with Different Nozzle Weld Sequences

	With Fixture			After Fixture Removal		
	Displacement Min (mm)	Displacement Max (mm)	Max Z Distortion (mm)	Displacement Min (mm)	Displacement Max (mm)	Max Z Distortion (mm)
Progressive Weld Sequence - I	-20.9	1.4	22.3	-23.7	13.7	37.4
Jumped Weld Sequence	-25	2.1	27.1	-24.5	17.5	42
Distortion Ratio (Jumped / Progressive)			**122%**			**112%**

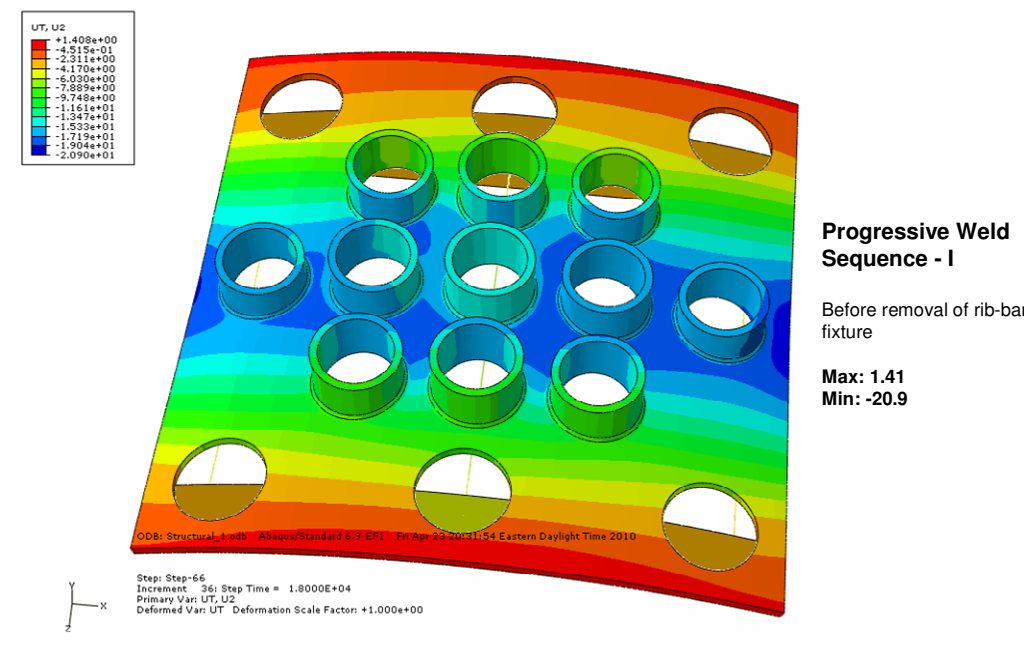

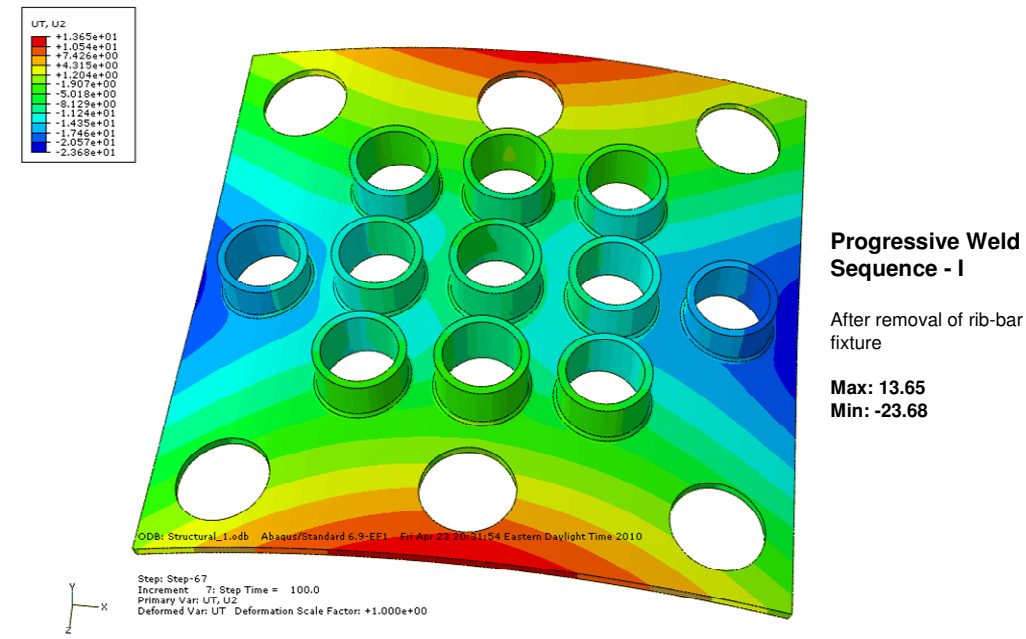

Figure 5-2 Multi-nozzle Weld Distortion – Progressive Nozzle Weld Sequence

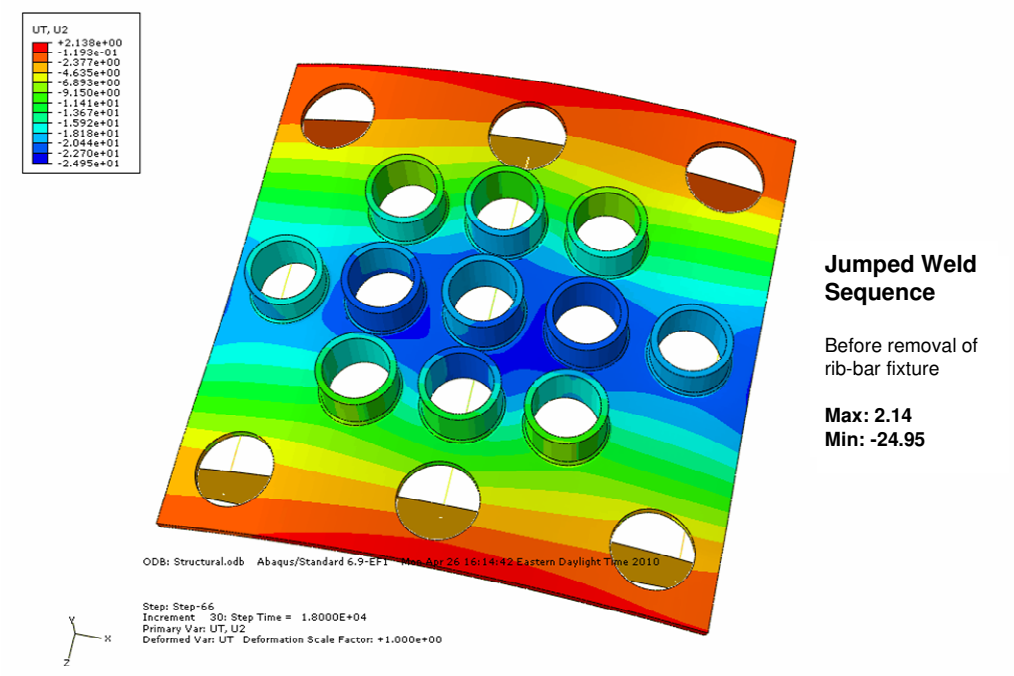

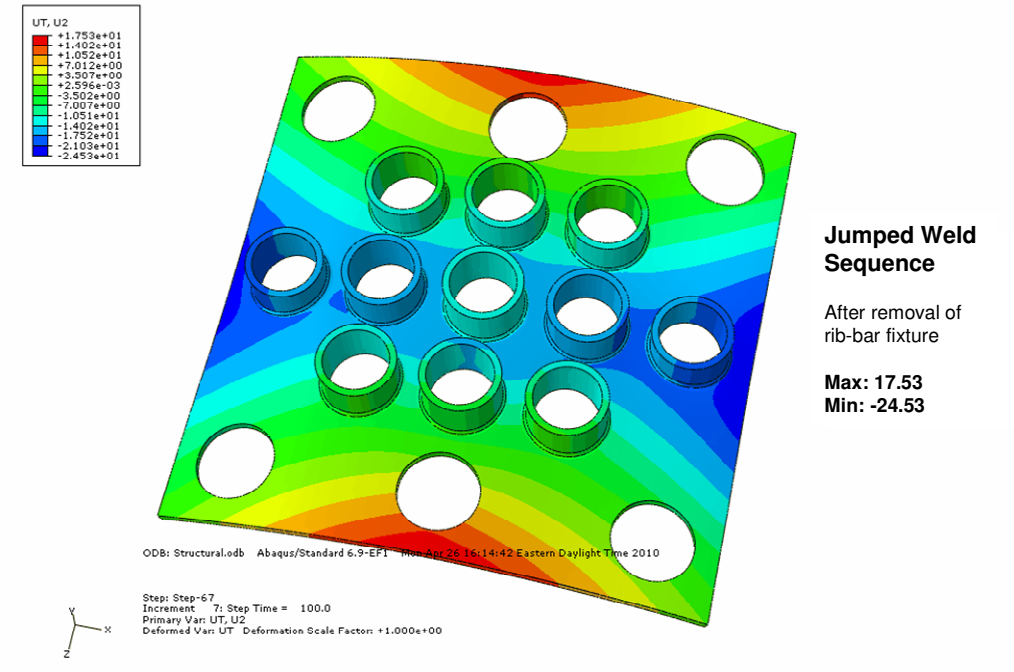

Figure 5-3 Multi-nozzle Weld Distortion – Jumped Nozzle Weld Sequence

5.2 Simulation of Nozzle Welding with Different Weld Pass Deposit Sequences

5.2.1 Effect of Weld Pass Deposit Sequence in Single Nozzle Welding

Due to the structural characteristics of the nozzle-to-shell weld joint, the weld pass deposit sequence will certainly affect the welding distortion. Four cases listed below were studied on the effect of weld pass deposit sequence,

1) No fixture, shell ID side is welded first
2) No fixture, shell OD side is welded first
3) With contour fixture, shell ID side is welded first
4) With contour fixture**,** shell OD side is welded first

All cases above have a nozzle angle of 45^{o}, and are with modified double J groove. Altogether 36 weld passes are deposited to the weld groove. The heat input is 13.8 KJ/cm, weld travel speed 7.6 cm/min, and interpass temperature 177^{o}C maximum.

The predicted shell plate distortions (after removal of fixture for the cases with contour fixture) are shown in Figures 5-4 and 5-5. A comparison of the distortions of the four FEA cases is presented in Table 5-2, which shows that much less distortion will be developed by welding the shell OD side first, especially when a fixture is applied. The distortion in the later case is only 31% of the case when the shell ID side is welded first.

The reason for the distortion behavior revealed by the FEA results above can be explained by Figure 5-6. For all cases in nozzle-to-shell welding, the shell plate region around the weld seam will be pulled toward the nozzle due to the shrinkage of the weld metal and the heat affected zone, ending up with the sinking of the nozzle toward the

shell can centerline. Figure 5-6 (a) shows the residual stress distribution after the welding of a single nozzle without fixture. Clearly it demonstrated that the outside portion of the shell plate had experienced higher tensile stress than the inside portion. The conceptual sketch of stress distribution in Figure 5-6 (b) should apply to all cases listed above. When the welding starts from the shell ID side, the shrinkage of the weld metal would experience less resistance than the level when the welding starts from the shell OD side. The first few weld passes will play a major role in determining the final amount of welding distortion.

Table 5-2 Single Nozzle Weld Distortion with Different Weld Pass Deposit Sequences

	After fixture removal			
	Displacement Min (mm)	Displacement Max (mm)	Max Z Distortion (mm)	Distortion Ratio
No fixture				
Weld shell ID side then OD side	-3.585	5.974	9.559	
Weld shell OD side then ID side	-2.7	3.757	6.457	**68%**
Contour fixture				
Weld shell ID side then OD side	-2.265	3.242	5.507	
Weld shell OD side then ID side	-0.5866	1.126	1.7126	**31%**

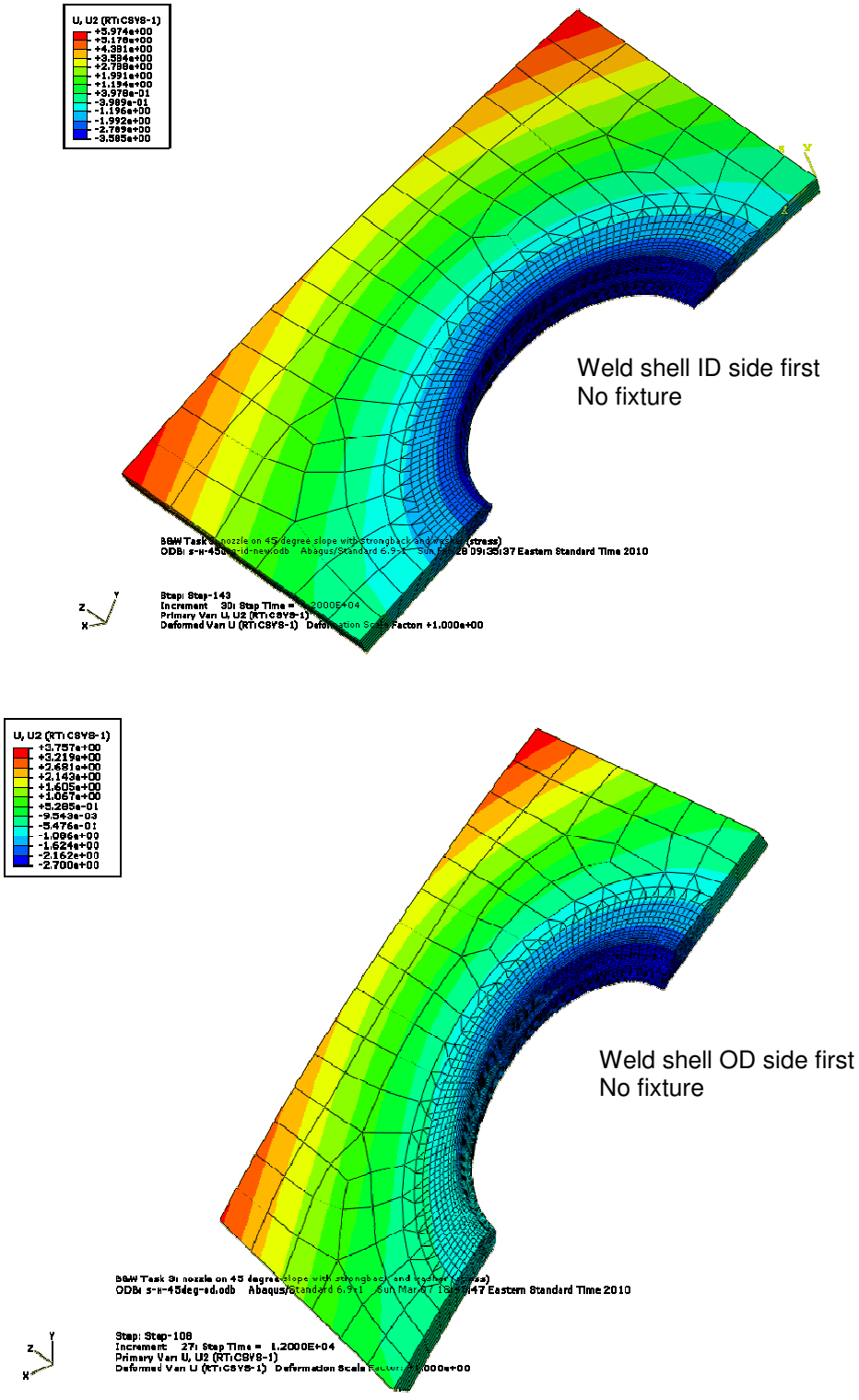

Figure 5-4 Single Nozzle Weld Distortion – Weld Pass Sequence – No Fixture

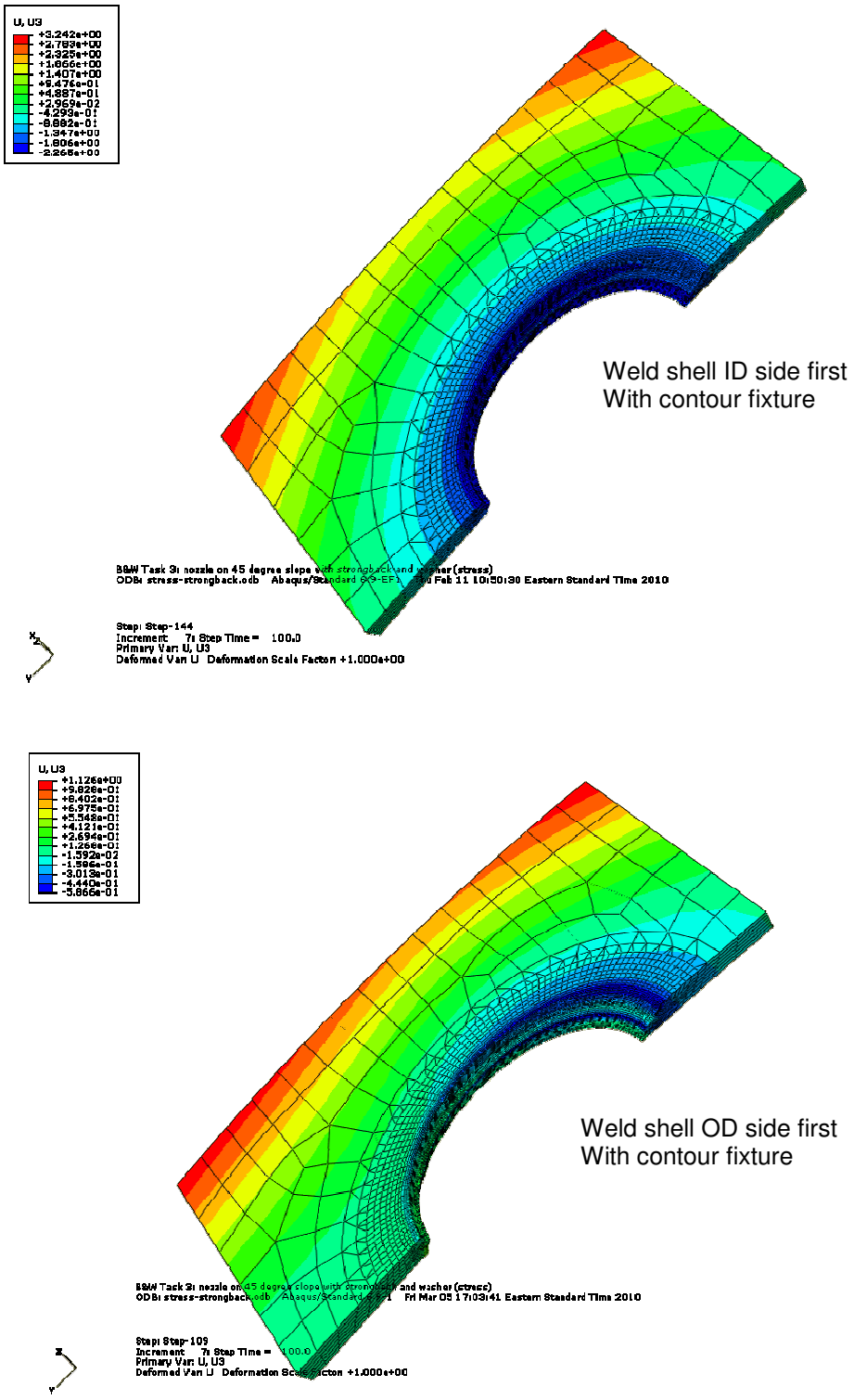

Figure 5-5 Single Nozzle Weld Distortion – Weld Pass Sequence – Contour Fixture

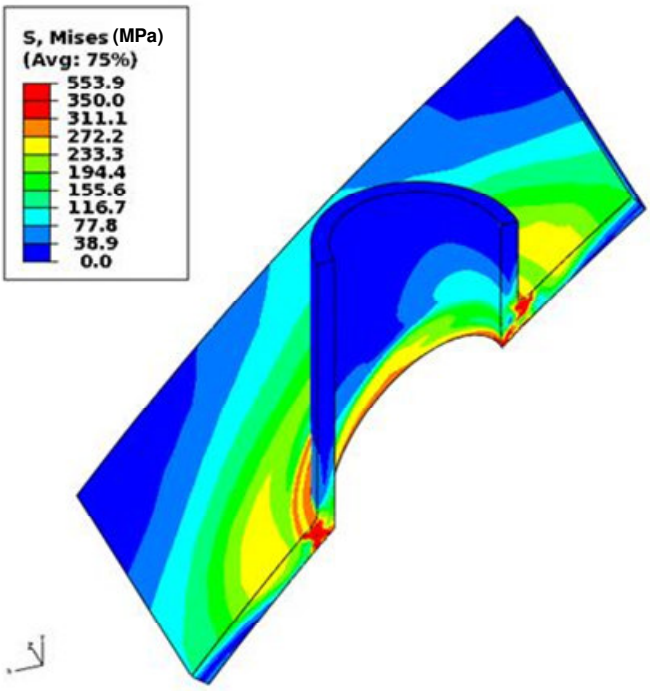

(a) Predicted Residual Stress Distribution – Welding Shell ID Side First, No Fixture

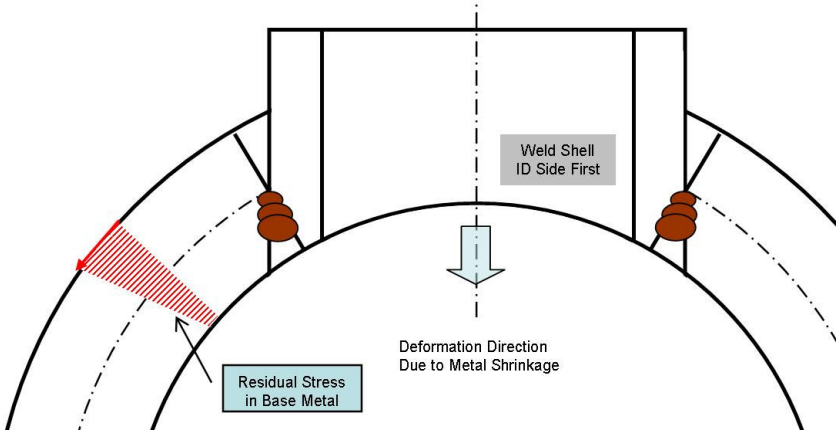

(b) Conceptual Sketch of Stress and Deformation in Single Nozzle Welding

Figure 5-6 Stress and Deformation in Single Nozzle Welding

5.2.2 Effect of Weld Pass Deposit Sequence in Multi-nozzle Welding

Combining the results of Sections 5.1 and 5.2.1, there would be two basic options for welding multiple nozzles to a shell can,

1) **Progressive weld sequence I**: following such as the progressive sequence in Figure 5-1, each nozzle is welded firstly on the shell OD side then on the shell ID side, followed by the welding of the next nozzle.
2) **Progressive weld sequence II**: the shell OD side of all nozzles is welded by following the progressive sequence in Figure 5-1, then the shell ID side is welded following the same sequence.

From the production point of view option II would be preferred. The reason is that, when there are dozens or even hundreds of nozzles to be welded, this would greatly reduce the amount of work for flipping the shell plate to facilitate the welding of every nozzle, hence effectively increase the productivity. However, this has to be evaluated to see whether there would be any major impact on the welding distortion.

A FEA study was therefore conducted to compare the two options. Both cases are with rib-bar fixture and double bevel weld groove. The FEA simulation results are shown in Figure 5-2 for the first case and in Figure 5-7 for the second case. The comparison between the two cases is listed in Table 5-3, which reveals that about 36% more distortion will be developed by option II. This sounds somewhat in contradiction with the single nozzle welding FEA results introduced in Section 5.2.1. The main cause possibly has come from the interaction between the neighboring nozzles due to the small nozzle spacing. The completion of the shell ID side of the neighboring nozzles would have created significantly higher resistance to the welding deformation of the next nozzle so

that the overall distortion of option II turned out to be less than the overall distortion of option I.

Table 5-3 Multi-nozzle Weld Distortion with Different Weld Pass Deposit Sequences

	With Fixture			
	Displacement Min (mm)	**Displacement Max (mm)**	**Max Z Distortion (mm)**	**Distortion Ratio**
Progressive Weld Sequence - I	-20.9	1.4	22.3	
Progressive Weld Sequence - II: welding shell ID side after completion of welding all nozzles from shell OD side	-29.3	1	30.3	**136%**

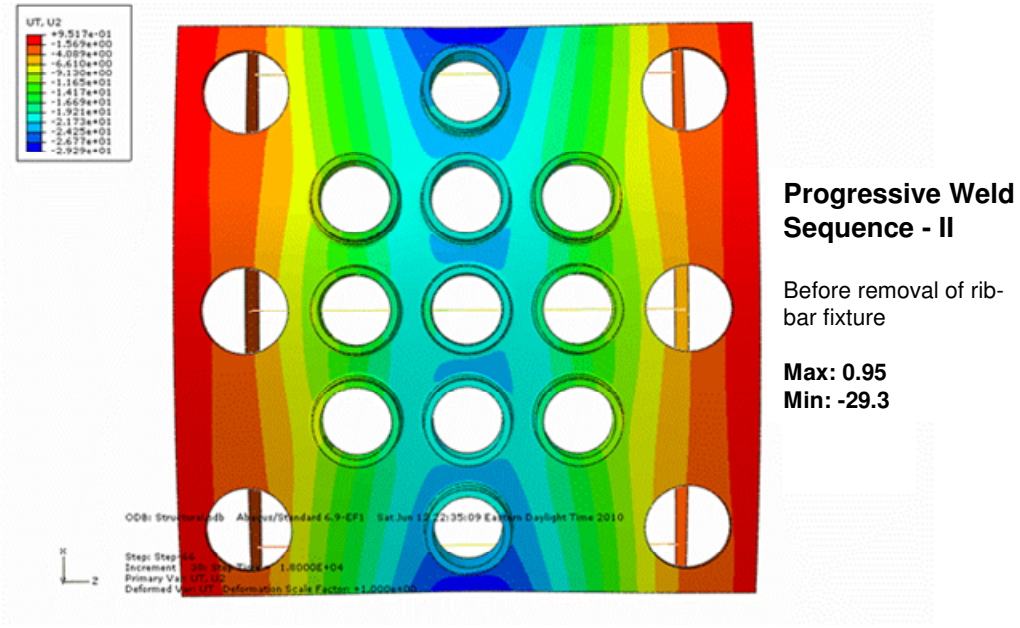

Figure 5-7 Multi-nozzle Weld Distortion – All OD Then All ID Welds

5.3 Single Nozzle Weld Mockup with Different Welding Directions

When the nozzle is not normal to the shell surface, it would be expected that the welding direction of the weld pass will affect the final angular distortion of the nozzle. Two single nozzle mockups were hence designed to investigate the influence of the welding direction,

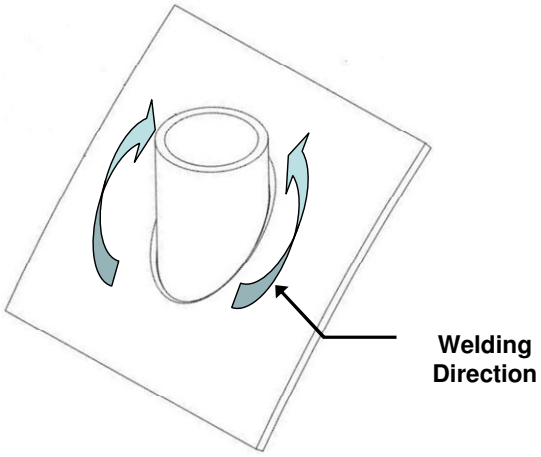

1) All weld passes are welded in uphill direction
2) Weld passes on shell OD side are welded in uphill direction, and weld passes on shell ID side in downhill direction. Refer to Figure 5-8 for the actual orientation of the mockups during welding.

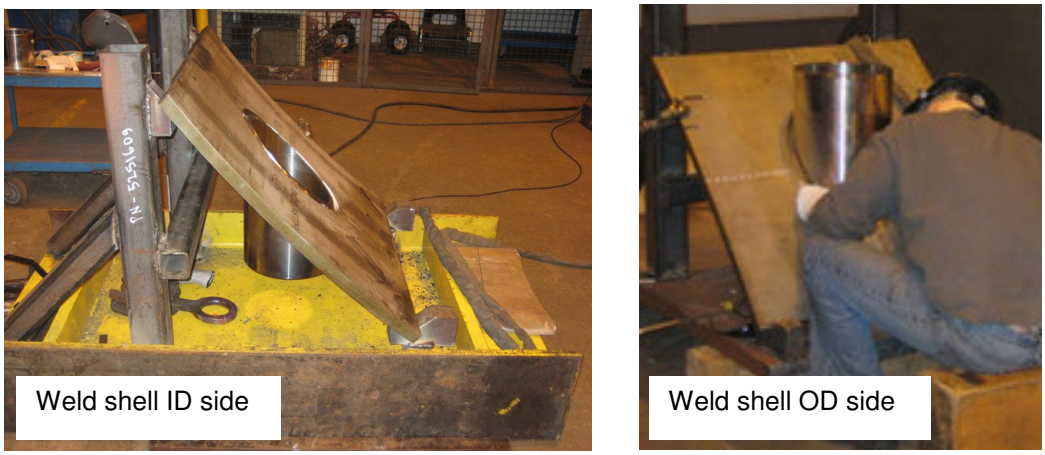

Figure 5-8 Mockup Orientations in Welding of Shell ID and OD Sides

Both mockups are with modified double J groove and without fixture. Manual GTAW process was used in the tests. The shell ID side was welded first. Welding parameters are listed in Table 5-4.

The mockup plate surface profiles were measured before and after welding. The results are shown in Figures 5-9 and 5-10. Welding distortions were summarized in Table 5-5, which shows that the welding direction had very little influence on the out-of-plane plate distortions or the plate shrinkages, but did show some influence on the nozzle angular distortion. The second mockup (shell OD side welded uphill, ID side downhill) developed less nozzle angular distortion, likely because the shorter/upper side of the nozzle was in this case always welded later than the longer/lower side. In general, the welding direction is not an important factor in nozzle-to-shell welding except when the nozzle angle becomes a critical quality index.

Table 5-4 Welding Parameters for Mockup Study on Welding Direction

Weld Direction	# of Weld Passes	Heat Input (kJ/cm)	Travel Speed (cm/min)	Estimated Total Heat Input (Mega J)
Uphill	38	27.6	7.6	117.0
Shell OD side: uphill Shell ID side: downhill	40	25.6	6.4	114.4

Table 5-5 Single Nozzle Weld Distortion from Mockup Study on Welding Direction

	MAX Z Distortion (mm)	RMS Z Distortion (mm)	X Direction Shrinkage (mm)	Y Direction Shrinkage (mm)	Nozzle Angle Change (deg)
Uphill	17.68	5.33	4.95	0.66	4.7
Shell OD side: uphill Shell ID side: downhill	17.30	5.26	4.52	0.56	3.9
Distortion Ratio (Uphill / (OD uphill & ID downhill))	98%	99%	91%	-	**83%**

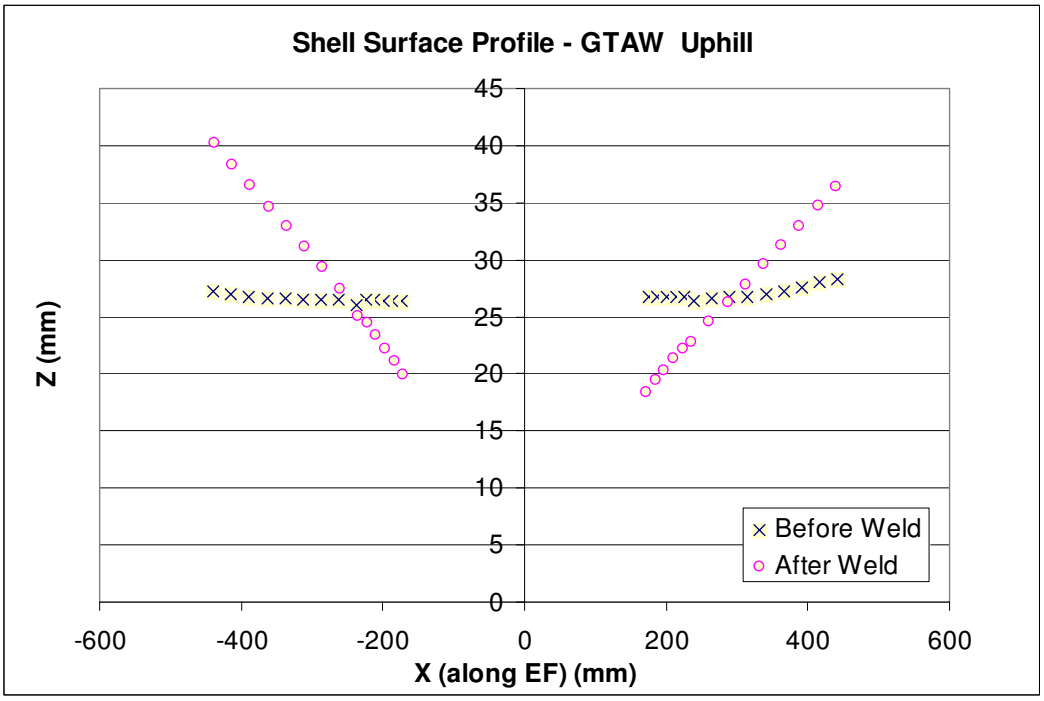

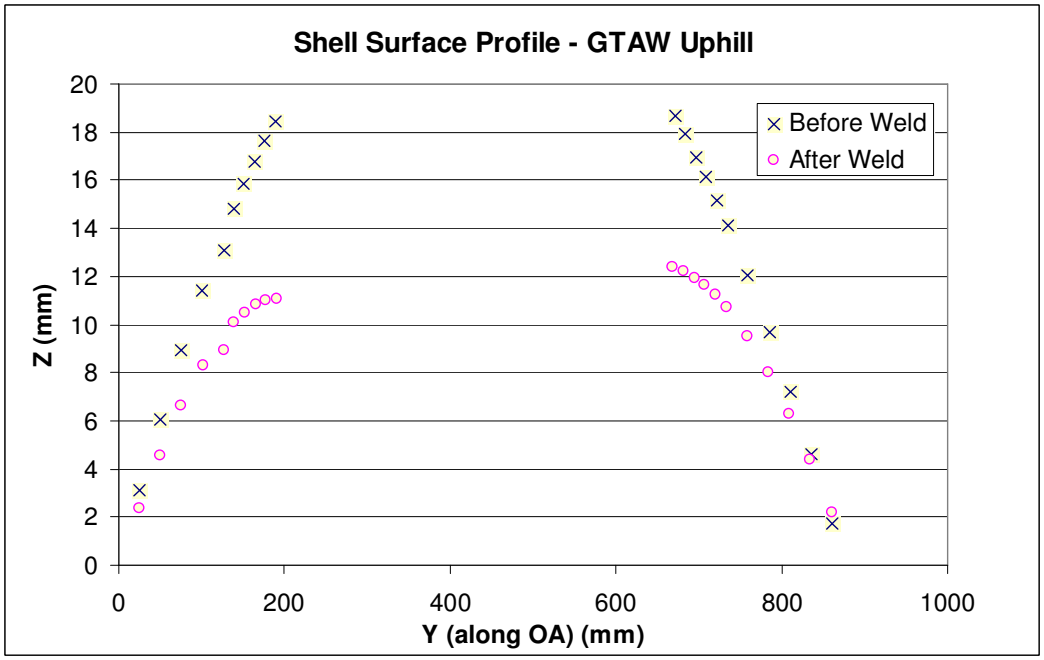

Figure 5-9 Single Nozzle Weld Mockup Distortion – All Uphill

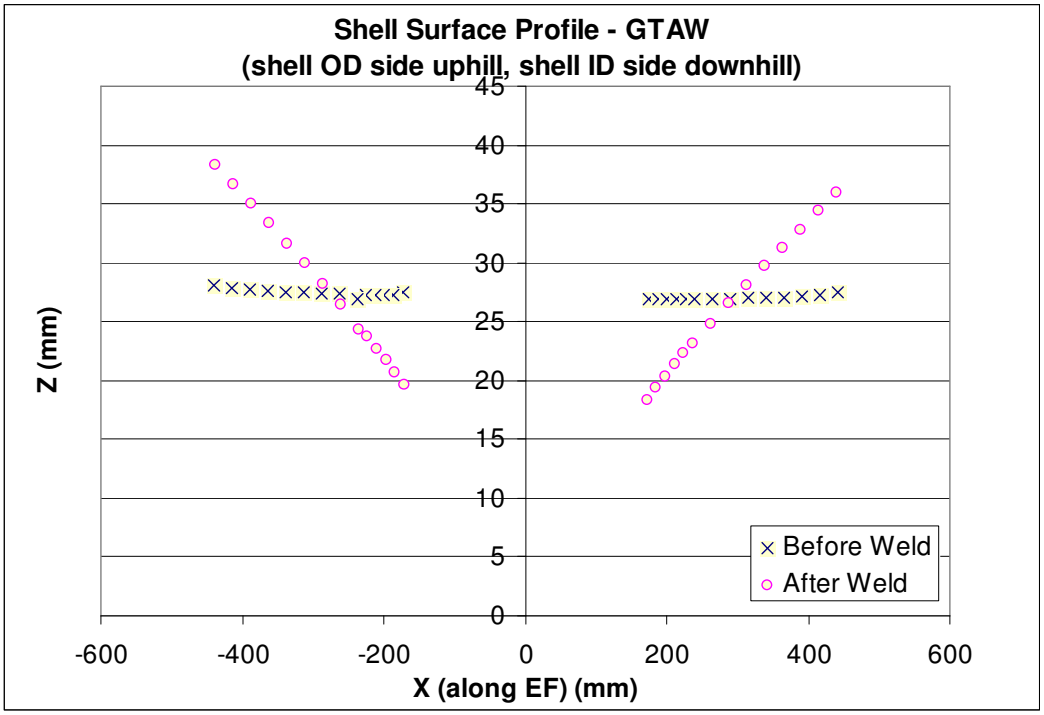

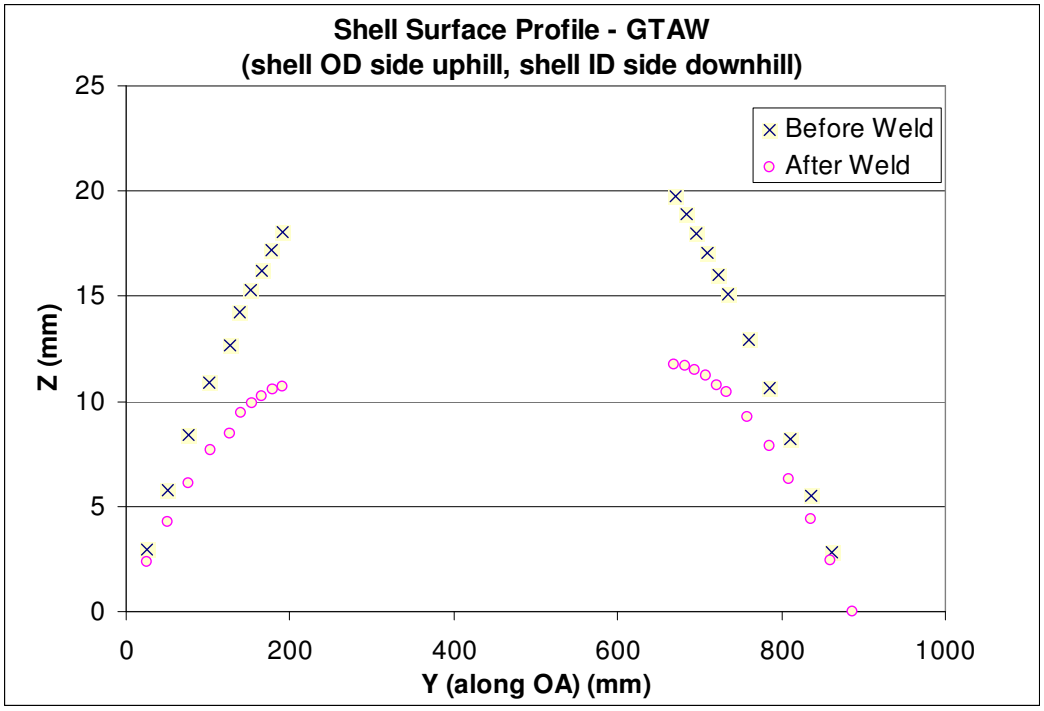

Figure 5-10 Single Nozzle Weld Mockup Distortion – OD Uphill ID Downhill

5.4 Summary

FEA simulations and mockup tests were carried out on the influence of the following factors on the welding distortion of stainless steel nozzle-to-shell-can weld assemblies,

1) Nozzle welding sequence in multi-nozzle welding
2) Weld pass deposit sequence in both single and multi-nozzle welding
3) Welding direction in single nozzle welding when the nozzle intersects into the shell plate with a nozzle angle of 45^{o}.

The FEA simulation results suggested that a progressive nozzle welding sequence would develop less welding distortion than a jumped sequence (Figure 5-1). Under the given structure and welding conditions, the welding distortion with progressive sequence was 22% less than the distortion with jumped sequence before the removal of the fixtures, and 12% less after the fixture removal.

The impact of the weld pass deposit sequence on the nozzle welding distortion was found significant. The FEA results of single nozzle welding without fixture showed 32% less distortion when the nozzle was welded from the shell OD side first as compared to the case when the nozzle welding was started from the shell ID side. When the nozzle welding started from the shell OD side, the distortion of single nozzle welding with contour fixture was 69% less as compared to the case when the nozzle welding was started from the shell ID side. For multi-nozzle welding under the given structure and welding conditions, the FEA simulation results suggested complete the welding of each nozzle, firstly on the shell OD side then on the shell ID side, then proceed to the next nozzle. However, the optimal weld pass deposit sequence for multi-nozzle welding may

change depending upon such as the nozzle spacing which would affect the interaction between the nozzles.

The influence of the welding direction on nozzle welding distortion appeared insignificant in the single nozzle mockup tests, except on the nozzle angle when the nozzle is on a 45^{o} slope on the shell plate.

Chapter 6 Effect of Welding Process on Nozzle Welding Distortion

All the studies introduced in Chapters 4 (fixture) and 5 (welding sequence) are based on an assumption that the compared cases use the same welding process. The studies in this Chapter address the welding process aspect, involving the type of welding process, the weld bead size, and the cooling time or interpass temperature. Single nozzle weld mockups or FEA models were employed in these studies.

6.1 Single Nozzle Mockups with Manual GTAW and SMAW Processes

As the most common processes for stainless steel nozzle welding, the manual GTAW and SMAW processes were compared regarding their welding distortions. Mockup was made for each process, with nozzle angle at 45^{o} and modified double J weld groove. No fixture was attached to the mockups. Uphill welding direction was chosen and the welding was done first on the shell ID side. Welding parameters are listed in Table 6-1.

Table 6-1 Welding Parameters for Mockup Study on Welding Process

Weld Process	# of Weld Passes	Heat Input (kJ/cm)	Travel Speed (cm/min)	Estimated Total Heat Input (Mega J)
GTAW	38	27.6	7.6	117.0
SMAW	26	19.7	8.4	57.2

The measured mockup plate surface profiles before and after welding are shown in Figures 4-2 (SMAW) and 5-8 (GTAW). Welding distortions were summarized in Table 6-2, which indicates that the distortion from SMAW process was only about 65~70% of the distortion from manual GTAW. The ratio of Y Direction Shrinkage was not calculated because the difference between the two mockup cases is very minor.

An outstanding observation from the welding parameters in Table 6-1 is that the manual GTAW process consumed much higher total energy than the SMAW process. This is because the total heat input of manual GTAW process heavily depends upon the skill of individual welders. The extra heat consumed by manual GTAW process would have been transferred into the base metal, thus causing more shell plate distortion. Skillful welder would be able to deposit more weld metal with given welding parameters, ending up with less total heat input, thus less weld distortion. This would be especially evident when facing difficult-to-weld applications such as the welding of nozzle on a 45^{o} slope on a shell can. The welders of average skill had been chosen for the mockup welding.

Another common observation from the mockup distortion data in Tables 4-2, 5-5 and 6-2 is that the distortion ratios of MAX Z Distortion and RMS Z Distortion between the two cases in comparison are fairly close. In Table 6-2 the ratios are 65% for MAX Z Distortion and 71% for RMS Z Distortion. It could therefore be concluded that using MAX Z Distortion or RMS Z Distortion for the evaluation of the nozzle-to-shell welding distortion be equally effective.

Table 6-2 Mockup Welding Distortion – Different Welding Processes

	MAX Z Distortion (mm)	RMS Z Distortion (mm)	X Direction Shrinkage (mm)	Y Direction Shrinkage (mm)	Nozzle Angle Change (deg)
GTAW	17.68	5.33	4.95	0.66	4.7
SMAW	11.53	3.78	3.20	0.28	3.4
Distortion Ratio (SMAW / GTAW)	65%	71%	65%	-	72%

6.2 Single Nozzle Mockups with Different Weld Bead Sizes

A common practice for distortion control is to use small weld beads and apply low heat input [38,53,55]. This would work fine when it is possible to reduce the weld seam size. When facing a large weld seam of which the pre-determined weld groove has to be filled up, the smaller weld bead size would mean more weld passes. Some research data showed that, for multi-pass weld seam, larger weld bead resulted in less final distortion [4]. However, it is unknown whether this observation would be applicable to nozzle-to-shell welding. Mockups were therefore designed to evaluate the impact of the weld bead size on stainless steel nozzle-to-shell welding distortion.

- **Welding conditions**: nozzle axis normal to shell surface (Figure 6-1), modified double J groove, no fixture, manual GTAW process, shell ID side welded first
- **Welding parameters**: see Table 6-3

The measured mockup plate surface profiles are shown in Figures 6-2 and 6-3. Welding distortions were summarized in Table 6-4, which indicates that the distortions of the two cases were very close (0.36 ~ 0.51mm difference), with most of the values by large weld bead slightly higher. The two mockups have similar level of total heat input (Table 6-3). In summary, under the given joint configuration and welding condition, the

variation in weld bead size didn't cause apparent impact on the stainless steel nozzle-to-shell welding distortion.

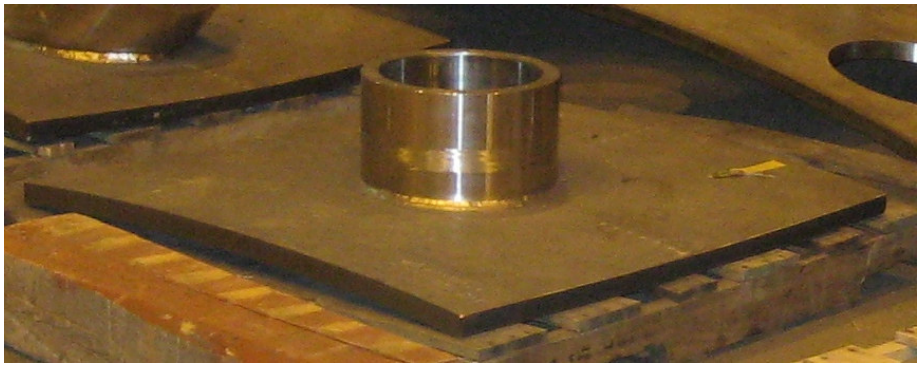

Figure 6-1 Mockup for Study on Effect of Weld Bead Size

Table 6-3 Welding Parameters for Mockup Study on Weld Bead Size

Weld Bead Size	# of Weld Passes	Heat Input (kJ/cm)	Travel Speed (cm/min)	Estimated Total Heat Input (Mega J)
Small	35	17.7	10.2	56.7
Large	26	26.8	10.2	53.9

Table 6-4 Mockup Welding Distortion – Different Weld Bead Sizes

	MAX Z Distortion (mm)	RMS Z Distortion (mm)	X Direction Shrinkage (mm)	Y Direction Shrinkage (mm)
Small weld bead	10.06	4.19	1.42	0.18
Large weld bead	9.70	4.62	1.93	0.61
Distortion Ratio (Large / Small bead)	96%	110%	136%	343%

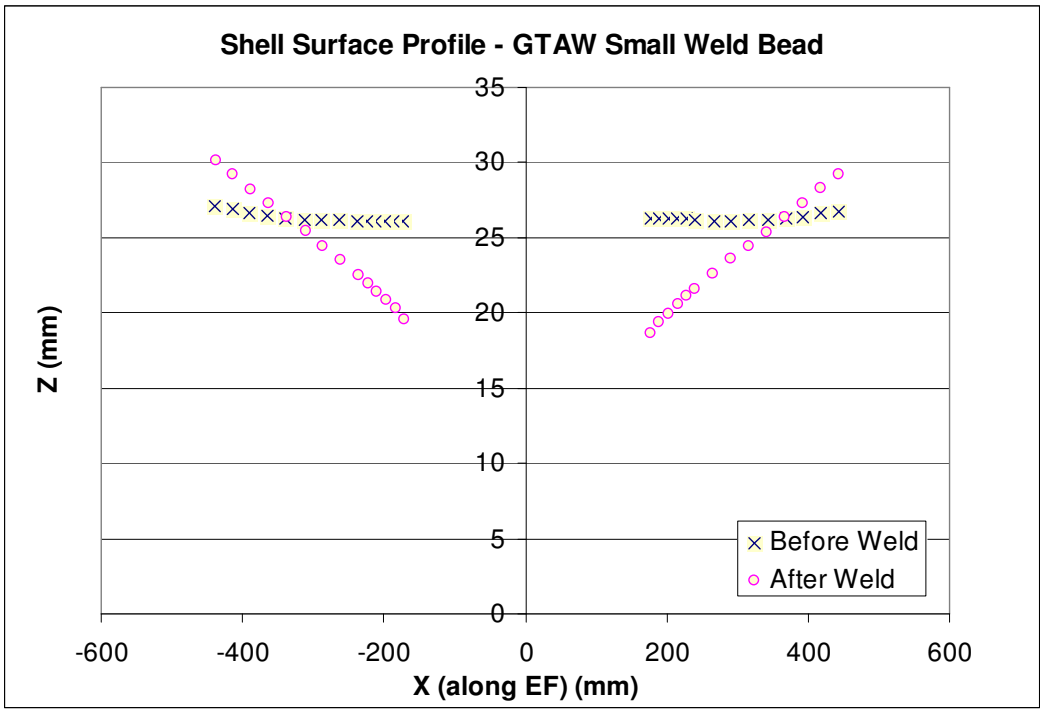

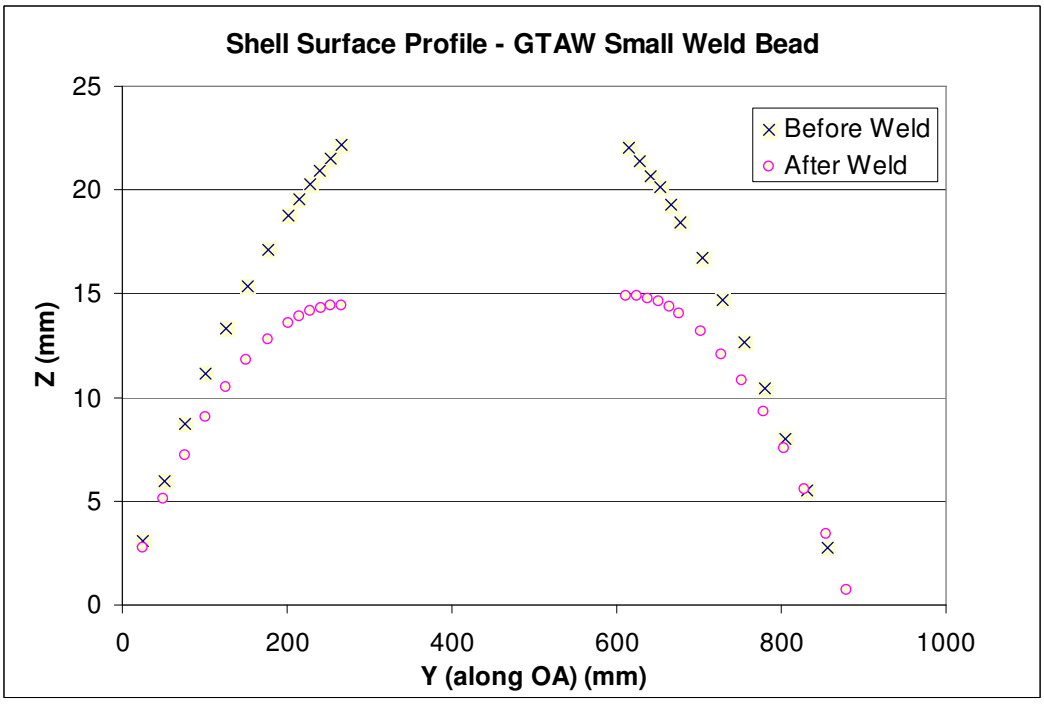

Figure 6-2 Single Nozzle Weld Mockup Distortion – Small Weld Bead

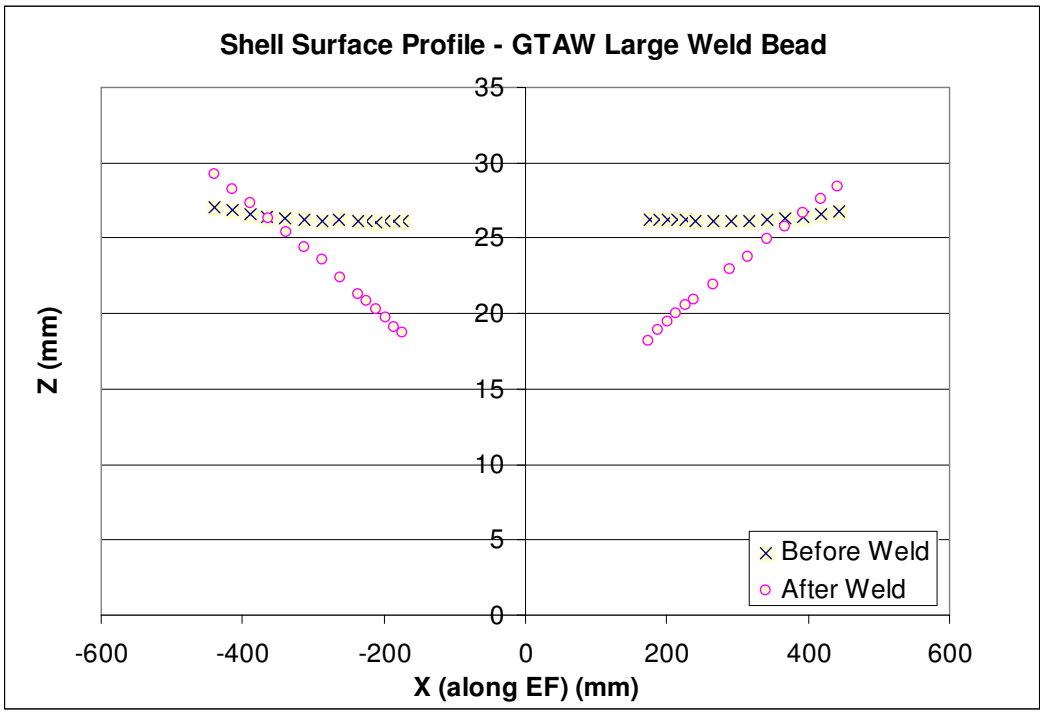

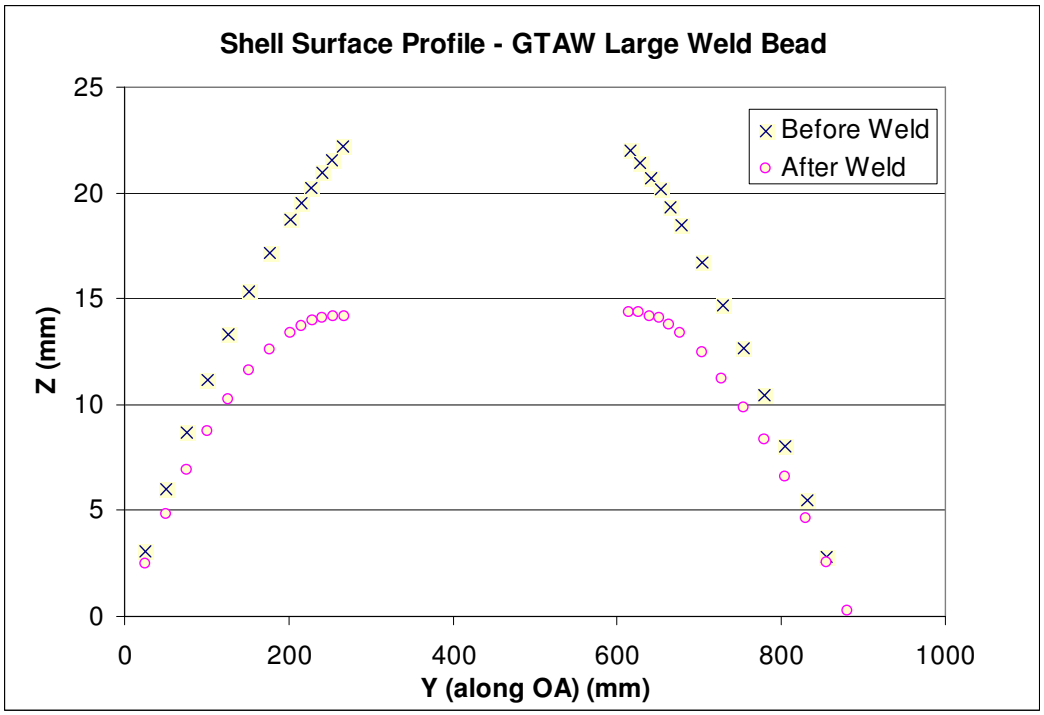

Figure 6-3 Single Nozzle Weld Mockup Distortion – Large Weld Bead

6.3 Simulation of Single Nozzle Welding with Different Lump Pass Sizes

The simulation study on the effect of the weld bead size on welding distortion was initiated with the intention for the application of high deposition rate processes, such as the use of large filler size, or even switching from GTAW or SMAW to SAW process.

- **Welding conditions**: contour fixture, nozzle angle 45^{o}, modified double J groove, shell ID side welded first
- **Welding heat input**: the relevant FEA analyses were designed as such that, with different weld bead sizes, the heat flux will just be enough to melt the weld bead and its immediate adjacent base metals.

The predicted shell plate distortions after fixture removal are shown in Figures 6-4 to 6-7. A comparison of the distortions of the four FEA cases is listed in Table 6-5, which shows that generally speaking less welding distortion will be developed with larger weld beads. This agrees with the results of similar studies introduced in Ref [4]. The reasons why they appear a little conflicting with the mockup test results in Section 6.2 might include,

- The difference between the weld bead sizes of the FEA cases are larger than that in the mockups, therefore able to better reveal the influence of the weld bead size
- The nozzle in the FEA analysis is on a 45^{o} slope, which may magnify the impact of the weld bead size as compared to the case of the mockups where the nozzles were normal to the shell

Nevertheless, the FEA simulation results suggest at least two things,

- Combined with the mockup results in Section 6.2, it could be concluded that large weld beads wouldn't have unfavorable major impact on the welding distortion of the given weld joint configuration under the given welding conditions
- Using large lumped passes in representation of an actually small-bead multi-pass process could produce reasonably close distortion prediction. This is very important for the application of FEA technology on large weld structures having large quantity of welds, because otherwise the FEA model would become very complicated and the FEA analysis would be very time-consuming, sometimes impossible.

Table 6-5 Predicted Welding Distortions with Different Weld Bead Sizes

Number of Weld Passes (with contour fixture)	After Fixture Removal Displacement Min (mm)	Displacement Max (mm)	Max Z Distortion (mm)	Distortion Ratio
Weld passes: 17 on ID, 19 on OD	-2.265	3.242	5.507	
Weld passes: 6 on ID, 6 on OD	-1.891	2.514	4.405	**80%**
Weld passes: 2 on ID, 2 on OD	-2.076	2.96	5.036	**91%**
Weld passes: 1 on ID, 1 on OD	-1.616	2.465	4.081	**74%**

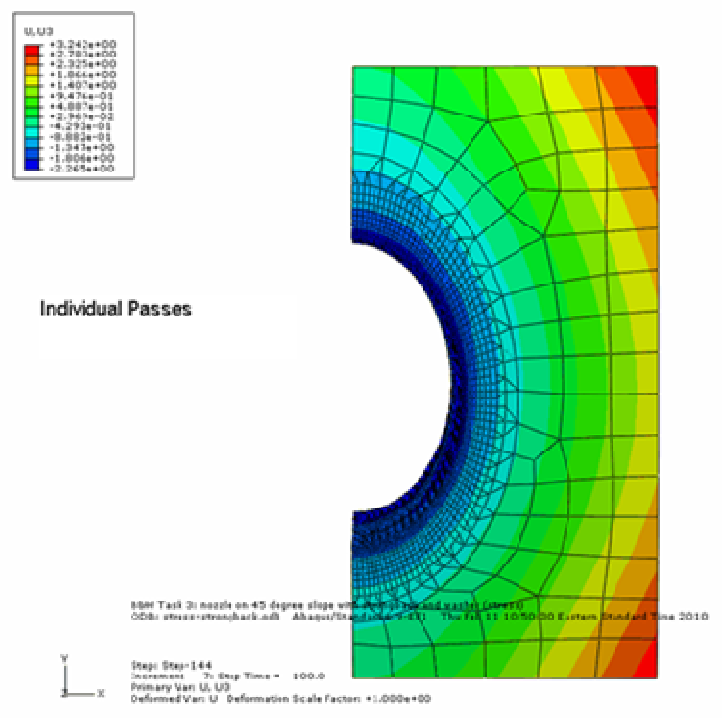

Figure 6-4 Predicted Welding Distortion – 36 Weld Passes

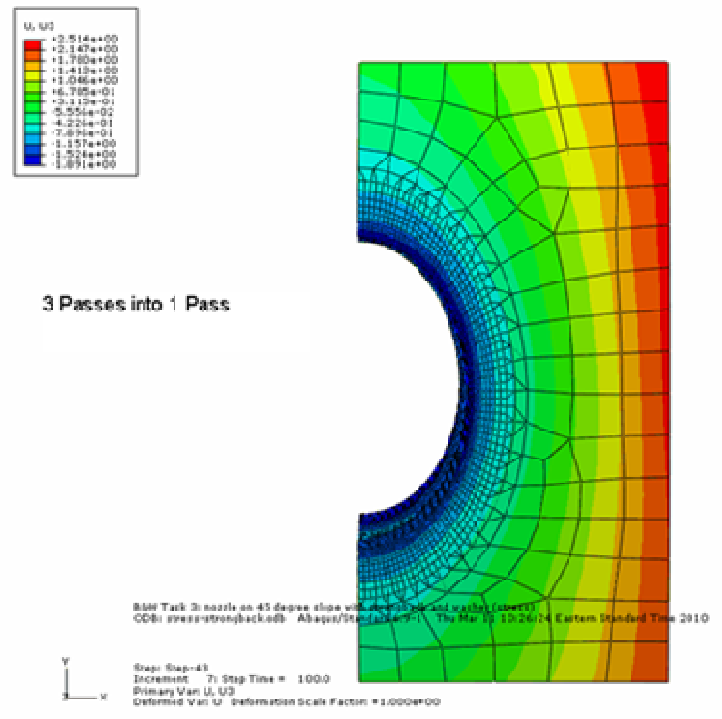

Figure 6-5 Predicted Welding Distortion – 12 Weld Passes

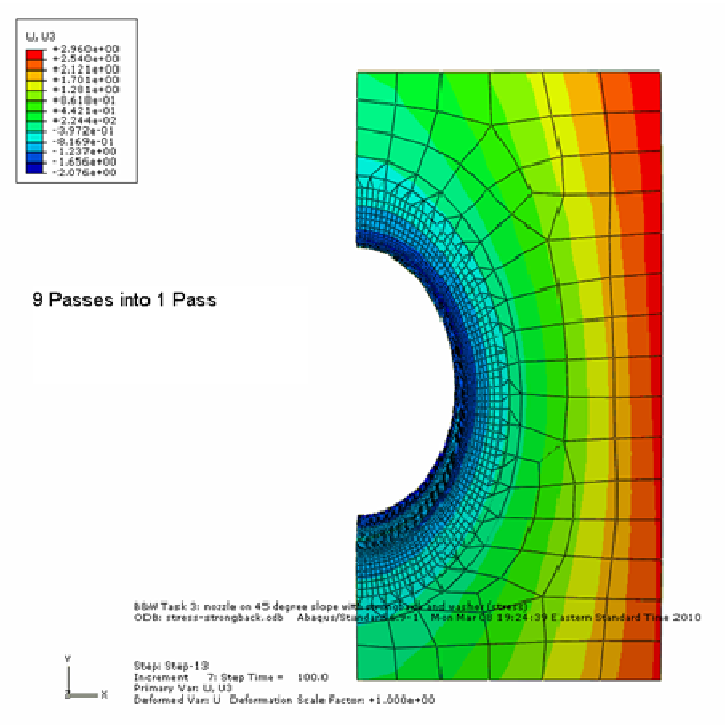

Figure 6-6 Predicted Welding Distortion – 4 Weld Passes

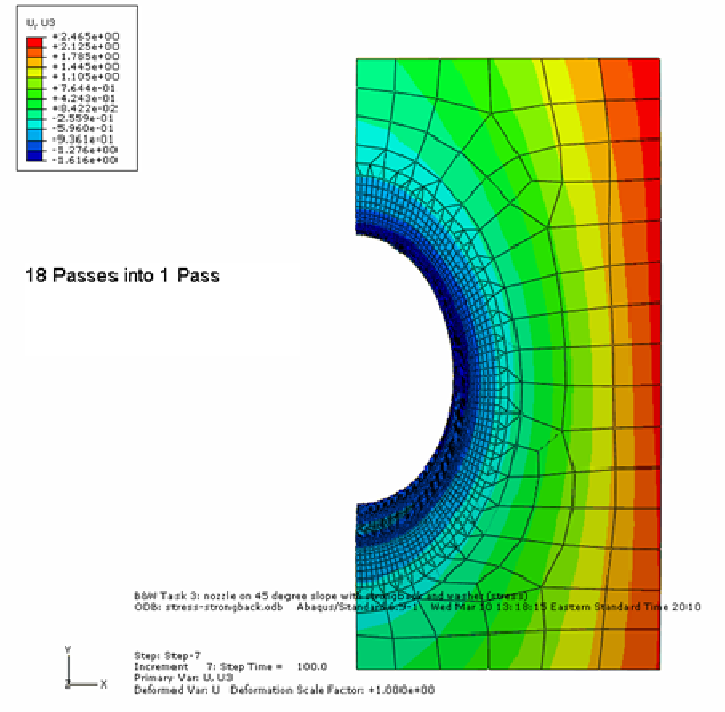

Figure 6-7 Predicted Welding Distortion – 2 Weld Passes

6.4 Simulation of Single Nozzle Welding with Different Cooling Times

The cooling time of each weld pass is another important factor that will affect the final welding distortion. This is related to the interpass temperature. Longer cooling time will result in a lower interpass temperature. Normally the low interpass temperature would help to reduce the welding distortion. The question is, for stainless steel nozzle-to-shell welding with the given dimensions, to what an extent the cooling time would affect the distortion. FEA simulation was thus conducted under the following conditions,

- Nozzle angle 45^{o}, modified double J groove, with contour fixture
- Shell ID side is welded first, 36 weld passes in total

The predicted welding distortions (after removal of fixture) together with the history of the interpass temperature are shown in Figures 6-8 to 6-10. The interpass temperature has been taken from a node on the FEA model that is 18mm below the shell OD surface and 22mm away from the weld prep root nose. A comparison of the distortions of the three FEA cases is presented in Table 6-6, showing an apparent trend that shorter cooling time, i.e. higher interpass temperature, has resulted in slightly higher welding distortion. Nevertheless, the impact of cooling time or interpass temperature on shell plate distortion doesn't seem to be high.

Table 6-6 Predicted Welding Distortions with Different Cooling Times

Cooling Time (sec)	Average Interpass (degC)	Total Weld Time (hrs)	MAX Z Distortion (mm)	Distortion Ratio
800~1000	100	9.4	5.507	
600~800	125	7.5	5.618	**102%**
200~400	200	3.3	6.352	**115%**

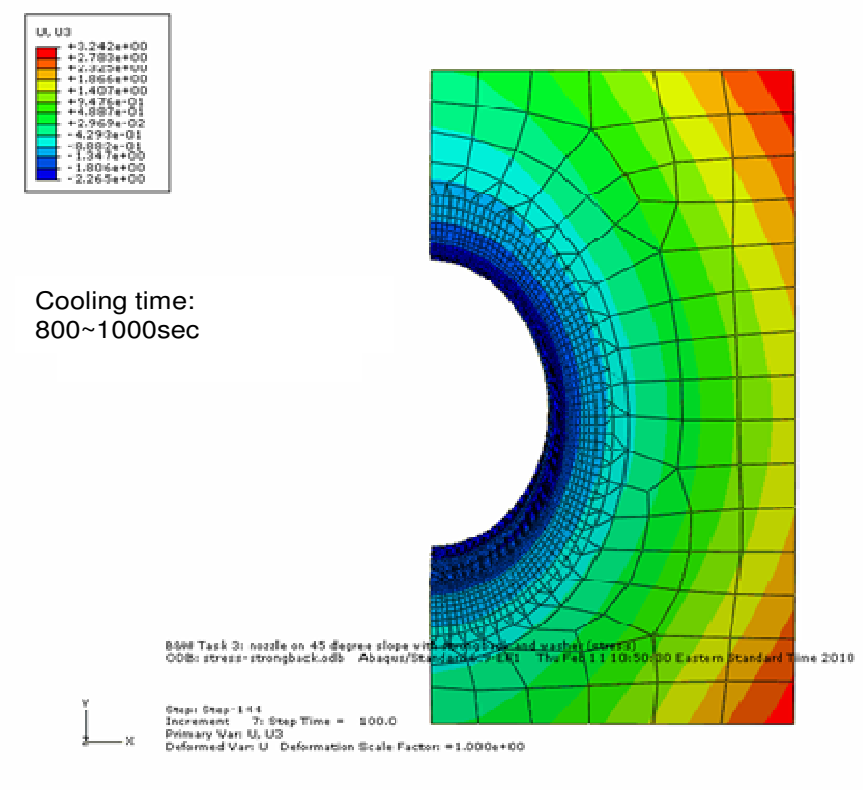

Figure 6-8 Weld Distortion and Interpass Temperature - Long Cooling Time

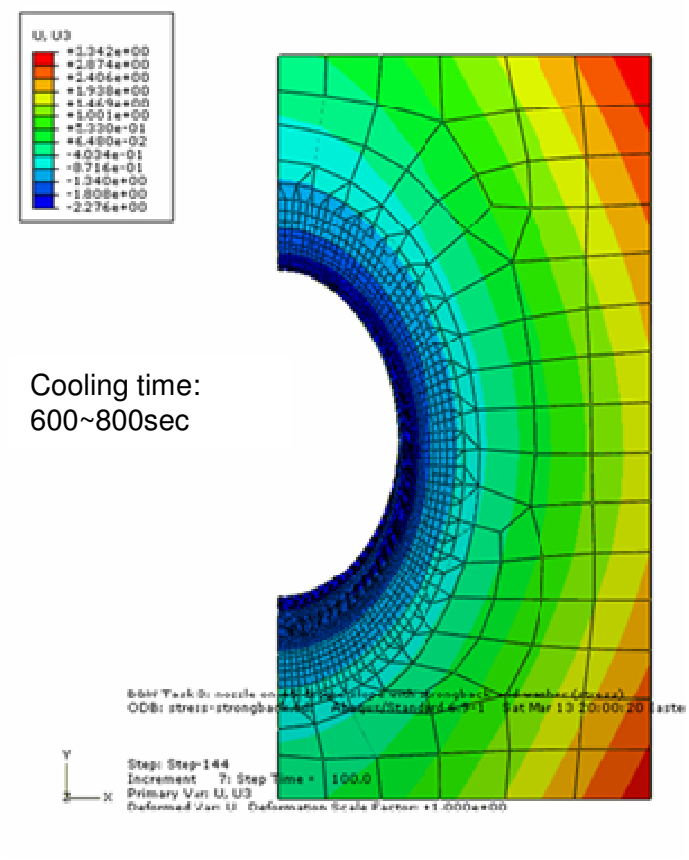

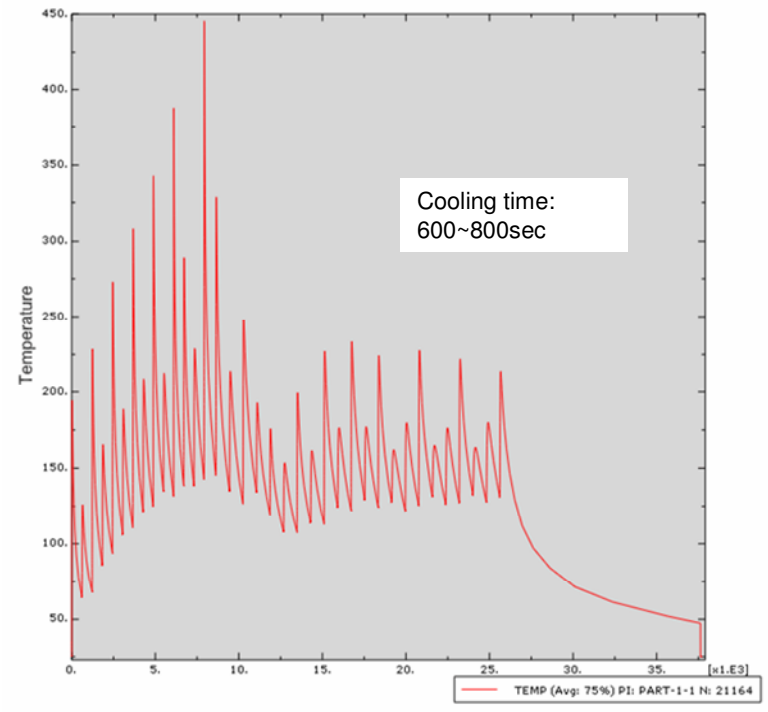

Figure 6-9 Weld Distortion and Interpass Temperature - Mid Cooling Time

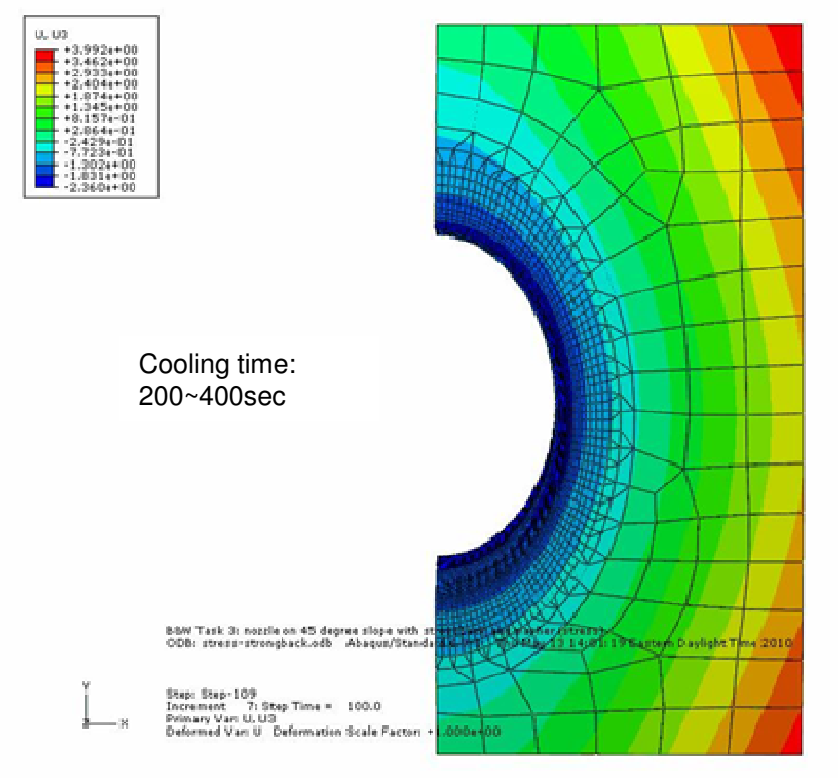

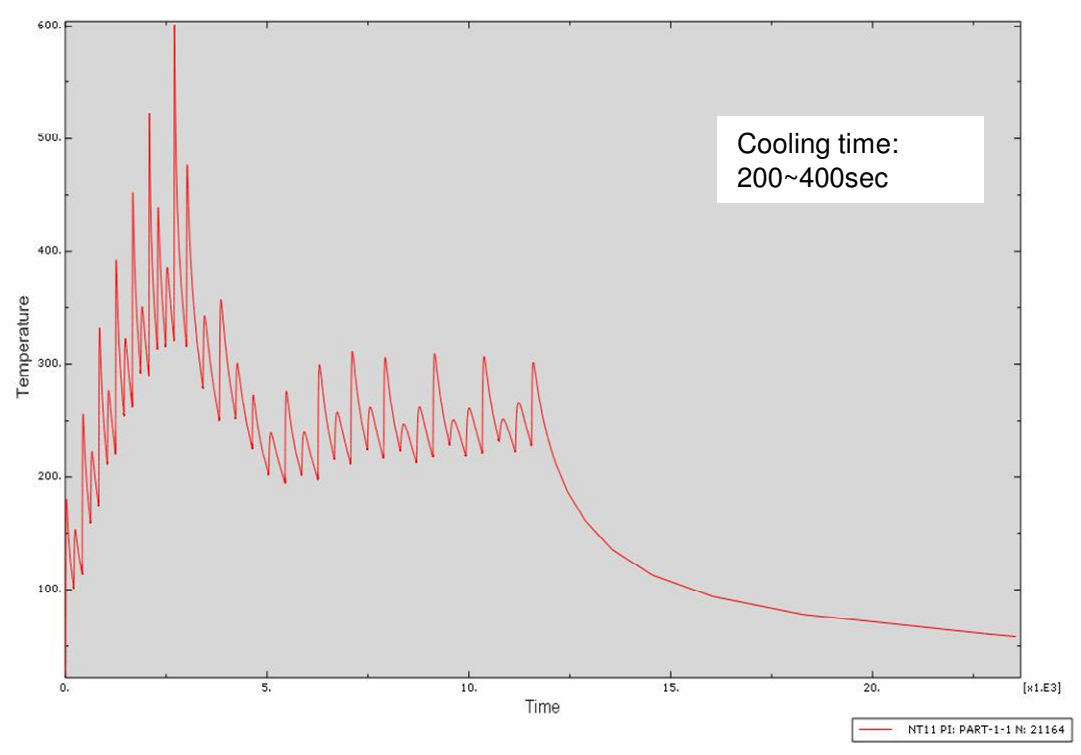

Figure 6-10 Weld Distortion and Interpass Temperature - Short Cooling Time

6.5 Summary

The influence of welding process on the welding distortion of stainless steel nozzle-to-shell-can weld assemblies was investigated through mockup tests and finite element analyses of single nozzle welding, with variations in welding process type, weld bead size and cooling time.

The mockups welded with manual GTAW and SMAW processes showed that the welding distortion produced with SMAW process was only about 2/3 of the distortion produced by manual GTAW. Manual GTAW is a low efficient process, with much heat being absorbed by the base metal resulting in large welding distortion.

The influence of weld bead size on nozzle welding distortion was found insignificant in the mockup tests where the nozzles were normal to the shell plate surface and the size of the larger weld bead was about 35% bigger than the size of the smaller bead. While in the FEA simulations where the nozzles were on a 45^{o} slope and the sizes of the larger weld beads were 3~18 times of the size of the smallest bead, a general trend of distortion decrease was observed along with the increase in weld bead size. It could be concluded that applying large weld bead wouldn't have detrimental impact on the welding distortion of the nozzle-to-shell weld assembly. The FEA results also support that using very large lumped weld pass to simulate an actual multi-pass welding application wouldn't cause too much difference in the predicted welding distortion. In the FEA cases studied, the predicted distortion with two very large lumped passes was 74% of the predicted distortion with 36 small lumped passes. But the saving in FEA computing time was very significant.

The FEA simulations of single nozzle welding with different cooling times demonstrated the influence on the welding distortion. The corresponding inter-pass temperatures varied from about 100^{o}C when with long cooling time to about 200^{o}C when with short cooling time. The FEA case with 200^{o}C inter-pass temperature resulted in 15% more distortion than the case with 100^{o}C inter-pass temperature.

Chapter 7 Welding Distortion in Multi-nozzle Weld Mockup

7.1 Introduction

The main purpose of carrying out a multi-nozzle weld mockup test was to find out the actual level of the welding distortions under typical welding conditions. As introduced in Section 3.2.2, the multi-nozzle mockup test was performed in two stages. In the first stage, the nozzle at the shell plate center was welded without fixture (Figure 7-1 (a)). Manual GTAW process and J groove were used for the center nozzle welding. This represents a condition where a high level of welding distortion would be developed. In the second stage, a rib-bar fixture (Figure 3-2) was attached to the shell plate and 10 nozzles were welded around the center nozzle using double bevel groove design. SMAW was employed as the main welding process except for root pass where manual GTAW method was used. All the nozzles were welded firstly from the shell OD side (Figure 7-1 (b)) following progressive welding sequence shown in Figure 3-6. Then the shell plate was flipped over to weld all the nozzles on the shell ID side following the same welding sequence. Refer to Section 3.4.2 for specific welding procedure details. Stage 2 represents the most common production condition.

7.2 Distortion after Welding of Center Nozzle without Fixture

A series of punch marks were created on the shell plate surface as shown in Figure 7-2, to facilitate the surface profile measurement with FARO-ARM device. The

shell plate surface was measured before and after the welding of the center nozzle. The Z direction welding distortions along X and Y axes were plotted in Figure 7-3. Based on the measurement data, the Max Z Distortion was found to be 16.8mm.

(a) Completion of Stage 1 (b) Stage 2 Welding on Shell OD Side

Figure 7-1 Welding of Multi-nozzle Weld Mockup

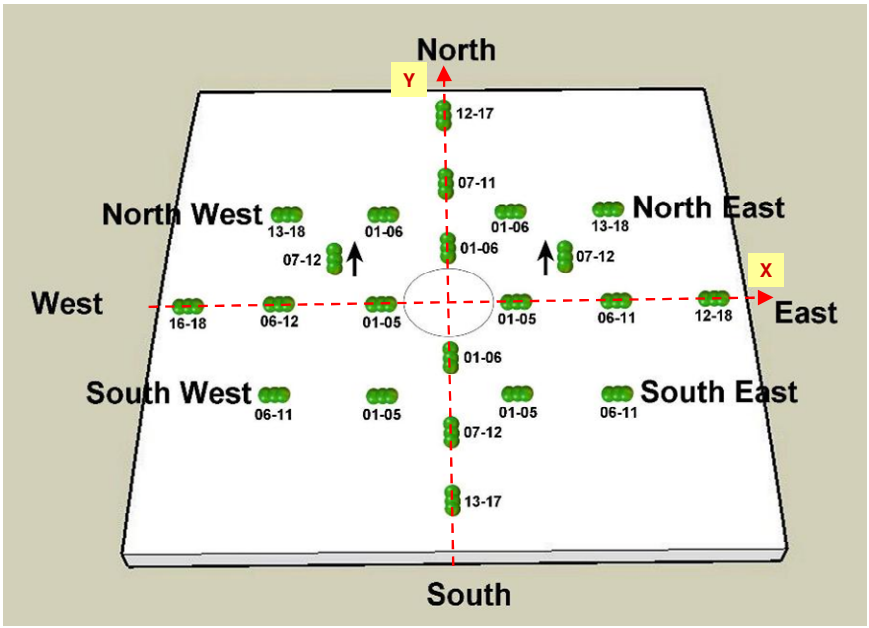

Figure 7-2 Shell Surface Measurement Map

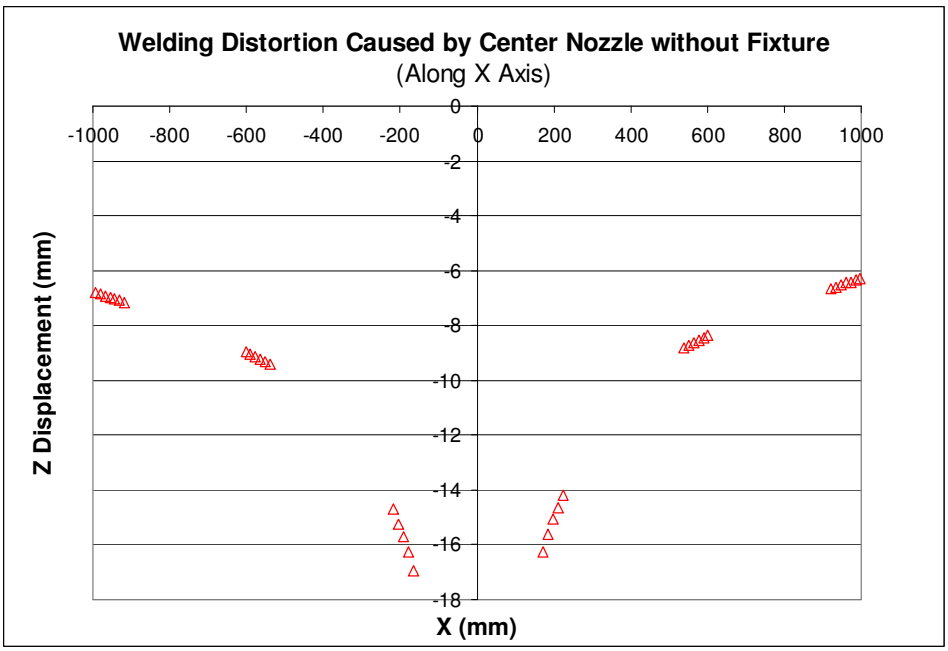

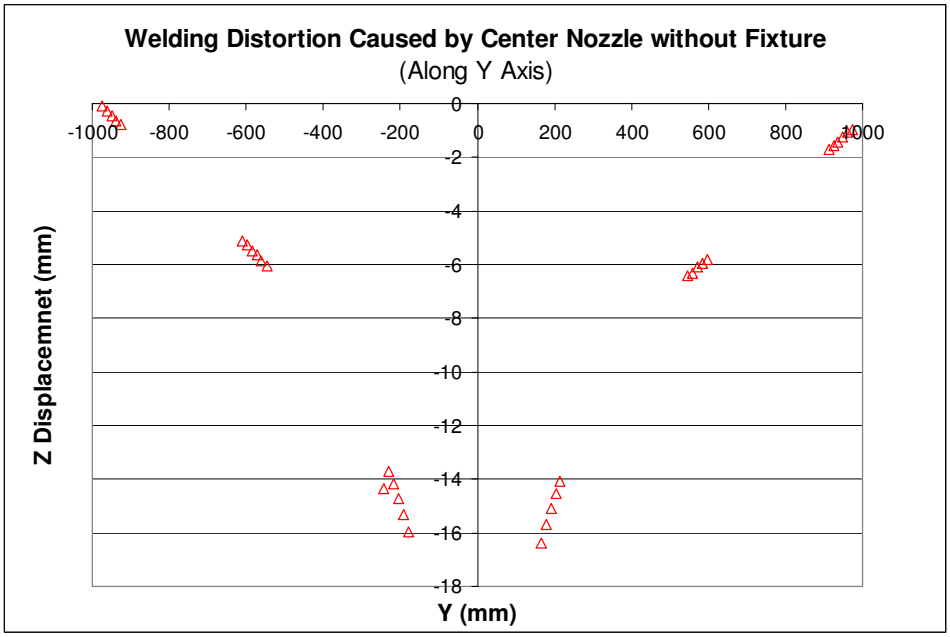

Figure 7-3 Distortion after Welding of Center Nozzle without Fixture

7.3 Distortion after Welding of Multiple Nozzles with Fixture

The shell OD side of the nozzle-to-shell weld assembly was scanned with laser scan device Handyscan 3D^{TM} EXAscan before and after the welding of nozzles #2~#11 (Figure 7-4). A series of data at locations shown in Figure 7-4 were extracted from the shell surface 3D model established after the laser scan, based on which Figures 7-5, 7-6 and 7-7 were obtained.

The Z direction displacement data of the shell surface (Figure 7-5) revealed a Max Z Distortion of 16.4mm. The maximum distortion occurred around nozzles #4 and #5 (the dark blue areas in Figure 7-4) which were least constrained by the fixture and the nozzle-shell structure around them. Comparing Figure 7-4 with the FEA result in Figure 5-7 a high similarity could be found. Both cases took the same welding sequence.

The maximum plate shrinkage, about 6mm, took place in Y axis direction around the plate center (Figure 7-7) for which the major reasons may include,

- More nozzles were welded along Y direction
- Naturally the distortion in Y direction is easier because of the shell curvature
- Low constraint from the fixture and the shell plate itself

Regarding the plate shrinkage in X direction (shell can axial direction), no clear trend can be found from Figure 7-6. This would be likely because the shrinkage was too small to be effectively detected by the measurement device employed. It suggests that, under the given mockup configuration, the shrinkage in shell can axial direction was negligible.

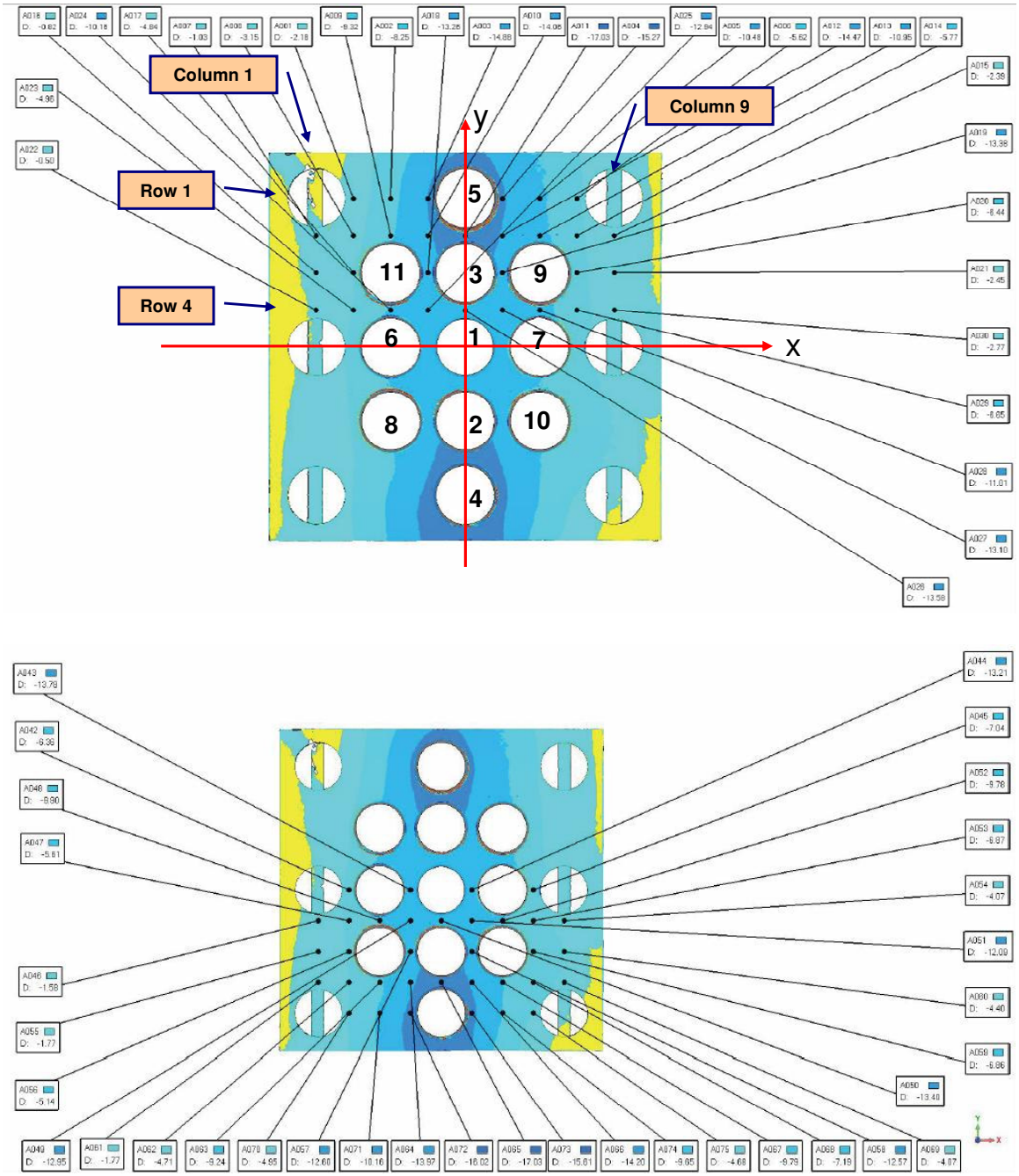

Figure 7-4 Welding Distortion Data Matrix of Multi-nozzle Weld Mockup

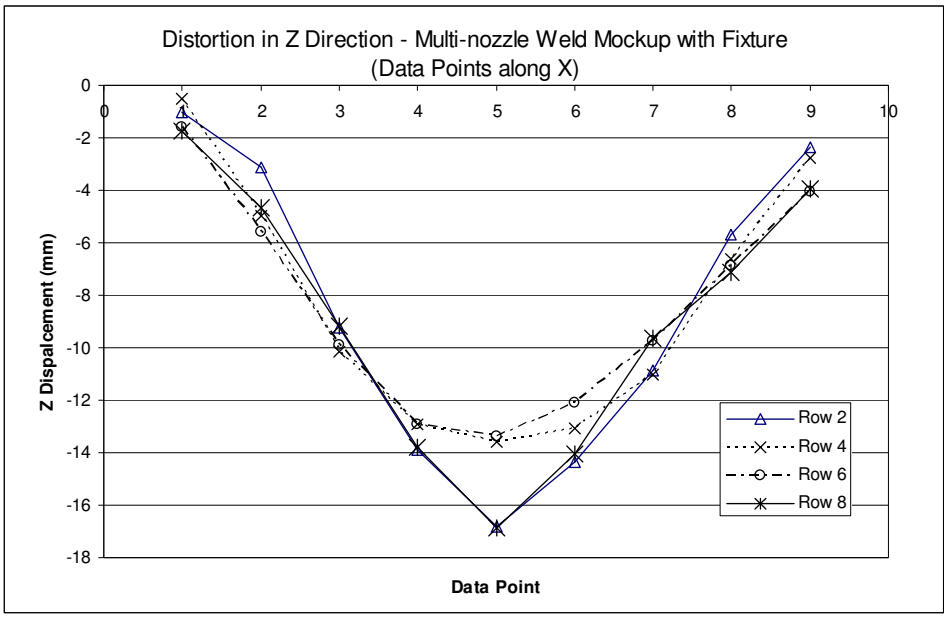

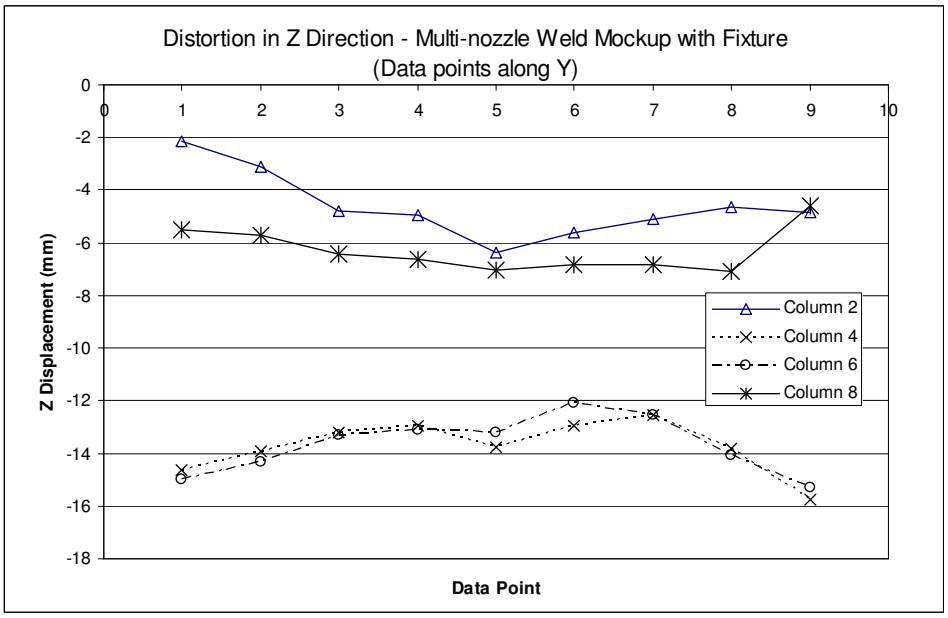

Figure 7-5 Distortion in Z Direction - Multi-nozzle Weld Mockup with Fixture

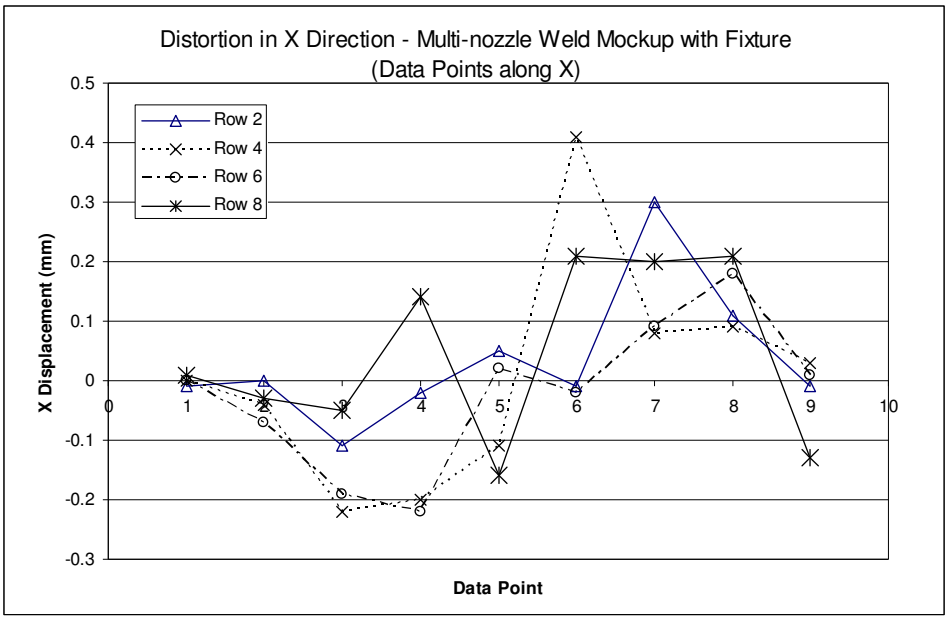

Figure 7-6 Distortion in X Direction - Multi-nozzle Weld Mockup with Fixture

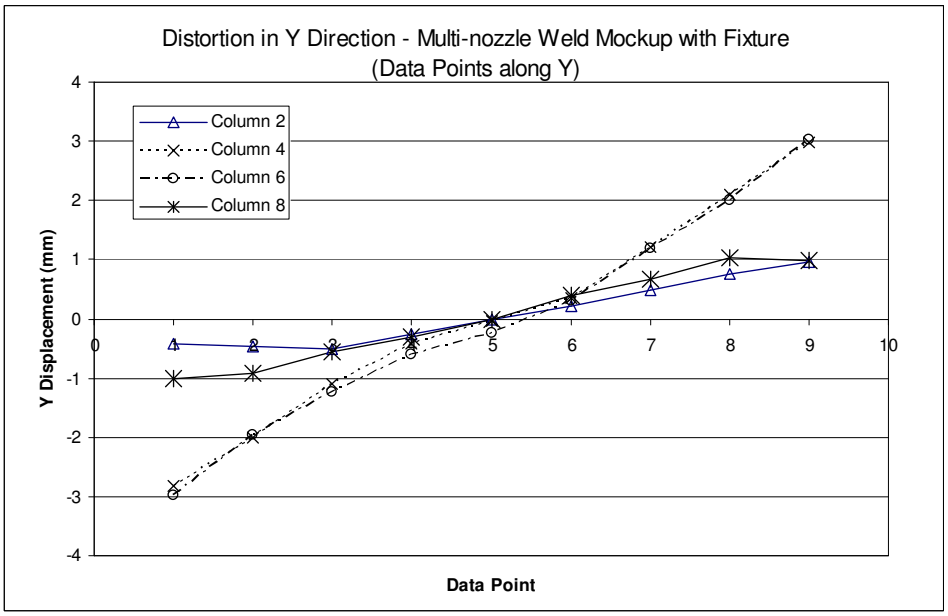

Figure 7-7 Distortion in Y Direction - Multi-nozzle Weld Mockup with Fixture

7.4 Summary

Large scale multi-nozzle weld mockup tests were designed to investigate the possible level of welding distortion under typical conditions of stainless steel nozzle-to-shell welding applications. The mockup tests were conducted in two stages, focusing firstly on the worst case scenario (no fixture, manual GTAW process, J groove) then the most common welding practice (rib-bar fixture, mainly SMAW process, double bevel groove, completing all nozzle welding from the shell OD side then proceeding to the shell ID side).

The welding (without fixture) of the center nozzle on the mockup plate produced a Max Z Distortion of 16.8mm, which would not be tolerable for most of the pressure vessel applications. Solutions have to be worked out to restrict the stainless steel nozzle welding distortion.

The multi-nozzle welding test under the most common welding conditions described above demonstrated a much better performance in terms of distortion control. After the welding of 10 nozzles, a Max Z Distortion of 16.4mm was developed, even less than the distortion of the first stage where only one nozzle was welded. The maximum plate surface shrinkage of 6mm was found in the direction across the shell can axis. No apparent shrinkage was found in the shell axis direction. The test results confirmed that the fixture design, the welding procedure, and the weld groove design of the second stage mockup test was effective in reducing the stainless steel nozzle welding distortion.

Chapter 8 Conclusions

Systematic studies were carried out through experiments and finite element analyses on the distortions developed in stainless steel nozzle-to-shell-can welding. The influences of welding fixture, welding sequence and welding process on the welding distortion were investigated in a comparative approach. Large nozzle-to-shell welding mockup was made under typical welding conditions to evaluate the actual level of the welding distortion. Major conclusions from these studies are as follows,

1. The contour fixture introduced in the thesis could effectively reduce the shell plate distortion. The results from single nozzle mockup tests and FEA (finite element analysis) simulations showed that the welding distortion was reduced by about 40% when the contour fixture was used. It was confirmed that the FEA models and techniques were effective for comparative study as well as for prediction of the nozzle welding distortion.
2. The comparison of different fixture designs suggests that, after the fixture removal, the contour fixtures would leave much less distortion than the conventional rib-bar fixture. The contour fixture will restrict the welding distortion to local area, resulting in less impact on the global distortion of a large weld structure. When rib-bar fixture is selected, it should be kept in place until all subassemblies are welded together, otherwise the shell pate of the welded subassembly would spring back to create significantly larger distortion.

3. Under the given shell-nozzle structure configuration, the nozzles shall be progressively welded onto the shell, starting from one nozzle then proceeding to its immediate neighboring nozzles.
4. For single nozzle welding with double-J groove, about 30~70% less distortion would be developed when the shell OD (outside diameter) side is welded first. From the distortion control point of view, the multi-nozzle welding under the conditions given in the thesis shall proceed one nozzle by one nozzle, each from shell OD side to ID (inside diameter) side, rather than finishing the shell OD side of all nozzles then proceeding to their ID side.
5. The influence of the welding direction of each weld pass on the shell distortion didn't appear to be significant, except when the nozzle angular distortion is concerned.
6. The distortion caused by SMAW (shielded metal arc welding) process was much less than the manual GTAW (gas tungsten arc welding) process, about 2/3 under the test conditions in the thesis.
7. The influence of the weld bead size on the shell distortion didn't seam to be significant under the given nozzle weld joint configuration and welding condition. This suggests that using larger filler size or higher power welding process wouldn't create unfavorable consequence in terms of welding distortion.
8. For FEA simulation of large weld structures, using a lumped pass much larger than the actual weld bead size would effectively reduce the computation time, with reduced level of the estimated distortion. The extreme case in the studies showed a reduction in distortion by 26%.

9. The cooling time after welding, or the inter-pass temperature, will slightly affect the shell plate distortion.
10. The multi-nozzle weld mockup with rib-bar fixture demonstrated a maximum out-of-plane distortion of 16.4mm after the welding of 10 nozzles by GTAW (for root pass) plus SMAW processes. This was about the same level when GTA welding only one nozzle to the center of the same shell plate with J-groove and without fixture. However, additional measures would be required to further reduce the welding distortion.

References

1. Ed. W.R. Oates et al, “Materials and Applications Part 2”, AWS Welding Handbook, Vol. 4, 8th Ed, (1998) 233-332
2. “Stainless Steel”, http://en.wikipedia.org/wiki/Stainless_steel
3. K.H. Tseng and C.P. Chou, “Effect of pulsed gas tungsten arc welding on angular distortion in austenitic stainless steel weldments”, Science and Technology of Welding & Joining, 6 (3) (2001) 149-153
4. Ed. C.L. Jenney et al, “Welding Science and Technology”, AWS Welding Handbook, Vol. 1, 9th Ed, (2001) 328-354
5. J. Mackerle, “Finite element analysis and simulation of welding: a bibliography (1976–1996)”, Modeling and Simulation in Materials Science and Engineering, 4 (1996) 501–533
6. Ed. Z. Feng, “Processes and Mechanisms of Welding Residual Stress and Distortion”, Woodhead Publishing Ltd., Cambridge, UK, 2005
7. F.W. Brust and P. Scott, “Weld Distortion Control Methods and Applications of Weld Modeling”, Transactions SMiRT 19, Toronto, August 2007
8. J. Goldak et al, “Computational Weld Mechanics”, Proceedings No. 398 Advanced Joining of Aerospace Metallic Materials, June 1985
9. M.I. Dawson, “Modeling and Analysis of Welding Processes in Abaqus using the Virtual Fabrication Technology (VFT) Analysis Software developed by Battelle and Caterpillar Inc”, 2008 Abaqus Users’ Conference
10. P. Michaleris et al, "Minimization of welding residual stress and distortion in large structures", Welding Journal, 78 (11) (1999) 361-s to 366-s
11. C.L. Tsai et al, “Welding Distortion of a Thin-Plate Panel Structure”, Welding Journal, 78 (5) (1999) 156-s to 165-s
12. D. Deng, “FEM prediction of welding residual stress and distortion in carbon steel considering phase transformation effects”, Materials and Design, 30 (2) (2009) 359–366
13. L.J. Zhang, “Parametric studies of welding distortion in fillet welded structure based on FEA using iterative substructure method”, Science and Technology of Welding and Joining 12 (8) (2007) 703-707
14. D. Camilleri and T.G.F. Gray, “Computationally efficient welding distortion simulation techniques”, Modeling and Simulation in Materials Science and Engineering, 13 (8) (2005) 1365-1382
15. D. Camilleri et al, “Computational prediction of out-of-plane welding distortion and experimental investigation”, Journal of Strain Analysis for Engineering Design, 40 (2) (2005) 161-166

16. C.L. Tsai et al, “Modeling Strategy for Control of Welding-Induced Distortion”, Modeling of Casting, Welding and Advanced Solidification Processes VII, The Minerals, Metals and Materials Society, (1995) 335±345
17. D. Deng and H. Murakawa, “FEM prediction of buckling distortion induced by welding in thin plate panel structures”, Computational Materials Science, 43 (4) (2008) 591-607
18. Z. Zeng et al, “Determination of welding stress and distortion in discontinuous welding by means of numerical simulation and comparison with experimental measurements”, Computational Materials Science, 49 (3) (2010) 535-543
19. S. Kiyoshima, “Influences of heat source model on welding residual stress and distortion in a multi-pass J-groove joint”, Computational Materials Science, 46 (4) (2009) 987-995
20. J. Guirao, “FEM simulation of a small EB welded mock-up and new sequence proposed to improve the final distortions”, Fusion Engineering and Design, 85 (2) (2010) 181-189
21. H. Long et al, “Prediction of welding distortion in butt joint of thin plates”, Materials and Design, 30 (10) (2009) 4126-4135
22. G.A. Moraitis and G.N. Labeas, “Prediction of residual stresses and distortions due to laser beam welding of butt joints in pressure vessels”, International Journal of Pressure Vessels and Piping, 86 (2-3) (2009) 133-142
23. M. Abid, “Prediction of welding distortions and residual stresses in a pipe–flange joint using the finite element technique”, Modeling and Simulation in Materials Science and Engineering, 13 (3) (2005) 455-470
24. M. Adak and N.R. Mandal, “Numerical and experimental study of mitigation of welding distortion”, Applied Mathematical Modeling, 34 (1) (2010) 146-158
25. J.J. del Coz Díaz et al, “Comparative analysis of TIG welding distortions between austenitic and duplex stainless steels by FEM”, Applied Thermal Engineering, 30 (16) (2010) 2448-2459
26. J. Guirao et al, “Use of a new methodology for prediction of weld distortion and residual stresses using FE simulation applied to ITER vacuum vessel manufacture”, Fusion Engineering and Design, 84 (12) (2009) 2187-2196
27. R. Wang et al, “Welding distortion investigation in fillet welded joint and structure based on iterative substructure method”, Science and Technology of Welding & Joining, 14 (5) (2009) 396-403
28. D. Camilleri et al, “Alternative simulation techniques for distortion of thin plate due to fillet-welded stiffeners”, Modelling and Simulation in Materials Science and Engineering, 14 (8) (2006) 1307-1327
29. J. Xu et al, “Prediction of welding distortion in multipass girth-butt welded pipes of different wall thickness”, The International Journal of Advanced Manufacturing Technology, 35 (9-10) (2008) 987-993
30. C. Liu and J. X. Zhang, “Numerical simulation of transient welding angular distortion with external restraints”, Science and Technology of Welding & Joining, 14 (1) (2009) 26-31
31. D. Deng and H. Murakawa, “Prediction of welding distortion and residual stress in a thin plate butt-welded joint”, Computational Materials Science, 43 (2) (2008) 353-365

32. D. Deng et al, “Numerical simulation of welding distortion in large structures”, Computer Methods in Applied Mechanics and Engineering, 196 (45-48) (2007) 4613-4627
33. M.V. Deo and P. Michaleris, “Mitigation of welding induced buckling distortion using transient thermal tensioning”, Science and Technology of Welding & Joining, 8 (1) (2003) 49-54
34. A. Bachorski et al, “Finite-element prediction of distortion during gas metal arc welding using the shrinkage volume approach”, Journal of Materials Processing Technology, 92 (93) (1999) 405-409
35. D. Deng et al, “Investigations on welding distortion in an asymmetrical curved block by means of numerical simulation technology and experimental method”, Computational Materials Science, 48 (1) (2010) 187-194
36. M. Mochizuki et al, “Computational simulation of weld microstructure and distortion by considering process mechanics”, Journal of Physics: Conference Series 165 (1) (2009) 012014
37. H. Zhang et al, “Fundamental studies on in-process controlling angular distortion in asymmetrical double-sided double arc welding”, Journal of Materials Processing Tech., 205 (1-3) (2008) 214-223
38. P. Colegrove et al, “Welding process impact on residual stress and distortion”, Science and Technology of Welding & Joining, 14 (8) (2009) 717-725
39. “Welding Simulation with Abaqus”, Abaqus Technology Brief TB-05-WELD-1, April 2007
40. M. Shubert et al, “An Abaqus Extension for Welding Simulations”, 2010 SIMULIA Customer Conference
41. J. Tejc, “SYSWELD – Complete Finite Element Solution for Simulation of Welding Processes”, MECAS ESI, 2003
42. “Weld Quality Simulation of Multi-Pass Designs”, ESI Group training course, April 2009
43. “SYSWELD® 2008 Welding Simulation - User’s Guide”, ESI Group, November 2007.
44. H. Yang and H. Shao, “Distortion-oriented welding path optimization based on elastic net method and genetic algorithm”, Journal of Materials Processing Tech., 209 (9) (2009) 4407-4412
45. S. Pal et al, “Radial basis function neural network model based prediction of weld plate distortion due to pulsed metal inert gas welding”, Science and Technology of Welding & Joining, 12 (8) (2007) 725-731
46. M.P. Lightfoot et al, “Artificial neural networks – an aid to welding induced ship plate distortion?”, Science and Technology of Welding & Joining, 10 (2) (2005) 187-189
47. T. Schenk et al, “A study on the influence of clamping on welding distortion”, Computational Materials Science, 45 (4) (2009) 999-1005
48. N.A. McPherson, “Correcting Thin-Plate Distortion in Shipbuilding”, Welding Journal, 89 (1) (2010) 30-34

49. M. Sammons, “Welding austenitic stainless steel - Tips for optimal GTAW performance”, http://www.thefabricator.com/article/arcwelding/welding-austenitic-stainless-steel#, April 2007
50. P. K. GHOSH et al, "Effect of Pulse Current on Shrinkage Stress and Distortion in Multipass GMA Welds of Different Groove Sizes", Welding Journal, 89 (3) (2010) 43-s to 53-s
51. J. Xu et al, “Effect of vibratory weld conditioning on the residual stresses and distortion in multipass girth-butt welded pipes”, International Journal of Pressure Vessels and Piping, 84 (5) (2007) 298-303
52. D.A. Price, “Distortion control in welding by mechanical tensioning”, Science and Technology of Welding & Joining, 12 (7) (2007) 620-633
53. J.R. Dydo et al, “Guidelines for Control of Distortion in Thin Ship Structures”, EWI Project No. 42372GDE, November 1999
54. T. Schenk et al, “Modeling buckling distortion of DP600 overlap joints due to gas metal arc welding and the influence of the mesh density”, Computational Materials Science, 46 (4) (2009) 977-986
55. T. Teng et al, “Analysis of residual stresses and distortions in T-joint fillet welds”, The International Journal of Pressure Vessels and Piping, 78 (8) (2001) 523-538
56. D. Deng et al, “Numerical and experimental investigations on welding residual stress in multi-pass butt-welded austenitic stainless steel pipe”, Computational Materials Science, 42 (2008) 234–244
57. M. Audronis and J. Bendikas, “The Welding Deformations of Chrome-nickel Stainless Steels”, Materials Science (MEDŽIAGOTYRA, ISSN 1392-1320), 9 (2) (2003) 169-173
58. K. Akikazu et al, “A study of laser welding on 304 stainless steel vessel fabrication”, Proceedings of Japanese Welding Society, 20 (2) (2002) 301-308
59. K. Akikazu et al, “A study on laser welding deformation of 304 stainless steel”, Proceedings of Japanese Welding Society, 20 (2) (2002) 295-300
60. M. Vural et al, “The effect of welding fixtures on welding distortions”, J. Achievements in Materials and Manufacturing Engineering, 20 (1-2) (2007) 511-514
61. Y. Ozcatalbas and H.I. Vural, “Determination of optimum welding sequence and distortion forces in steel lattice beams”, Journal of Materials Processing Tech., 209 (1) (2009) 599-604
62. L. Gannon et al, “Effect of welding sequence on residual stress and distortion in flat-bar stiffened plates”, Marine Structures, 23 (3) (2010) 385-404
63. I. Voutchkov et al, “Weld sequence optimization: The use of surrogate models for solving sequential combinatorial problems”, Computer Methods in Applied Mechanics and Engineering, 194 (2005) 3535–3551
64. J. Goldak et al, “Why Power per Unit Length of Weld Does Not Characterize a Weld”, http://cat.inist.fr/?aModele=afficheN&cpsidt=22585988, July 2009